Infrared Contrast Analysis Technique for Flash Thermography Nondestructive Evaluation

Ajay Koshti
NASA Johnson Space Center

September 11, 2014

Table of Contents

List of Figures

Nomenclature

Uppercase Symbols

A_c = flaw size parameter

A_{cA} = adjusted flaw size parameter

C_1 through C_9 = contrast evolution shape or profile constants

C_A = amplitude constant

$C_{A,d}$ = amplitude constant for a given depth d

$C_{AF,d}$ = amplitude factor for a given depth d

$C_{A,b,\mu}$ = amplitude constant from the calibration curve for a base depth and given attenuation μ

$C_{AF,b}$ = amplitude factor at base depth, usually 1

C_{Ae} = amplitude constant for anomaly evaluation

$C_{A,\mu}$ = amplitude constant for attenuation μ

$C_{A,0}$ = amplitude constant at for no attenuation

C_D = diameter constant

$C_{D,\mu}$ = diameter constant for attenuation μ

$C_{D,0} = C_D$ =diameter constant for no attenuation

C_d = depth (or diffusivity) constant

$C_{d\text{-}ref}$ = depth constant for reference material

$C_{d,d}$ = depth constant at depth d

$C_{d\,b}$ = depth constant for base depth

C_f = transformation coefficient

$\overline{C}^{Steady}$ = steady state normalized contrast

$\overline{C}^{t}$ = normalized temperature contrast or modulation temperature contrast

$\overline{C}^{t}_{adjusted}$ = adjusted normalized contrast evolution

$\overline{C}^{t}_{\%}$ = normalized contrast expressed as percentage

$\overline{C}^{t}_{W}$ = normalized pixel intensity contrast

$\overline{C}^{t}_{W,\%}$ = percent normalized pixel intensity contrast

$\overline{C}^{t-peak}_{w,a}$ = peak contrast (amplitude) on (actual) data

$\overline{C}_{w,ref}^{\,t_{ref}}$ = normalized contrast of reference contrast evolution

$\overline{C}_{w,a}$ = measured normalized contrast

$\overline{C}_{w,e}$ = estimated normalized contrast

$\overline{C}_{w,af}$ = measured normalized contrast that is filtered or smoothed

$\Delta\overline{C}_{w}^{\,2}$ = delta square

$\Delta\overline{C}_{w}^{2-f}$ = delta square for filtered contrast evolution

$\Delta\overline{C}_{w,av}^{2}$ = delta square average

$\Delta\overline{C}_{w,av}^{2-f}$ = delta square average for filtered contrast evolution

$\Delta\overline{C}_{w,\%}^{2}$ = percent delta square

$\Delta\overline{C}_{w,\%}^{2-f}$ = percent delta square for filtered contrast evolution

D = diameter (cm, m or in)

D_a = diameter (cm, m or in) estimated by analysis

D_{EFBH} = diameter estimated by equivalent flat bottom hole analysis

$D_{EUG,\,\mu 50\%}$ = equivalent gap estimation of diameter with 50 percent attenuation

$E_{50L-50R}$ = persistence energy time (sec, hr)

H = average heat flux incident on the surface (cal-cm^{-2}sec^{-1}, kcal-m^{-2}sec^{-1} or BTU-ft^{-2}hr^{-1})

L = conduction layer thickness (cm, m or in)

N_{Bi} = Biot Number

Q = total heat incident on the test object per unit surface area (cal-cm^{-2}, kcal-m^{-2} or BTU-ft^{-2})

R = width of region of interest (cm, m or in)

$S_{AF,d}$ = slope for the amplitude factor (e.g. -0.1)

S_d = slope for the depth constant

$S_{D,\mu}$ = slope for the diameter constant

$S_{A,\mu}$ = slope for the amplitude constant

T = surface temperature at the measurement point (usually center of the anomaly) (°C, K or °F)

ΔT = temperature change (rise) from the preflash temperature on the front surface (°C, K or °F) at the center of anomaly at time t

T^0 = surface temperature of the measurement point before flash

T_R = surface temperature at reference point (usually outside the anomaly area) footprint

T_R^0 = surface temperature of the reference area before flash

ΔT_R =temperature rise at the reference area outside the anomaly at time *t*.

$W_{50\text{-}50}$ = withholding heat time (sec, hr)

ΔW = rise in the pixel intensity at the measurement point at time *t*

ΔW_R = rise in the pixel intensity at the reference point at time *t*

Lowercase Symbols

c = specific heat (cal- gm^{-1} -$^oC^{-1}$, kcal- kg^{-1} -$^oC^{-1}$ or BTU- lbm^{-1} -$^oF^{-1}$)

d = thickness of layer above anomaly or anomaly depth (cm, m or ft), depth of a flat bottom of FBH from flash surface or depth of a uniform gap from flash surface

d_b = delamination or FBH base depth

d_{th} = thickness of the test object in the form of a plate

$d_{threshold}$ = threshold thickness

d_{EFBH} = depth estimated by equivalent flat bottom hole analysis

$d_{EUG,\,\mu 50\%}$ = equivalent gap estimation of depth with 50 percent attenuation

f = frequency used in FFT filtering of the contrast evolution (for a 1024 point evolution, 1024 points represent *f* =1, 524 points represent *f* =2 and so on)

g = gap thickness of a delamination (cm, m or in)

h = thermal convection film coefficient, (cal- cm^{-2}-oC^{-1} s^{-1}, kcal- m^{-2} K^{-1} s^{-1} or BTU- ft^{-2} $^oF^{-1}$ hr^{-1})

k = thermal conductivity, (cal- cm^{-2} -$^oC^{-1}$ s^{-1} , kcal- m^{-2} -K^{-1} s^{-1} or BTU- ft^{-2} -$^oF^{-1}$ hr^{-1})

l = length of the anomaly (cm, m or in)

l_1 , l_2, l_3 = transit time multipliers

n = natural number

ns, nf = starting and end frame numbers used in delta square calculations

ns1 and *nf1* = starting and end frame numbers used in delta square calculations using filtered contrast evolution

r = radius of a round anomaly (cm, m or in)

t = time (sec or hr) measured from the end of flash

t' = normalized time (dimensionless)

Δt = flash time (sec or hr)

t_{appear} = earliest appearance or detection of anomaly in the raw frame of IR data (sec or hr)

t_{peak} = time at which peak contrast occurs (sec or hr)

t_{ref} = time of reference contrast evolution (sec or hr)

t_{peak}^{ref} = peak of reference contrast evolution (sec or hr)

t_{end} = end time of contrast evolution (sec or hr)

t_{50L} = time less than the peak time at which the contrast intensity is 50 percent of the peak contrast (sec or hr)

t_{50L}^{ref} = time less than the peak time at which the contrast intensity is 50 percent of the peak contrast for the reference contrast evolution (sec or hr)

t_{50R} = time greater than the peak time at which the contrast intensity is 50 percent of the peak contrast (sec or hr)

t_{50R}^{ref} = time greater than the peak time at which the contrast intensity is 50 percent of the peak contrast for the reference contrast evolution (sec or hr)

t_{10R} = time greater than the peak time at which the contrast intensity is 10 percent of the peak contrast (sec or hr)

t_{10R}^{ref} = time greater than the peak time at which the contrast intensity is 10 percent of the peak contrast(sec or hr)

$t_{50L-50R}$ = persistence time (sec or hr)

w = anomaly width (cm, m or in)

w_{hm} = half-max width estimation (cm, m or in)

Uppercase Greek Symbol

Γ = thermal mismatch factor at the anomaly (Γ is the Greek letter capital gamma)

Lowercase Greek Symbols

α = thermal diffusivity, (cm^2 -sec^{-1}, m^2 -sec^{-1} or ft^2-hr^{-1})

α_l = thermal diffusivity for lateral heat flow, (cm^2 -sec^{-1}, m^2 -sec^{-1} or ft^2-hr^{-1})

α_{ref} = thermal diffusivity of reference material, (cm^2 -sec^{-1}, m^2 -sec^{-1} or ft^2-hr^{-1})

β = thermal effusivity of the layer above the anomaly, (cal-cm^{-2} -$^oC^{-1}$-$sec^{-1/2}$, kcal-m^{-2} -K^{-1}-$sec^{-1/2}$ or BTU-ft^{-2} -$^oF^{-1}$-$hr^{-1/2}$)

β_d = thermal effusivity of the layer below the anomaly (cal-cm^{-2} -^{o}C^{-1}-sec$^{-1/2}$, kcal-m^{-2} -$^{K-1}$-sec$^{-1/2}$ or BTU-ft^{-2} -^{o}F^{-1}-hr$^{-1/2}$)

ε = emissivity of the flashed surface

ε' = ratio of normalized pixel contrast to normalized temperature contrast

ε'' = emissivity factor

η = best fit exponent, depends upon μ

φ = anomaly aspect ratio, i.e. ratio of length to width or diameter

γ = diameter or width to depth ratio

γ_a = apparent diameter or width to depth ratio

γ' = adjusted diameter or width to depth ratio

γ_{ref} = diameter or width to depth ratio in the reference contrast evolution

λ = pixel resolution ratio

λ' = ratio of width of the anomaly to size of pixel

$\lambda_{texture}$ = pixel resolution ratio for texture

$\lambda_{anomaly}$ = pixel resolution ratio for anomaly

ν = frame rate in frames per second (Hz)

ρ = density (g-cm^{-3} kg-m^{-3} or lbm-ft^{-3})

ψ = width ratio

$\psi_{\mu 50\%}$ = width ratio at 50 percent attenuation

μ = attenuation or transmissivity measure (fraction between 0 and 1)

$\mu_{\%}$ = percent attenuation

τ = normal transit time, normal transit time is related to the Fourier Modulus, (sec or hr)

τ_l = lateral transit time

τ_n = multiples of heat transit time to the anomaly

θ = heat flow angle, degree

ω = ratio of anomaly depth to object thickness

ω_{ref} = ratio of anomaly depth to object thickness in the reference contrast evolution

χ = depth ratio

ζ = amplitude ratio

Acronyms

ASTM = American Society for Testing and Materials

EFBH = equivalent flat bottom hole

EUG = equivalent uniform gap

FBH = flat bottom hole

FFT = fast Fourier transform

FSP = flaw size parameter

IFOV = instantaneous field of view

IR = infrared

NDE = nondestructive evaluation

POD = probability of detection

RCC = reinforced carbon carbon

ROI = region of interest

SRF = slit response function

Infrared Contrast Analysis Technique for Flash Thermography Nondestructive Evaluation

1. Abstract

The paper deals with the infrared flash thermography inspection to detect and analyze delamination-like anomalies in nonmetallic materials. It provides information on an IR Contrast technique that involves extracting normalized contrast verses time evolutions from the flash thermography infrared video data. The paper provides the analytical model used in the simulation of infrared image contrast. The contrast evolution simulation is achieved through calibration on measured contrast evolutions from many flat bottom holes in the subject material. The paper also provides formulas to calculate values of the thermal measurement features from the measured contrast evolution curve. Many thermal measurement features of the contrast evolution that relate to the anomaly characteristics are calculated. The measurement features and the contrast simulation are used to evaluate flash thermography inspection data in order to characterize the delamination-like anomalies. In addition, the contrast evolution prediction is matched to the measured anomaly contrast evolution to provide an assessment of the anomaly depth and width in terms of depth and diameter of the corresponding equivalent flat-bottom hole (EFBH) or equivalent uniform gap (EUG). The paper provides anomaly edge detection technique called the half-max technique which is also used to estimate width of an indication. The EFBH/EUG and half-max width estimations are used to assess anomaly size. The paper also provides some information on the "IR Contrast" software application, half-max technique and IR Contrast feature imaging application, which are based on models provided in this paper.

2. Introduction

Infrared (IR) flash (or pulsed) thermography is a Nondestructive Evaluation (NDE) method used in the inspection of thin nonmetallic materials such as laminated composites in the aerospace industry. It is primarily used to detect delamination-like anomalies, although, surface cracks are also detected to some extent. In most circumstances, a single sided or reflection technique is used where the flash lamp (heat source) and the IR camera (detector) are on the same side of the test object inspected. In some situations, a through-transmission or forward scattering flash thermography technique is used. In the through-transmission technique, the source and the detector are on the opposite sides of the test object. Here, the area of the test object under inspection has more or less constant thickness. Maldague[1] provides general information on flash thermography including practical examples and mathematical analysis. Carslaw[2] provides analytical solutions for thermal conduction in isotropic material for many cases of heat source and boundary conditions. Spicer[3] provides information on both theory and applications in active thermography for nondestructive evaluation. This paper deals only with the single-sided flash thermography.

3. Flash Thermography Equipment

The IR Flash thermography equipment consists of a flashhood, flash power supply/trigger unit, flash duration controller, camera data acquisition electronics and a personal computer (PC). The PC is used for controlling the flash trigger, camera data acquisition, data display and post processing of the acquired data. The flash-hood has three major components. The first component is a box (or hood). It is made from a sheet metal. One of the six sides of the hood is open. The side opposite to the open side has a hole in the center to provide a window for lens of the IR camera which is mounted from outside of the hood. The IR camera is focused at the test object (part) surface located at the hood opening. Two flash lamps are located at inner wall of the hood on the camera side. These flash lamps direct the illumination towards the hood opening where the part is located without directly shining the light into the camera lens. The hood contains most of the intense flash. See Figure 1.

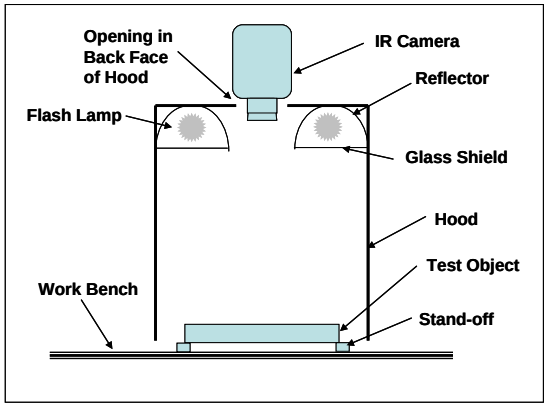

Figure 1: Schematic of the Flash Thermography Set-up

4. One-Sided Flash Thermography Technique

If the test object can be accommodated inside the hood, then it is located at the hood opening or slightly inside the hood. Otherwise, the part is located slightly outside of the hood opening. A short duration (e.g. 5 msec), intense (12 kJ) flash is triggered using a computer keyboard. The data acquisition is triggered a few seconds before the flash and it continues until the prescribed time. The camera provides a sequence of IR images (or frames) called the datacube (or digital video) of the part surface taken at the chosen frame rate (e.g. 60 Hz or 60 frames per sec). The intensity (numerical value) of each pixel in the image is function of the surface temperature of the corresponding area on the part at the time of image frame. The flash causes the surface to warm up slightly and the heat starts to dissipate rapidly. The surface cools through thermal radiation, convection and conduction. It is assumed that the heat conduction within the part is the dominant heat transfer mode until the temperature gradients within the part become small. At later times, the heat conduction is of the order of the combined effect of heat convection and

radiation. The IR data acquisition and data analysis utilizes the thermal data in the short duration immediately after the flash where the thermal dissipation is dominated by the heat conduction within the part.

The heat exchange across the boundaries due to convection can be assumed to be zero[5,6] if Biot number (N_{Bi} =hL/k) < 0.1. Consider an example of ½ cm thick graphite/epoxy (k = 0.64 W/mK) plate. Using h = 10 W/m^2, the Biot number is 0.078. Therefore, the heat conduction is the dominant mode of heat transfer in this example. Thinner parts tend to equalize the temperature within the part very quickly and have relatively longer cooling time by heat loss to environment. These parts are not suitable for IR Contrast simulation analysis provided here. Koshti[7] defines a term called threshold thickness ($d_{threshold}$) to classify parts as thin or thick for heat conduction in flash thermography.

5 IR Flash Thermography Anomaly Detection

Let us assume that the part is a plate made of a thermally isotropic material with constant thickness and it fits inside the hood. The plate is supported at the corners on insulating standoffs and the hood is oriented vertically. If we assume that the flash intensity is uniform over the plate top surface, then the heat conduction will be in a direction normal to the part surface in most of the acreage area (area away from edges of the part and flash boundary). The heat is conducted uniformly from the top surface to bottom surface of the plate. The normal heat conduction will be obstructed by an anomaly such as a small round gapping delamination at the center of a plate, as depicted in Figure 2. The volume bounded by the anomaly on one side and the part top surface on the other side is called the heat trapping volume.

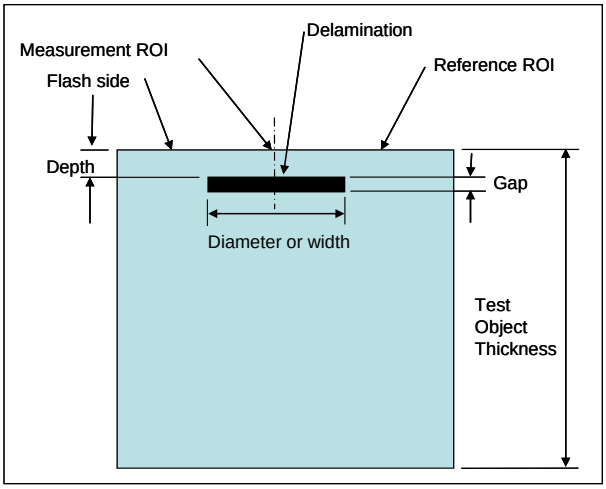

Figure 2: Cross Sectional View of the Test Object, Measurement and Reference Points

The top surface area surrounding the anomaly cools faster than the top surface (footprint) area above the anomaly. The IR camera captures the surface temperature image in terms

of the pixel intensity and shows the anomaly as a hot spot (e.g. an area warmer than the surrounding area) which is about the size and shape of the anomaly footprint. Relative pixel intensity of the hot spot changes with the time. Deeper anomalies appear at later times in the IR video compared to the near surface anomalies. After the appearance of an anomaly in the IR video, its relative pixel intensity continues to increase with time. The anomaly relative pixel intensity reaches a peak at a certain time and then the relative intensity decays until the indication area temperature and the surrounding area temperature become equal. Figure 3 shows an IR image of a plate with round flat-bottom holes (FBH's) machined from the back side to simulate gapping delaminations of differing depths. The part continues to cool down to ambient temperature through heat convection and radiation. If any objects contact the part or the part has significant area that does not receive the flash, then the heat conduction to unflashed area or to the contacting object also causes cooling.

6. Flash Thermography IR Data Analysis Using Commercial Software

Commercially available IR data analysis software analyzes the data to detect the anomalies by providing enhanced processed images. Commercial software's called EchoTherm[4] and Mosaic[4] by Thermal Wave Imaging Inc., provide many post-processing options such as, frame subtraction from other frames, frame averaging, pixel intensity rescaling etc. They also provide first and second derivative (of pixel intensity with respect to frame number or time) images. The derivative images are drawn from fitted data. The fitted data is created by fitting curves in the pixel intensity versus time profile of each pixel. The pixel intensity (average of one or more neighboring pixels) versus time (T-t) curve can be displayed in logarithmic (log-log) scale. An ideal temperature-time decay log-log curve on a thick plate with no anomalies is a straight line with a slope[1] of -0.5. The measured log-log curve on an anomaly would have a constant negative slope for some time after the flash but at a time related to the heat transit time to the anomaly, the decay curve would start departing from the linear constant slope (see ASTM E 2582). The departure time or the early appearance time (t_{appear}) can be used to estimate the depth of the anomaly. The software also allows a calibration of a ruler for measuring the distance between the pixels and provides the pixel coordinates. Thermofit Pro[5] also provides many of the above image post-processing routines such as derivatives of pixel intensities. Thermofit also defines a running contrast and normalized contrast. The definition of Thermofit normalized contrast is different than used in this paper. The Thermofit software does not define normalized image contrast and the normalized temperature contrast separately and therefore does not make distinction between the two. Both EchoTherm and Thermofit implicitly assume that the pixel intensity is proportional to the surface temperature and is a complete indicator of the surface temperature.

The EchoTherm software provides simple pixel "contrast" which is defined as the difference in the pixel intensity of any two selected areas on the test object surface. The ThermoCalc simulation provides simple temperature "contrast" which is defined as the difference in the temperature of any two selected areas on the test object surface. The

simple contrast evolution looks similar to the normalized contrast but is not as useful to correlate to the flaw parameters due to its dependence on flash intensity.

7. IR Contrast Objectives

The subject simulation model, software application, data analysis technique and approach are named "IR Contrast" by the author. The IR Contrast technique is geared towards anomaly characterization and not towards detection. The IR Contrast approach relates thermal measurements, such as the contrast evolution (or contrast signal) amplitude of an anomaly, in terms of the normalized anomaly contrast as a function of the frame number or the post-flash time. Under some constraints, the normalized anomaly contrast is mainly influenced by factors "related" to an anomaly such as the material thermal properties (diffusivity and emissivity), anomaly size, depth and the heat transmissivity or thermal mismatch factor. The contrast is also affected by factors that are "unrelated" to the anomaly such as the part curvature, uneven part cross section, changing thermal properties along the part surface, surface cracks, surface texture, uneven flash heating, camera pixel size, focusing and proximity to the part edge or the flash boundary. The IR Contrast technique seeks to either minimize effect the unrelated factors in order to improve accuracy of the IR Contrast analysis or to control the unrelated factors to improve repeatability of the IR Contrast analysis. Several amplitude and time related thermal measurements (e.g. peak contrast and peak contrast time, persistence energy time etc.) are computed from the measured contrast evolution. These parameters bear some correlation to the anomaly depth, width and bridging/contact (or heat transmissivity through the anomaly). The approach also involves measurement of width of the indication using the half-max technique explained later.

The IR Contrast also uses calibrated simulation of the contrast evolution. The software calculates the diameter and depth as input iteratively, called equivalent flat bottom hole (EFBH) inputs, to the simulation that provides the best match to the measured contrast evolution. Thus, the anomaly depth and width are mapped into an EFBH diameter and depth. It is hypothesized that if the ratio of EFBH diameter to half-max diameter is close to one, then the anomaly is similar to a FBH or a gapping round delamination. Similarly, if the ratio of EUG diameter to half-max diameter is close to one, then the anomaly is similar to a round void with uniform gap. It is hypothesized that the EFBH depth is an estimation of the anomaly depth if the anomaly is similar to a gapping delamination or a FBH. Similarly, the EUG depth is an estimation of the anomaly depth if the anomaly is similar to a void with a uniform gap. The IR Contrast allows better characterization of the anomaly in terms of anomaly depth and width and assesses bridging, contact within the anomaly or effect of the gap thickness. The IR Contrast application is programmed for many materials and therefore provides a quick approximate prediction of the contrast on a given delamination-like anomaly. It can be used as a training tool for the application of flash thermography.

8. Temperature Rise on a Large Diameter Anomaly

Consider a laminated thick plate with a large diameter anomaly at a shallow depth (i.e. diameter of anomaly to depth ratio is very large). Consider center point of the anomaly footprint on the top or flash illumination surface. The temperature decay after the flash for the center point does not depend on the diameter. It is however, dependent on the depth of the anomaly especially after the time when the heat wave-front reaches the anomaly. The time at which the effect of the heat wave-front, reaching the bottom surface, is felt on the top surface is called the normal transit time. Consider an instantaneous pulse of heat radiation applied to the plate. If we assume that there is no heat transfer from the plate to the environment after receiving the flash, then the surface temperature is governed by heat conduction within the plate. Carslaw and Jaeger[2] provide many analytical solutions for heat conduction problems. An approximate solution for the surface temperature rise at the center-point as given by Spicer[3] is,

$$\Delta T(t) = \frac{\varepsilon\, Q}{\beta\sqrt{\pi t}}\left[1 + 2\sum_{n=1}^{\infty}(-\Gamma)^n e^{\left(\frac{-\tau_n}{t}\right)}\right], \tag{1}$$

where,

$$\Gamma = \frac{\beta_d - \beta}{\beta_d + \beta}, \tag{2}$$

$$\tau_n = \frac{n^2 d^2}{\alpha}, \tag{3}$$

$$\alpha = \frac{k}{\rho c}, \tag{4}$$

$$\beta = \sqrt{k\rho c}, \tag{5}$$

$$H = \frac{Q}{\Delta t}, \tag{6}$$

ΔT = temperature change from the preflash temperature on the front surface (^{o}C, K or ^{o}F),

t = time (sec or hr) measured from end of the flash,

τ_n = multiples of heat transit time to the anomaly,

α = thermal diffusivity of the material or effective diffusivity, (cm^2 -sec^{-1}, m^2 -sec^{-1} or ft^2-hr^{-1}),

β = thermal effusivity of layer above the anomaly, (cal-cm^{-2} -^{o}C^{-1}-sec$^{-1/2}$, Kcal-m^{-2} -K^{-1}-sec$^{-1/2}$ or BTU-ft^{-2} -^{o}F^{-1}-hr$^{-1/2}$),

β_d = thermal effusivity of layer below the anomaly (cal-cm^{-2} -^{o}C^{-1}-sec$^{-1/2}$, Kcal-m^{-2} -K^{-1}-sec$^{-1/2}$or BTU-ft^{-2} -^{o}F^{-1}-hr$^{-1/2}$),

c = specific heat (cal- gm^{-1} -^{o}C^{-1} , Kcal- Kg^{-1} –K^{-1} or BTU- lbm^{-1} -^{o}F^{-1}),

d = thickness of layer above the anomaly or anomaly depth (cm, m or ft),

ε = emissivity of the flashed surface,

Δt = flash time (sec or hr),

H = average heat flux incident on the surface (cal-cm^{-2}sec^{-1} , Kcal-m^{-2}sec^{-1} or BTU-ft^{-2}hr^{-1}),

Q = total heat incident on the test object per unit surface area (cal-cm^{-2} , Kcal-m^{-2}or BTU-ft^{-2}),

k = thermal conductivity, (cal- cm^{-1} -^{o}C^{-1} sec^{-1} , Kcal- m^{-1} -K^{-1} sec^{-1} or BTU- ft^{-1} -^{o}F^{-1} hr^{-1}),

ρ = material density (g- cm^{-3} , kg- m^{-3} or lbm- ft^{-3}) and

Γ = thermal mismatch factor at the anomaly (Γ is the Greek letter capital gamma).

The above equation assumes that the surface temperature is affected solely by the diffusion of heat within the test object by conduction. The heat conduction at the center point is assumed to be in a direction normal to the top surface. The flash from the photographic flash lamps is assumed to approximate the instantaneous heat pulse. The anomaly is modeled as contact between two dissimilar layers with a mismatch factor.

Γ = 0, no thermal mismatch factor, no anomaly, perfect contact between layers of same material, transmissive anomaly.

Γ = 1, bottom layer is a perfect conductor or a heat sink, perfect contact with the conductor.

Γ = -1, bottom layer is a perfect insulator, a gapping delamination, no heat transmissivity.

We assume that air is present in the delamination gap causing heat transmission by conduction across the gap. For thin gap delaminations, the delamination gap thickness also factors in the thermal mismatch with values ranging typically between -1 and 0. Similarly, for bridging within a delamination and uneven contact pressure within the delamination, the thermal mismatch values would range from -1 to 0 indicating partial transmission of the heat.

For a thick test object, with no anomaly ($\Gamma = 0$), the above equation simplifies to,

(7a) $$\Delta T(t) = \frac{\varepsilon\, Q}{\beta\sqrt{\pi t}}$$

The above equation implies that the test object continues to cool to its initial temperature indefinitely.

The above equations are not applicable at zero (flash) time and earlier times. The temperature at zero time, which occurs immediately after the flash is given by,

(7b) $$\Delta T_0 = \frac{\varepsilon Q}{\beta\sqrt{\pi \Delta t}}$$

It is difficult to measure the temperature at zero time because it changes very rapidly within the camera measurement period or the instrument response time. There may be variation in the delay between flash trigger with respect to the camera frame trigger causing the camera to measure varying flash response. Some cameras may saturate momentarily due to the high intensity of flash. Therefore, measurements immediately after the flash (1 frame) may have lower repeatability and we would provide options to block or omit use of these frames in the IR Contrast model and data analysis.

Let us start with a large gapping anomaly ($\Gamma = -1$). In this situation, Eq. (1) simplifies to,

(8) $$\Delta T(t) = \frac{\varepsilon\, Q}{\beta\sqrt{\pi t}}\left[1 + 2\sum_{n=1}^{\infty} e^{\left(\frac{-\tau_n}{t}\right)}\right].$$

9. Transit Times

In the IR image video sequence, the anomaly appears at a time related to the normal transit time given by,

(9) $$t_{appear} = l_1 \tau\ , \qquad 0 < l_1 < 1$$

where,

(10) $$\tau = \frac{d^2}{\alpha}.$$

The normal transit time, τ is related to the Fourier Modulus. Intensity of the anomaly indication is strongest at another time called the optimal time (or peak contrast time defined later) and is given by,

(11) $$t_{peak} = l_2 \tau\ , \qquad \text{such that } l_2 > l_1 > 0.$$

The anomaly has a lateral heat flow around the center point. The heat is conducted over the edges of the anomaly to cooler surrounding area and material below the anomaly. Effect of boundary of the anomaly on temperature of the center of the anomaly footprint is influenced by the lateral transit time given by,

(12) $$t_{appear}^{transverse} = l_3 \tau_l \,, \qquad 0< l_3 <1.$$

Where, the lateral transit time τ_l, is given by,

(13) $$\tau_l = \frac{r^2}{\alpha_l} \,.$$

Where, r = radius of the anomaly (cm, ft) and,

α_l = lateral (or transverse) diffusivity which is same as the through thickness diffusivity for isotropic materials. Later on, when we develop the IR Contrast model, we will use a single value for diffusivity that provides an acceptable calibration match. This value is likely to be between the two diffusivities e.g. the normal and the lateral but can be dependent on the depth of the anomaly. The model addresses the difference in diffusivities through calibration constants and limits on the applicability of the model. l_3 is similar to l_1 and is used here conceptually to illustrate that the temperature of the center point is affected by the diffusion transit times to the lower boundary defined by the flaw depth and the edge boundary defined by the radius.

Effect of an anomaly edge (diameter) on the center point temperature will be felt before the effect of depth if $\tau_l < \tau$. The ratio of these two transit times play an important role in relative contribution of the depth and diameter in the peak contrast time of the anomaly. The ratio of the transit times is proportional to the square of the diameter to depth ratio e.g. $\frac{\tau_l}{\tau} \propto \left(\frac{D}{d}\right)^2$.

Let us define three ratios based on dimensional measurements. Gamma is the ratio of diameter of the anomaly (or width of a long anomaly $\varphi \geq 3$, φ is defined in Eq. (14c)) to its depth below the surface,

(14a) $$\gamma = \frac{D}{d} \quad \text{or} \quad \gamma_a = \frac{D_a}{d}$$

In the above equation the subscript $_a$ indicates an apparent value referring to value provided by the analysis rather than the actual measurement. For an anomaly described by depth and diameter, the heat trapping volume is given by $d\,\frac{\pi D^2}{4}$. Let us also define anomaly depth to test object thickness ratio, omega as follows,

(14b) $$\omega = \frac{d}{d_{th}},$$

where, d_{th} = the test object thickness.

We define an aspect ratio φ (phi) of the anomaly length to its width or diameter as

(14c) $$\varphi = \frac{l}{w},$$

where, w = width of the anomaly. For a linear anomaly, the width is defined as the shorter of the two dimensions along the orthogonal axes. l = length of the anomaly. The length is defined as the longer of the two dimensions along the orthogonal axes.

10. Normalized Contrast Definition

Let us define the anomaly temperature contrast as,

(15a) $$\overline{C}^{t} = \frac{\left(T - T^{0}\right) - \left(T_R - T_R^{0}\right)}{\left(T - T^{0}\right) + \left(T_R - T_R^{0}\right)},$$

(15b) $$\overline{C}^{t}_{\%} = \frac{\left(T - T^{0}\right) - \left(T_R - T_R^{0}\right)}{\left(T - T^{0}\right) + \left(T_R - T_R^{0}\right)} \times 100$$

where, $\overline{C}^{t}$ = normalized temperature contrast or modulation temperature contrast. It is a function of time, t. Time is measured from the moment of the flash (e.g. flash time = 0 sec).

$\overline{C}^{t}_{\%}$ = normalized contrast expressed as percentage

T = surface temperature at the measurement point (usually center of the anomaly) (°C, K or °F),

T_R = surface temperature at the reference point (usually outside the anomaly area) footprint,

T^{0} = surface temperature of the measurement point before flash,

T_R^{0} = surface temperature of the reference area before flash.

Equation (15) can be written as,

(16a) $$\overline{C}^{t} = \frac{\Delta T - \Delta T_R}{\Delta T + \Delta T_R},$$

where, $\Delta T = T - T^{0}$ = temperature rise at center of the anomaly at time t,

$\Delta T_R = T_R - T_R^{0}$ = temperature rise at the reference area outside the anomaly at time t.

Thus, the normalized contrast, as defined here, is a measure of the ratio of the difference in temperature rise between the anomaly center point and the reference point and the sum of the two temperature rises. This definition is similar to the definition of signal modulation and the values would range from -1 to +1 in normal situations. In some abnormal situations the values beyond customary range of -1 to +1 are possible and are outside the domain of this analysis. In normal measurement situations, the reference area

is always cooler than the anomaly area. Therefore, the contrast shall always be positive. But in practice, surface heat gradients caused by factors including the proximity of the anomaly to the edge of the flash zone or uneven thickness of the cross section may cause the anomaly to appear cooler at later times compared to the temperature of reference area. The pre-flash surface temperature distribution and emissivity variation also affects the contrast.

Ideally, $T^0 = T_R^0$ and Eq. (15) simplifies to,

(16b) $$\overline{C}^t = \frac{T - T_R}{T + T_R - 2T^0}.$$

The denominator in the contrast definition normalizes the numerator. The contrast changes with the time. The contrast increases rapidly after the flash; reaches its peak value and then slowly diminishes and achieves a more or less constant value. In practice, the contrast should ultimately reach zero when the temperature equalizes in the test object. However, the denominator also becomes very small due low temperature rises increasing noise in the contrast evolution at times beyond the end time defined later. In the above anomaly definition, the measurement area can be considered to be a plate with thickness equal to the anomaly depth and the reference area can be considered to be a plate with infinite thickness. We assumed no heat loss from the test object and no thermal connection between the reference area and anomaly area. Therefore, the contrast would not reach zero but would mostly level out or reach close to a steady state value after certain time.

Most radiometric capable IR cameras are calibrated to measure the surface temperature. These cameras provide a surface temperature map using a color pallet or gray scale. The contrast formula is directly applicable. However, the IR cameras used in the flash thermography set-up may not be calibrated for temperature. These cameras have a linear pixel intensity response with the irradiance or the total radiation incident on the camera detector pixel. In this situation, the total radiation incident on the detector has three main components e.g. emitted radiation from the test object surface, reflected radiation from the object surface and radiation from the air between the test object and the camera. The main component is assumed to be due to emission (due to high test object emissivity). The normalized pixel intensity contrast is defined as follows.

(16c) $$\overline{C}_W^t = \frac{\Delta W - \Delta W_R}{\Delta W + \Delta W_R}$$

Where, $\Delta W_R = W_R - W_R^0$ rise in the pixel intensity at the reference point at time *t*,

$\Delta W = W - W^0$ rise in the pixel intensity at the measurement point at time *t*,

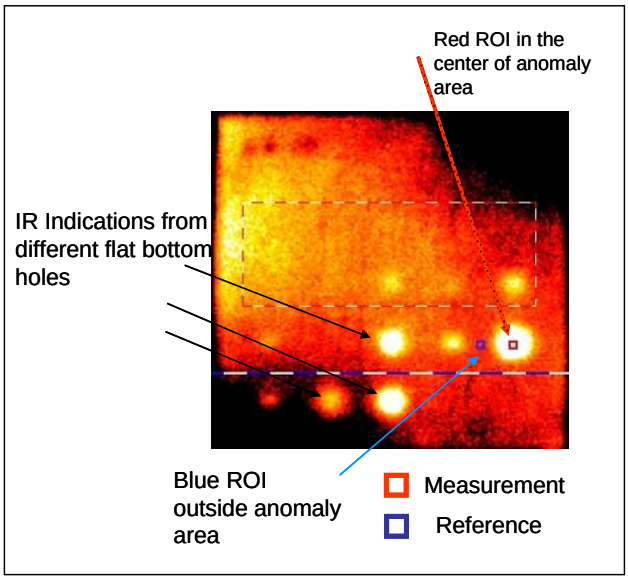

Figure 3: IR Image of Flat Bottom Holes in a Test Piece

Figure 3 provides one of the frames in a sample IR data cube from an RCC sample with flat bottom holes. The measurement and the reference areas are indicated. The area in dotted rectangle is used to adjust the color display or visible contrast.

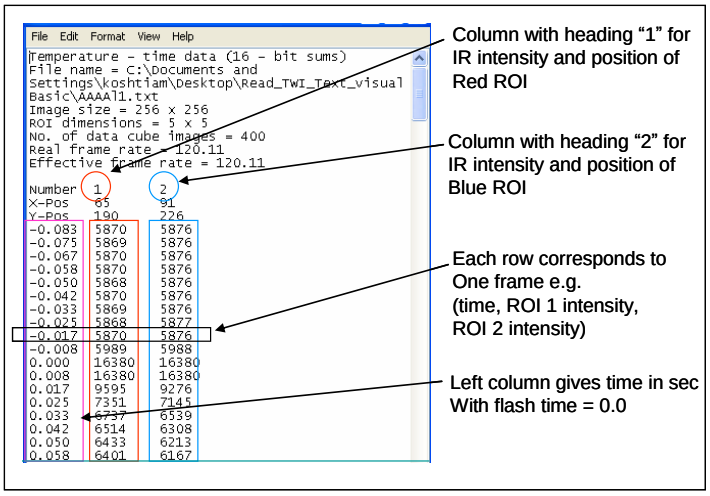

Figure 4: Example of Data File for Single Pair of Measurement and Reference ROI

The pixel intensity registered by the camera due to thermal emissions is approximately proportional to the fourth power of the surface temperature of the object areas imaged in the pixel. However, it is expected that if we apply the contrast definition to the total incident radiation (or pixel intensity), the contrast would be approximately same as the contrast calculated from true surface temperatures (e.g. $\overline{C}^t \cong \overline{C}_W^t$) for high emissivity (>0.95) surfaces. In this paper, we assume that the thermal emissivity (within the range of camera sensing wavelength) is high (>0.8) and constant over surface of the test object

under inspection. Also, we assume that the flash intensity on the object surface, flash duration and the part/camera/hood geometry are kept constant. With these assumptions, we would assume that pixel contrast and temperature contrast are approximately the same. Influence of small variation in the emissivity will be modeled approximately as emissivity factor ratio defined later.

11. Contrast Leveling

The flash time marks the beginning of the contrast evolution where normally it has a zero value. On acreage delaminations, the contrast rises rapidly above zero with time to reach a peak and then slowly decays to zero at long times (t_{tail} defined later). An ideal shape of the contrast evolution is similar to a skewed Gaussian distribution that is skewed to the left. Confidence in the analysis of contrast evolution is higher if the shape of contrast evolution is close to the ideal shape. But factors such as the part curvature, proximity to the part edge, step in the part and uneven flash intensity may cause the contrast evolution to have a non-ideal shape. Some factors cause lateral heat flows that are not related to the anomaly under investigation causing a non-ideal contrast shape. In such situations, it is preferred to extract the contrast evolution with proper choice of measurement and reference region of interest (ROI) such that the shape of the evolution is as close to the ideal shape as possible. Here, a method of artificially leveling or shifting the evolution vertically is provided but it should be used only after validation.

In practice, the contrast may not start at zero. It may dip below zero after reaching the peak and then slowly come back to zero as the temperature equalizes. In this situation, there may be a time period beyond the peak time when it is below zero but leveled out providing a steady value for a considerable time. The steady state contrast is given by.

(17a) $$C^{Steady} = \frac{\Delta T^S - \Delta T_R^S}{\Delta T^S + \Delta T_R^S}$$

(17b) $$C_W^{Steady} = \frac{\Delta W^S - \Delta W_R^S}{\Delta W^S + \Delta W_R^S}$$

The superscript "S" is used to indicate the time when the change in contrast with time is very small. This time is called the steady state time. ΔT^S and ΔT_R^S temperature rises at steady state time at the measurement ROI and the reference ROI respectively. ΔW^S and ΔW_R^S are pixel intensity rises at steady state time at the measurement ROI and the reference ROI respectively.

To achieve leveling of the tail portion (time t_{tail}) of the contrast evolution, we may apply an adjustment to the contrast using the following expression,

(18a) $$\overline{C}^t_{adjusted} = \frac{\Delta T - \Delta T_R}{\Delta T + \Delta T_R} - l_4 \overline{C}^{Steady}. \qquad 0 < l_4 < 1$$

(18b) $$\overline{C}^{t}_{W,adjusted} = \frac{\Delta W - \Delta W_R}{\Delta W + \Delta W_R} - l_4 \overline{C}^{Steady}_{W} \quad . \quad 0 < l_4 < 1$$

If we choose a value of l_4 to be one, this would result in bringing the contrast at the steady state time to zero. Under ideal conditions of flash uniformity and test object geometry, the contrast on the flat-bottom holes is near zero at steady state times. In the analysis, if we shift the contrast evolution curve (l_4 >0), the effect of the shift needs to be studied as it correlates to anomaly characteristics, otherwise it is better not to shift the contrast even if it goes negative. In practice, choosing the reference point closer to the anomaly is advantageous in reducing the negative incursion of the contrast. Uniformity of the flash intensity also helps. The flash intensity is usually most uniform in the center of hood. Locating the anomaly away from the edges of flash boundary also helps. Ideally, one should not apply the contrast adjustment but, rather, mitigate factors that cause the negative incursion and keep the contrast evolution positive so that the model developed here is applicable.

12. Normalized Time and Contrast

Let us define a new variable *t'* (pronounced *t* prime) called the normalized time. This is also known as the Fourier Modulus in heat conduction problems and is dimensionless. It is related to the time by following equation.

(19) $$t' = t / \tau$$

The time ratio in Eq. (1) is written as

(20) $$\frac{\tau_n}{t} = \frac{n^2}{t'}$$

By substituting in Eq. (1) we get,

(21a) $$\Delta T = \left(\frac{\varepsilon Q}{\beta d} \sqrt{\frac{\alpha}{\pi}} \right) \frac{1}{\sqrt{t'}} \left[1 + 2 \sum_{n=1}^{\infty} e^{\left(-\frac{n^2}{t'} \right)} \right]$$

(21b) $$\frac{\Delta T \beta d}{\varepsilon Q} \sqrt{\frac{\pi}{\alpha}} = \frac{1}{\sqrt{t'}} \left[1 + 2 \sum_{n=1}^{\infty} e^{\left(-\frac{n^2}{t'} \right)} \right]$$

Note that the right hand side of Eq. (21b) is only a function of normalized time. Eq. (7a) is rewritten as,

(22) $$\Delta T_R = \left(\frac{\varepsilon Q}{\beta d} \sqrt{\frac{\alpha}{\pi}} \right) \frac{1}{\sqrt{t'}}$$

Substituting Eq. (21a) and (21b) into Eq. (16a) we get,

(23) $$\overline{C}^{t'} = \frac{\sum_{n=1}^{\infty} e^{\left(-\frac{n^2}{t'}\right)}}{1 + \sum_{n=1}^{\infty} e^{\left(-\frac{n^2}{t'}\right)}} \qquad 0 < \overline{C}_N^{t'} < 1$$

The normalized contrast is solely a function of the normalized time. It should always be positive per above equation. The equation implies that the normalized contrast evolution against the normalized time is the same for all isotropic materials and anomaly depths. Therefore, the evolution is called the invariant contrast evolution. The normalized contrast is also considered to be the thermal response of the anomaly. Equation (23) is plotted in Figure 5A and Figure 5B in semi-log and linear form, respectively.

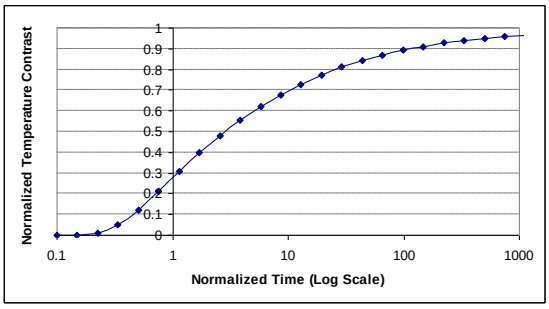

Figure 5A: Approximate Normalized Temperature Contrast in Semi-Log from Eq. (23)

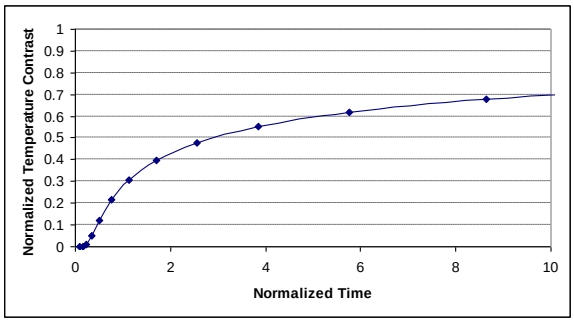

Figure 5B: Approximate Normalized Temperature Contrast in Linear Scale from Eq. (23)

There is an inflection point at t' = 0.5. If we define early detection time (t_{appear}) as 1 percent contrast then it occurs at t' = 0.2 and l_1 = 0.2 per Eq. (9). Here, the normalized contrast keeps increasing with time and is asymptotic to 1. The above contrast evolution is applicable to high values of diameter to depth (D/d ratio γ) ratio. Essentially, the

contrast evolution is drawn from the center points of two plates of the same material. The measurement point is on a plate with thickness equal to the anomaly depth. The reference point is on a plate with infinite thickness. Due to separation of the plates, there is no cross heat flow between the two plates and the two plates cannot reach the same temperature after the flash. While the thinner plate reaches a constant temperature, the thicker slab continues to cool down indefinitely. We can obtain the contrast evolution for any isotropic material with a large FBH-like anomaly by using the above contrast evolution and by simply transforming the normalized time to real time by using Eq. (19). The concept of use of the invariant contrast evolution for prediction of the normalized contrast is developed further to design the IR Contrast prediction model.

As the γ ratio becomes smaller, the lateral heat conduction contributes to the cooling rate and the contrast evolution has a shorter peak. We take the IR video frame sequence data for a specified duration of normalized time (e.g. 2). In practice, the contrast rarely approaches 1, because heat from the trapped volume is dissipated to the surrounding area (cross heat flow) and for delaminations, the heat from the trapped volume is also conducted to material below the delamination through the delamination gap. Peak in the contrast is reached below a contrast value of 1.0 with a subsequent gradual reduction in the contrast to zero due to temperature equalization by the cross anomaly heat flow. At later normalized times, the heat loss mechanisms influence the surface temperature as much as the internal conduction. In practice, the contrast rarely goes above 0.7 on true delaminations if reference area is chosen significantly larger (10 times) than the size of texture (see Section 43) and the measurement area is larger (minimum 2 times) than the texture size.

13. Contrast Prediction Using Reference Contrast Evolution Curve

In order to accommodate lower values of the γ ratio and to apply the contrast evolution curve prediction to a practical situation, we depart from the Eq. (23) invariant contrast evolution curve which is approximate and is only applicable for very high γ ratios. Instead we use a measured contrast evolution curve (normalized contrast versus time) taken on a flat-bottom hole (FBH) in an isotropic material (e.g. 1 inch diameter, 0.05 inch depth, γ_{ref} = 20) to generate a "reference contrast evolution" curve to capture the effects of most factors in contrast measurement. The reference contrast evolution is considered to be a modified instance of the invariant contrast evolution. It is hypothesized that the reference contrast evolution curve would be applicable to a range of γ ratios in the neighborhood of its reference γ value. Figure 6 shows a normalized reference contrast evolution curve. The reference contrast evolution curve is similar to the invariant contrast evolution curve (Figure 5A) in that it is the source to generate the simulated contrast evolution curve but the process also uses calibration and empirical relationships explained later.

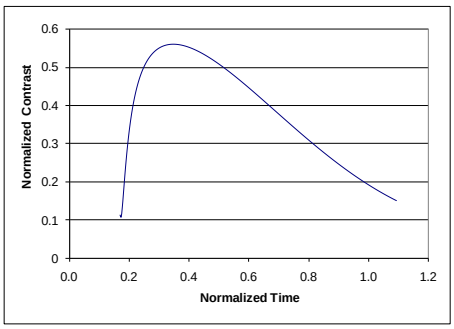

Figure 6: An Example of Normalized Reference Contrast Evolution Curve

In the above example, l_1= 0.2, l_2 = 0.35 per Eq. (9) and Eq. (11) respectively. Here, all material properties are known. The surface emissivity is also known. We transform the actual time to the normalized time to generate the normalized contrast versus normalized time. In order to generate the simulated (predicted) contrast evolution of a flat-bottom hole, we need to know material properties, flat-bottom hole depth and diameter. The normalized time (with known contrast) is transformed to the real-time. Thus, the contrast versus the real-time evolution is obtained. We make many changes to this approach to allow calibration on known contrast evolutions. Here, calibration refers to defining values of certain calibration constants to obtain a better match between the predicted contrast and measured contrast evolutions.

Here, we use the reference normalized contrast (contrast with normalized time) and the ratio γ, and three calibration constants (defined later) to fine tune the predicted contrast evolution within the diameter and depth range validated during calibration. The normalized time expression in Eq. (19) is further modified as follows to accommodate the smaller diameter of the anomaly.

(24a)
$$t' = \frac{C_3\left(e^{\frac{-C_6}{\gamma'}}\right)}{(1-e^{-\frac{\gamma'}{C_1}})}\left(C_d\frac{\alpha t}{d^2}+C_7\right)+C_8$$

Here we define the transformation coefficient C_f to illustrate effects of terms within the above equation.

(24b)
$$t' = C_f\left(C_d\frac{\alpha t}{d^2}+C_7\right)+C_8$$

(24c)
$$C_f = \frac{C_3\left(e^{\frac{-C_6}{\gamma'}}\right)}{(1-e^{-\frac{\gamma'}{C_1}})}$$

To set up calibration based on the diameter, a diameter constant C_D is introduced.

(25a)
$$\gamma' = C_D\gamma$$

(25b) $$D' = C_D D$$

Where, C_D = diameter or width calibration constant. Nominal value is equal to 1,
α = effective diffusivity (cm^2sec^{-1}),
C_f = transformation coefficient.

C_3, C_6, C_7, C_8 are the contrast evolution shape (or profile) constants and are derived empirically.

Here, α is defined as the effective diffusivity or an estimate of effective diffusivity rather than the actual diffusivity. The effective diffusivity refers to a value of diffusivity used in this model that provides an acceptable prediction match after calibration. For isotropic materials, the effective diffusivity is the same as the material diffusivity. For anisotropic materials, it is related to material diffusivity and direction of the heat flow. An appropriate value of effective diffusivity may provide adequate calibration on selected flat bottom holes of a test object.

C_d = depth (or diffusivity) calibration constant. It is assumed to be constant for a given isotropic material within the validated range of flaws. Nominal value is equal to 1.

We provide an expression for the simulated (predicted) contrast evolution as follows,

(26a) $$\overline{C}^{t}_{w,e} = \zeta \varepsilon'' C_A C_5 A_c \overline{C}^{t_{ref}}_{w,ref}$$

(26b) $$\overline{C}^{t}_{T,e} = \zeta C_A C_5 A_c \overline{C}^{t_{ref}}_{T,ref}$$

(27a) $$\varepsilon'' = \frac{\varepsilon'}{\varepsilon'_{std}}$$

(27b) $$\varepsilon' = \frac{\overline{C}^{t}_{w}}{\overline{C}^{t}_{T}}$$

Where, C_5 is the contrast evolution shape (or profile) constant and is derived empirically. ε'' is the emissivity factor ratio used to account for differences in the emissivity between the calibration standard and the test object. ε' is the ratio of normalized pixel intensity contrast to normalized temperature contrast. Higher emissivity or flash power provides higher temperature rise and better signal to noise ratio. Lower emissivity or flash power provides lower temperature rise and lower value of simple contrast. Lower emissivity also reflects more heat. The reflected heat causes the image contrast to decrease due to increase in the denominator of Eq. (16a), (16b) and (16c). The emissivity factor ratio is introduced to approximately account for small change in emissivity or power. The value of emissivity factor is 1 for object emissivity of 1. Usually, the flash power setting is not changed and emissivity of the test article is required to be high (> 0.8) and same as the calibration standard. Under these circumstances, the emissivity factor ratio is assumed to be unchanged with value of one. The emissivity factor ratio is not needed for prediction of the temperature contrast, provided we assume that the part emissivity is uniform.

Here, we start with realtime t (e.g. a frame at 1/60 or 1/120 sec). We transform the realtime to normalized time t' using Eq. (24b). We inverse transform t' to realtime t_{ref} for a reference material flat bottom hole. We read the contrast from the reference curve (Figure 6). The transformation/calculation process steps are given below. The reference contrast evolution may be obtained from a material different from the NDE reference standard. The transformation is indicated by $\rightarrow$ and the calculation is indicated by $\Rightarrow$.

(28) $$t \rightarrow t' \rightarrow t_{ref} \Rightarrow \overline{C}_{w,ref}^{\,t_{ref}}$$

A flaw size parameter (FSP), A_c defined as a function of γ, is given by,

(29) $$A_c = 1 - e^{-\left(\frac{\gamma'^{C9}}{c_4}\right)} \qquad 0 < A_c < 1$$

C_4 and C_9 are contrast evolution shape constants. The flaw size parameter (also called parameter 1) is used for amplitude and diameter calibration. Figure 7 shows plot of flaw size parameter as a function of depth and diameter.

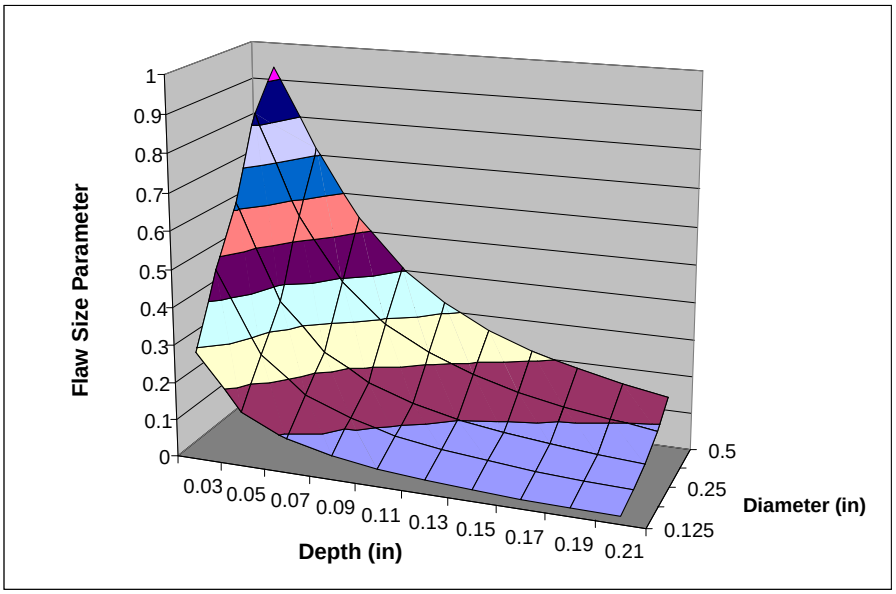

Figure 7: Flaw Size Parameter A_c as a Function of Diameter and Depth

Figure 8 show a plot of the flaw size parameter as a function of gamma. For high values of gamma, the value of flaw size parameter is equal to 1.

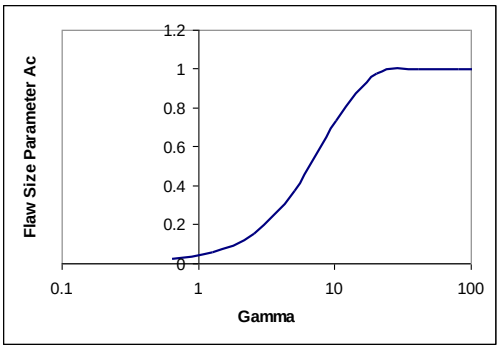

Figure 8: Flaw Size Parameter A_c as Function of Gamma

Figure 9 shows the transformation coefficient C_f as a function of the flaw size parameter A_c. For high values of the flaw size parameter, the value of transformation coefficient C_f is equal to one. The value of transformation coefficient increases with decrease in value of the flaw size parameter.

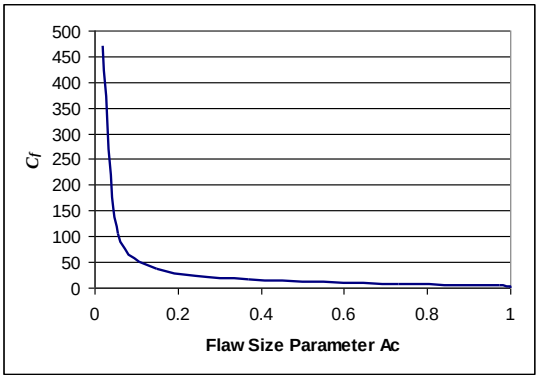

Figure 9: Transformation Coefficient C_f as a Function of Flaw Size Parameter A_c

Inverse of the transformation coefficient is plotted against the flaw size parameter in Figure 10. It indicates that for high values of gamma, the value of transformation coefficient is equal to one.

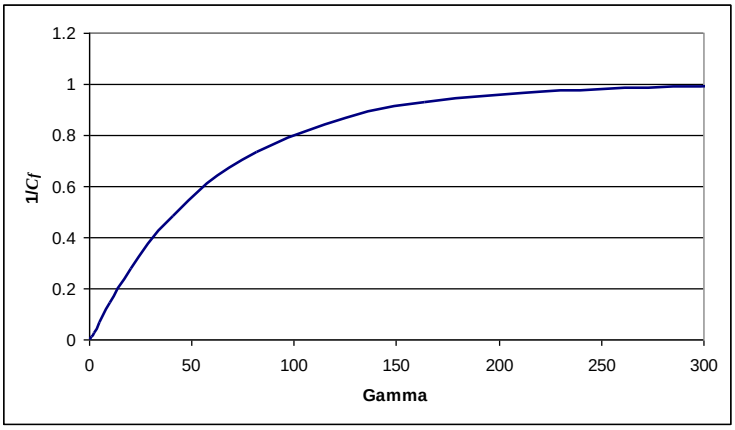

Figure 10: Transformation Coefficient C_f as a Function of Gamma

During the calibration process, the amplitude constant (C_A) and the diameter constant (C_D) are determined by trial and error for the given flat-bottom hole. Many flat-bottom holes are used to establish the calibration/correlation relationship between the FSP and amplitude constant; FSP and the diameter constant. Usually, a curve fit in the calibration data is used to establish these functions. Figure 11 shows example of the diameter constant and amplitude constant calibration curves.

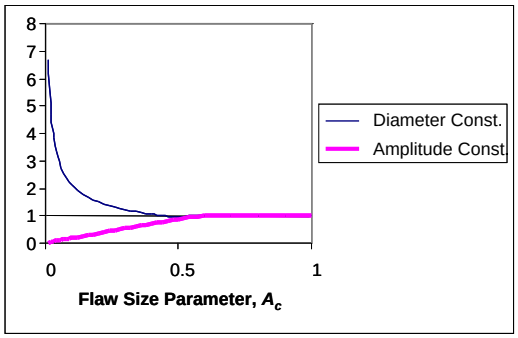

Figure 11: Example of Correlation of Calibration Constants

C_5 is an evolution shape constant based on the values of evolution shape constants C_4 and C_9. C_5 has an effect of normalizing the effect of the FSP.

(30) $$C_5 = \frac{1}{1 - e^{-\left(\frac{20^{C_9}}{C_4}\right)}}$$, here d = 0.05 inch, D = 1.0 inch; and $\gamma' = D/d = 20$

The values of the evolution shape constants are derived empirically. A flow chart explaining the process of the above calibration is provided in Figure 12.

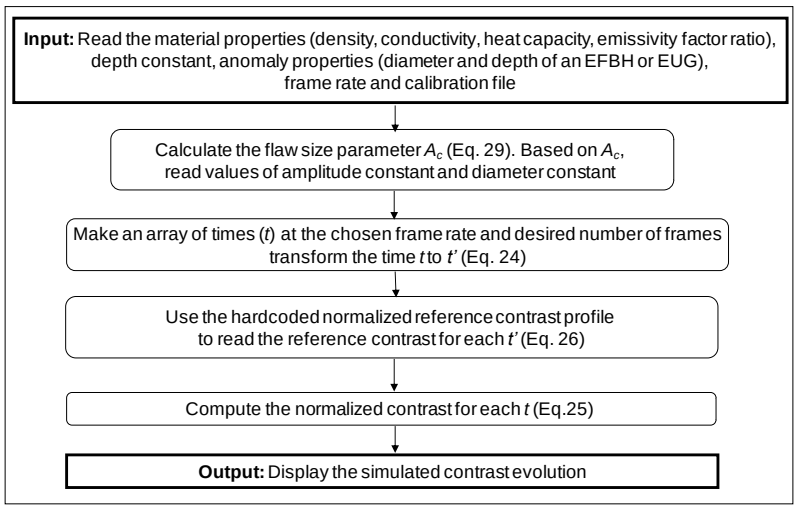

Figure 12: Flowchart for Computation of the Simulated Contrast

Figure 13 shows an example of simulated contrast using the IR Contrast application.

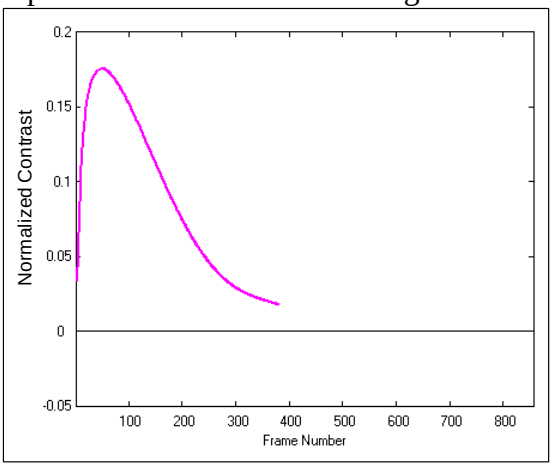

Figure 13: Example of Predicted Contrast Evolution from a Flat Bottom Hole

14. Direct Depth Estimation

Expression for the depth of anomaly can be obtained by manipulating Eq. (24a) as follows.

$$\frac{1}{d^2} = \left(\frac{\left(t' - C_8\right)\left(1 - e^{-\frac{\gamma'}{C_1}}\right)}{C_3\left(e^{\frac{C_6}{\gamma'}}\right)} - C_7 \right) \frac{1}{C_d \alpha t}. \tag{31}$$

If we can estimate γ', the above expression can be used at many t and t' values to estimate the depth. First we need to have the measured contrast data. This would be

typically a two-column array (column 1 provides time or frame number, column 2 provides contrast) with time spacing of 0.017 sec (1/60 of sec based on 60 Hz frame rate). We need to find the peak contrast of the measured data. Here, we define a multiplier, *M* using Eq. (26) as follows,

$$M \equiv \varepsilon'\zeta C_A C_5 A_c = \frac{\overline{C}_{w,a}^{t-peak}}{\overline{C}_{w,ref}^{t'-peak}} = \frac{\overline{C}_{a}^{t-peak}}{0.56}. \tag{32}$$

Here, subscript "$_a$" indicates actual or measured contrast. The denominator (0.56) comes from the peak amplitude of the invariant evolution from Figure 6. Manipulating Eq. (32), we can write an expression for A_c.

$$A_c = \frac{M}{\varepsilon'\zeta A_r C_A C_5}. \tag{33}$$

Manipulating Eq. (29), we can write an expression for γ' as,

$$\gamma' = \left(-\left(\ln\left(1 - A_c\right)\right)C_4\right)^{\frac{1}{C_9}}. \tag{34}$$

Manipulating Eq. (25) we can write an expression for the diameter.

$$D = \frac{\gamma' d}{C_D} \tag{35}$$

We can use Eq. (35) to estimate the equivalent diameter of the flat-bottom hole, if we know all quantities on the right hand side. We cannot use Eq. (34) to estimate γ' until we know the value of A_c. We don't know the value of A_c until we know the value of C_A per Eq. (33). However, an iterative loop can be set up between Eq. (31) through Eq. (35). The starting values for C_D and C_A are their nominal values equal to 1. *M* is calculated using Eq. (32) as a constant for the iterative loop. Equation (33), followed by Eq. (34), is used to provide the value of γ'. Here, we calculate the calibration constant for C_D and C_A as they are functions of A_c. Next we use Eq. (31) to estimate the depth. Use Eq. (35) to estimate the diameter. Estimate A_c again using Eq. (33) with the latest value of amplitude constant C_A and repeat the process until change in the depth estimation in successive iterations is less than a set value. This process is called the direct estimation of the equivalent FBH depth.

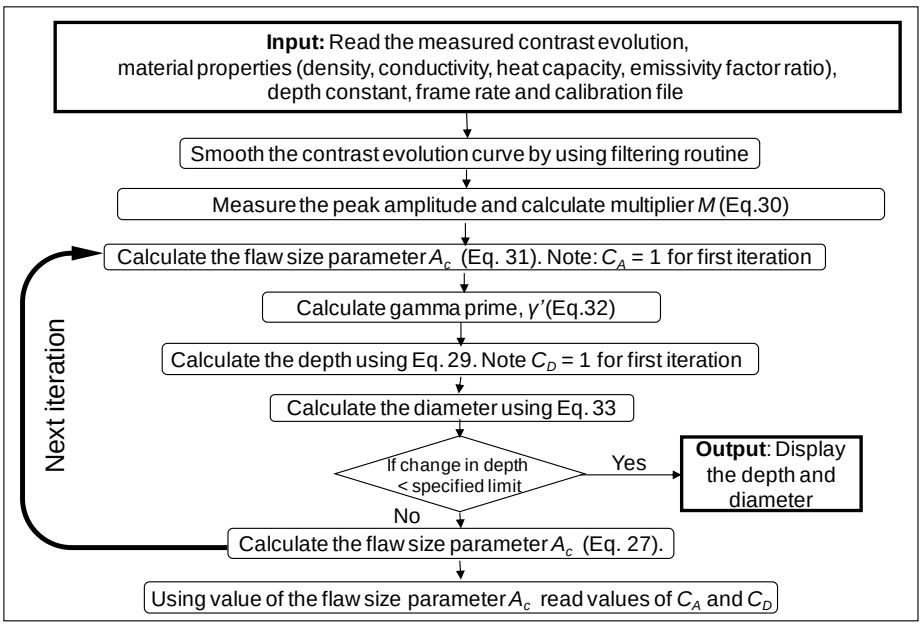

Figure 14: Flowchart for Computation of Direct Depth Estimation

Typically, the depth estimation is done at many points in the measured contrast evolution to improve confidence in the depth estimation. It can be done at the time of peak contrast time (see calculation time 1 input below). The points of interest could be the left 50 percent peak point (see calculation time 2 input). The other points of interest are 50 percent right of peak contrast and 10 percent right of peak contrast. The recommended range is up to t_{50R}. Beyond this time, the influence of lateral heat diffusion processes may be noticeable in the contrast evolution. This may be observed as significant change in the contrast evolution beyond t_{50R} due change in the reference ROI location. An average of these estimations will have a better confidence. An example of the calculation inputs are given below.

Table 1: An Example of Calculation Inputs in Direct Depth Estimation

Calculation #	Measure	Reference time symbol	Reference time, sec	t'	M
1	t_{peak}	t_{peak}^{ref}	0.43	0.211	1.0
2	t_{50L}	t_{50L}^{ref}	0.075	0.169	0.5
3	t_{50R}	t_{50R}^{ref}	1.62	0.349	0.5
4	t_{10R}	t_{10R}^{ref}	2.8	1.315	0.1

15. Commentary on Constants

IR Contrast model uses many constants in Eq. (24a) and Eq. (25a). Equation 24a is the time transformation equation. Therefore, the constants appearing the Eq. (24a) are called the "transformation constants". These include C_1, C_3, C_6, C_7, C_8,C_d and C_D. The constants C_1, C_3, C_6, C_7 and C_8 have fixed values. C_7 and C_8 are used to set the time offset in the transformation. Constants C_1, C_3 and C_6 are used to manipulate effect of γ. The effect of change in γ is not fully accounted for by these internal constants especially for the lower γ values. The effect of change in γ on the shape of the contrast evolution curve (e.g. amplitude, peak time etc.) may need to be adjusted or calibrated for change in the in diffusivity from material to material due to change in anisotropy and layer thickness. Therefore, an external constant C_D as a multiplier to γ is introduced. This constant is calibrated to capture the behavior of measured contrast on a given material and therefore considered as one of the calibration constants. Since C_D multiplies to γ, it is also called the "diameter constant". The effect of change in C_D is more complex. It changes both the amplitude and the peak time (or time scale) of the contrast evolution and change in estimation of EFBH diameter.

External constant C_d is used as a multiplier to diffusivity. Change in C_d causes the change in the time scale or the shape of the profile but the peak amplitude is not affected. The constant is used to choose or calibrate to effective diffusivity of the material and can be determined by matching simulated contrast evolutions to measured contrast evolutions of FBH with known diameter and depth. It multiplies to the depth ($1/d^2$). Therefore, it is also called the depth constant. Since, C_d also multiplies to diffusivity, it can also be called the diffusivity calibration constant. The effect of change in diffusivity in analyzing a given contrast data results in change in time scale and depth estimation of the anomaly. The calibration process is intended to minimize errors due to small differences between the actual diffusivity and the effective diffusivity.

Equation (26) involves additional constants. These are C_A, A_c and C_5. These quantities only have effect of changing the amplitude of the contrast (amplification of Y-scale) and have no effect on the time. Therefore, C_A and C_5 are called the "amplitude constants". C_5 has a fixed value.

Flaw size parameter A_c is not a constant. A_c is a function of γ. Internal constants C_4 and C_9 are used in computation of A_c. The effect of change in γ on the contrast amplitude is not fully accounted for by A_c.

Also, effect of γ on amplitude may need adjustment or calibration for the change in diffusivity from material to material. Therefore, an external constant C_A, used as a multiplier to A_c, is introduced. This constant is calibrated to capture the behavior of measured contrast amplitude and therefore is considered as one of the calibration constants. The effect of C_A is to change amplitude without affecting the time scale. Therefore, C_A is called the amplitude calibration constant.

Constants C_1 through C_9 are internal constants with fixed values. These are not visible to the user. They are used in time transformation as well as computation of the contrast amplitude. Internal constants are not part of the calibration constants.

The IR Contrast uses three external constants for calibration. These are C_A, C_D and C_d. The calibration constants capture effect of variation in γ or the flaw size parameter (A_c) on the contrast evolution. Therefore, calibration profiles of C_A and C_D, as functions of A_c, are established. The nominal value for the constants is one and usually for high values of the A_c (> 0.5) the corresponding values of C_A and C_D are expected be close to the nominal value of 1.

A typical calibration process for isotropic material involves use of various acreage FBH's in the subject material providing the A_c values from 0.01 to at least 0.5. An optimized contrast evolution is obtained on each of the flat bottom holes. Each contrast evolution is analyzed separately starting with the highest A_c ($\geq$ 0.5) values. The data contrast evolution is displayed in the IR Contrast application and a simulation contrast evolution is generated by choosing inputs for (material, emissivity factor ratio, FBH depth and FBH diameter and depth constant = 1, diameter constant = 1, amplitude constant =1). The process of matching simulation would reveal any changes needed in the depth constant. The exercise is repeated on contrast data from many high flaw size parameter value holes and a value of depth constant providing the best match on the contrast evolution curve is determined. Once the depth constant has been determined, contrast evolution curves with lower flaw size parameter values are analyzed with the calibrated (fixed) depth constant. The analysis involves matching the simulation with measured contrast by using following inputs. Use actual FBH depth and actual FBH diameter and depth constant as determined above. In addition, diameter constant and amplitude constant are adjusted in an iterative manner to provide a best match of the simulation. The best match values of the diameter and amplitude calibration constants are plotted against the respective flaw size parameter value. Curves fitted through the plotted data are called the calibration curves. The amplitude and the diameter constant curves diverge with reduction in the flaw size parameter value.

The emissivity factor ratio ε'' is normally set to 1 during calibration instead of choosing the actual value for emissivity. Normally, it is impractical to assess emissivity at the measurement region. It is assumed that the emissivity is high and uniform over the test object surface. Thus, the emissivity factor ratio can be set to one during calibration.

Similarly, amplitude ratio ζ explained later is set to 1 during calibration on the FBH's. The emissivity factor ratio and the amplitude ratio have identical effect on the contrast prediction.

The IR Contrast simulation assumes that the flaws are located at a shallow depth compared to the part thickness. It also assumes that the part thickness is considered to be very thick (>> threshold thickness[7]).

16. Indirect Depth and Diameter Estimation and Simulation Match to Measured Contrast Evolution

Even if we use the average of four points to find a better match of simulation contrast with the measured contrast, it is not likely to provide the optimum solution due to differences between the shape of the simulated contrast evolution and the measured contrast evolution. The direct depth estimation may provide a solution very close to the optimum solution. Thus, the direct depth estimation is considered to be the starting point for a more accurate depth estimation using the following method.

The second method of estimating depth is based on scanning possible values of depth and diameter. An array of "I" depth values and an array of "J" diameter values is defined. Both I and J are natural numbers. The direct estimation of depth and diameter are captured in these arrays possibly as the center values. This results in I times J diameter and depth pairs. We calculate the simulation contrast for one depth-diameter pair at a time and calculate simulation match or fit index "delta square" from the measured contrast using the following expression.

$$\Delta\overline{C_w}^2 = \sum_{n=ns}^{nf}\left(\overline{C}_{w,e} - \overline{C}_{w,a}\right)^2 . \tag{36}$$

Fit index, "delta square average" is calculated using the following expression.

$$\Delta\overline{C}^2_{w,av} = \frac{\sum_{n=ns}^{nf}\left(\overline{C}_{w,e} - \overline{C}_{w,a}\right)^2}{nf - ns + 1} \tag{37}$$

Fit index "percent delta square" is calculated using the following expression.

$$\Delta\overline{C}^2_{w,\%} = 100\frac{\sum_{n=ns}^{nf}\left(\overline{C}_{w,e} - \overline{C}_{w,a}\right)^2}{\sum_{n=ns}^{nf}\left(\overline{C}_{w,a}\right)^2} \tag{38}$$

where, *ns* and *nf* are the starting and the ending frame numbers. Typically, the range may span from a frame at left 50 percent peak contrast to a frame at right 10 percent peak contrast. The delta square, Eq. (36), is calculated for all depth/diameter pairs and the minimum of all delta squares is sorted out. The diameter-depth input providing the minimum delta square is the best possible match within the selected range of frames. Equation 37 provides the average difference (difference square per frame) as an indicator of the fit between the simulation and the measured data. The method of array search is called the "scan fit" here. When the array is constructed around the direct depth estimation solution, then the method is termed as the "search fit". Equation 38 provides percent difference between the simulation and the measured data.

17. Signal Smoothing

The raw contrast data contains the camera pixel noise. The signal can be filtered by a signal processing routine to improve the IR Contrast calculations. The filtered contrast is

shown in red and the raw contrast is shown in black in Figure 15. Detection of frames that provide the peak contrast, left 50 percent of peak frame etc. is affected by the noise incursion in the selected frame. Signal smoothing using signal processing filters (e.g. low pass FFT) helps to locate the above frames more precisely. Also, the delta square calculation is affected somewhat by the noise. Therefore, it is advisable to perform the delta square calculation on the smoothed (or smooth) data.

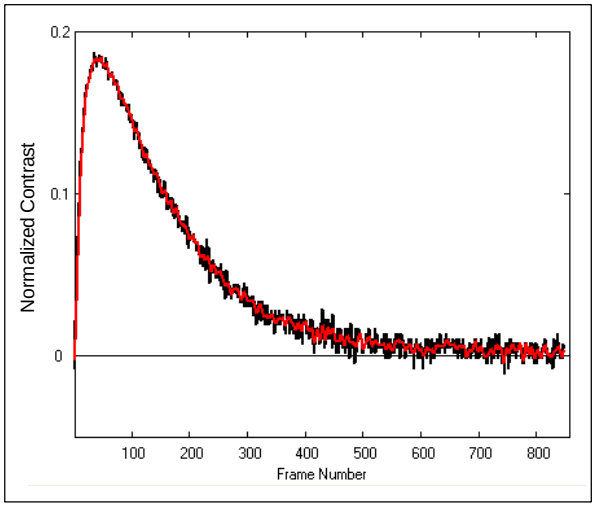

Figure 15: Example of Filtered Contrast Evolution (in Red) from a Flat Bottom Hole

A smoothing index is defined as a sum of square of difference between the raw (unfiltered) contrast evolution and the filtered contrast evolution using the following equation which is similar to Eq. (36). The smoothing index, "delta square" is calculated using the following expression.

$$\Delta\overline{C}_w^{2-f} = \sum_{n=ns1}^{nf1}\left(\overline{C}_{w,af} - \overline{C}_{w,a}\right)^2 \tag{39}$$

The smoothing index, "delta square average" is calculated using the following expression.

$$\Delta\overline{C}_{w,av}^{2-f} = \frac{\sum_{n=ns1}^{nf1}\left(\overline{C}_{w,af} - \overline{C}_{w,a}\right)^2}{nf1 - ns1 + 1}. \tag{40}$$

The smoothing index "percent delta square" is calculated using the following expression.

$$\Delta\overline{C}_{w,\%}^{2-f} = 100\frac{\sum_{n=ns1}^{nf1}\left(\overline{C}_{w,af} - \overline{C}_{w,a}\right)^2}{\sum_{n=ns1}^{nf1}\left(\overline{C}_{w,a}\right)^2}. \tag{41}$$

where, *ns1* and *nf1* are the starting and ending frame numbers used in this calculation. Subscript "*af*" is used to indicate the filtered or smooth contrast evolution. Lower values of the smoothing index imply a better match but not necessarily better smoothing which is controlled by the degree of smoothing input. If we start from a highly low-pass-filtered

(low-pass frequency *f*) signal and decrease the filtering, (i.e. increase *f*), we would decrease the delta square values. The derivative of slope, $\left|\frac{d^2\Delta\overline{C}_w^{2-f}}{df^2}\right|$ decreases to zero with low-pass frequency. The slope $\left|\frac{d\Delta\overline{C}_w^{2-f}}{df}\right|$ reduces with low-pass frequency and at one point no significant reduction in the delta square is observed at the cost of increasing the low-pass frequency. Therefore, we choose a compromise between the degree of smoothing and the smoothing index as the optimized smoothing solution. If a consistent degree of filtering (filter type and setting) is used, then, Eq. (41) can be viewed as a measure of noise-to-signal ratio. The measured noise-to-signal ratio is higher than this estimation as the filtered signal is not completely smooth similar to the predicted evolution.

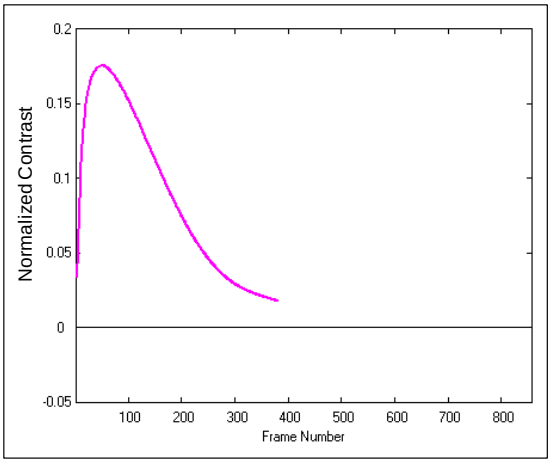

Figure 16: Example of Predicted Contrast Evolution from a Flat Bottom Hole

Figure 16 shows the predicted contrast curve that provides the best match to the measured contrast evolution. The EFBH depth and diameter input to the simulation providing the best match to measured contrast data is obtained in an automated way. The IR Contrast application calculates the approximate depth and diameter of the EFBH directly based on the peak contrast, peak contrast time and other times including t_{50L}, t_{50R} and t_{10R} (see section 19). The simulation matching provides an indirect method of assessing the EFBH depth and diameter. Figure 17 shows the measured raw contrast (in black), filtered contrast (in red) and the simulation (predicted) contrast (in purple) evolutions plotted on the same graph.

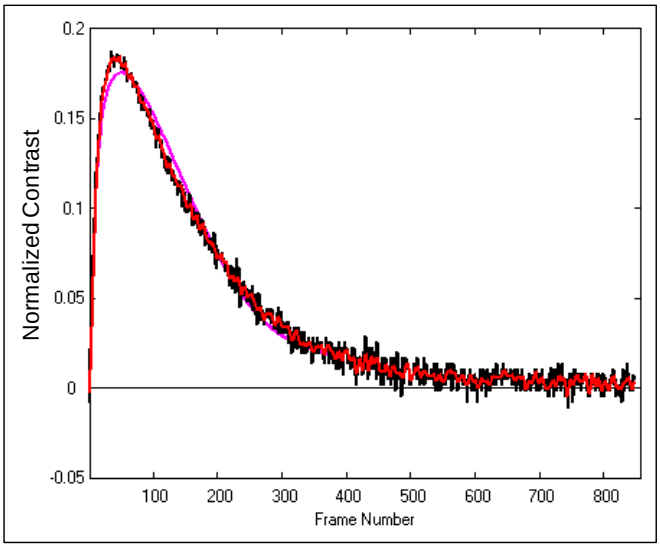

Figure 17: Three Contrast Evolutions (Raw, Filtered and Predicted) Overlaid for Comparison

18. Contrast and Feature Imaging

A separate contrast imaging application is written to work with EchoTherm. The application allows choosing the reference area and then converts the raw data cube into the contrast data cube using the reference area. The temperature versus time profile of each pixel is replaced by the normalized contrast versus time evolution. The contrast data cube images look similar to the raw data cube images. Figure 18 shows a frame from a raw data cube with temperature versus time curves at selected regions of interest (ROI's). Here, all pixels are used as the measurement pixels. Thus, the pixels within the reference ROI would have a contrast value of zero or close to zero.

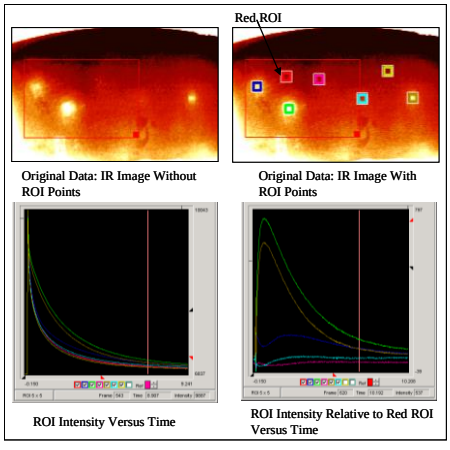

Figure 18: Unprocessed Data Cube

The red ROI is chosen as the reference area for conversion to the contrast data cube. Figure 19 shows a frame from the contrast data cube with the contrast versus time curves

at selected ROI's. The contrast data cube allows a quick view of the contrast evolution and forms the basis for feature images based on signal processing (e.g. filtering) and the thermal measurements (e.g. peak time) defined below.

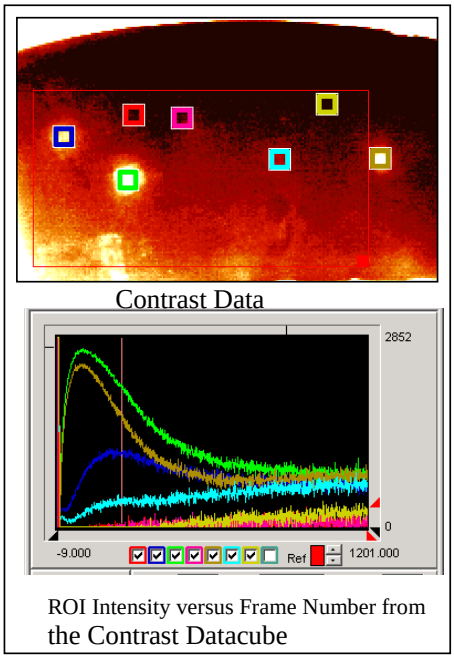

Figure 19: IR Contrast Processed Data Cube

19. Thermal Measurements on the Contrast Evolution

The contrast evolution on a FBH has a shape close to the ideal shape of the contrast evolution. The ideal shape is similar to a skewed statistical distribution. Therefore, measurements based on the ideal shape of the evolution are possible. The shape of contrast evolution is affected by two pixel intensity decay curves e.g. the pixel intensity decay at the measurement ROI and the pixel intensity decay at the reference ROI. Figure 20 shows the measurement (in red) and reference (in blue) ROI decay curves plotted in log time. In Figure 20, the reference pixel intensity versus log of decay time is more or less linear until about frame 248. After this frame the curve turns and becomes horizontal. The bend in the curve signifies the effect of heat reaching to the lower surface and affecting the heat diffusion from the reference ROI. For isotropic materials the pixel intensity log decay is linear until equilibrium temperature (t_{tail}, defined in this section) is reached. In the normalized contrast definition, it is assumed that the reference decay curve with log of time is linear. The reference decay curve is dictated by the heat diffusion or diffusivity in normal direction.

Apart from using the simulation contrast, we can perform thermal feature measurements on the IR Contrast evolution. Explanation of each measurement terminology follows.

Peak Contrast, $\overline{C}_{w,a}^{t-peak}$: Peak contrast is defined as the "amplitude" or value of the highest point in the contrast evolution curve. It may also be referred to as the peak amplitude or contrast amplitude. See Figure 21. This is a very important quantity. The peak contrast is related primarily to the dominant feature of the anomaly. When surface texture (not like delamination) is present, it provides its own peaks which may be superimposed on the peak caused by the sub-surface anomaly. The surface texture indications occur at earlier times and the subsurface delamination indications at later times depending upon the depth. The peak in contrast is reached at later times if surface texture indications are not present. However, the texture indications may provide significant contrast at earlier times and may advance the resultant peak contrast time. Thus, it is advisable to use peak contrast as a measure of the resultant of the surface and subsurface anomaly.

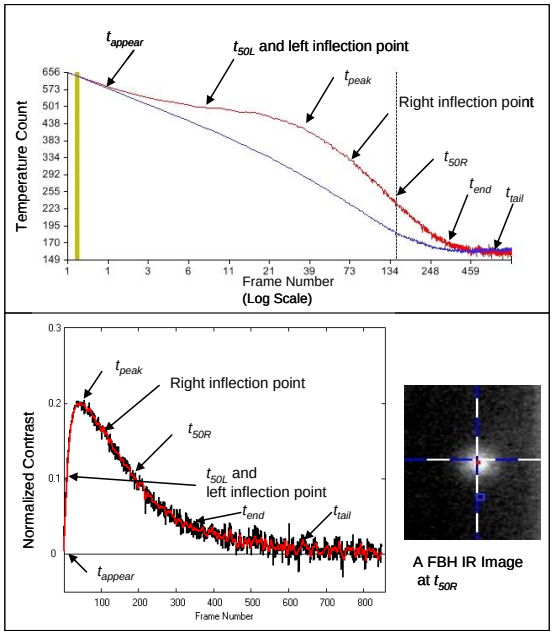

Figure 20: Temperature Count and Contrast Evolution

Peak Contrast Time (sec), t_{peak}: Peak contrast time is defined as the time (flash time = 0 sec) at which the peak in contrast occurs. The peak contrast time is influenced by the superimposition of effects of the surface/near surface texture and sub-surface anomaly. The two material conditions may provide either a single merged peak or two distinct peaks in the contrast evolution. It is assumed that the peak contrast and peak contrast time represent the dominant of the two effects if the subsurface peak is expected to occur at later time compared to the texture peak.

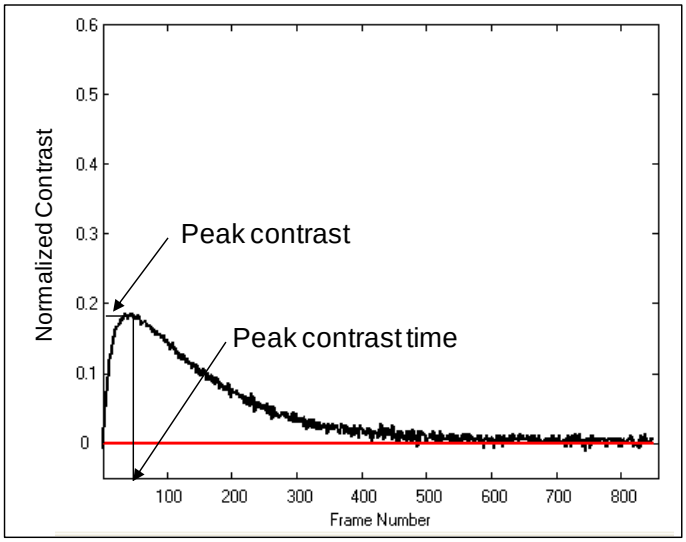

Figure 21: Example of Raw Contrast Evolution (in Black) from a Flat Bottom Hole

50 Percent Left of Peak Time (Sec), t_{50L}: This is the time (flash time = 0 sec) at which the 50 percent of the peak contrast occurs before the peak contrast time. The contrast evolution before t_{50L} may be useful if the surface/texture anomalies are needed to be analyzed. The IR indications of the surface anomalies are sharpest after the flash and diffuse away with time. Depending upon the location and size of the measurement ROI with respect to the texture indication and the severity of the texture effect, the contrast evolution shows variation in early times ($< t_{50L}$)after flash.

50 Percent Right of Peak Time, t_{50R}: This is a time (flash time = 0 sec) at which the 50 percent of peak contrast occurs after the peak contrast time. The contrast evolution beyond this time is significantly influenced by slow diffusion and cooling processes. The lateral heat diffusion, if present, can affect contrast noticeably between the t_{50R} and t_{end}. Therefore, portion of contrast evolution between t_{50L} and t_{50R} is recommended to be used for comparison with the simulated contrast evolution in evaluation of subsurface delaminations.

10 Percent Right of Peak Time, t_{10R}: This is a time (flash time = 0 sec) at which the 10 percent of peak contrast occurs after the peak contrast time.

End Time, t_{end}: The time corresponding frame *ns* in calculation of the delta square.

(42A) $$t_{end} = 2t_{50R} - t_{peak}$$

Another time used in leveling of the contrast signal or in optimizing location of the reference point is the tail time. The IR Contrast model assumes that the contrast value is nearly zero at t_{tail} time.

(42B) $$t_{tail} = 3t_{50R} - 2t_{peak}$$

50 percent Persistence Time, $t_{50L\text{-}50R}$: The time between 50 percent left of peak time and 50 percent right of peak time

(43) $$t_{50L-50R} = t_{50R} - t_{50L}$$

The times defining the persistence can be different (e.g. $t_{50L\text{-}10R}$).

Withholding Heat Time (sec):

(44) $$W_{50\text{-}50} = \overline{C}_{w,a}^{t-peak} t_{50L-50R},$$

Withholding heat time is a measure of area under the contrast evolution curve.

Persistence Energy Time (sec):

(45) $$E_{50L-50R} = \frac{\sum_{n_{50L}}^{n_{50R}} \overline{C}_{w,a}}{v},$$

where, v = the frame rate in frames/sec (Hz). n_{50L} and n_{50R} are the frame numbers corresponding to times. t_{50L} and t_{50R} respectively. These frame numbers could be different as chosen by the user (e.g. n_{50L} and n_{10R}). Both, the persistence energy time and the withholding heat time are related to the heat trapping volume or the depth and diameter of the anomaly.

The adjusted flaw size parameter (also known as flaw size parameter 2) is given by,

(46) $$A_{cA} = C_A A_c,$$

The adjusted FSP relates to the peak contrast per Eq. (26) and is illustrated in Figure 22.

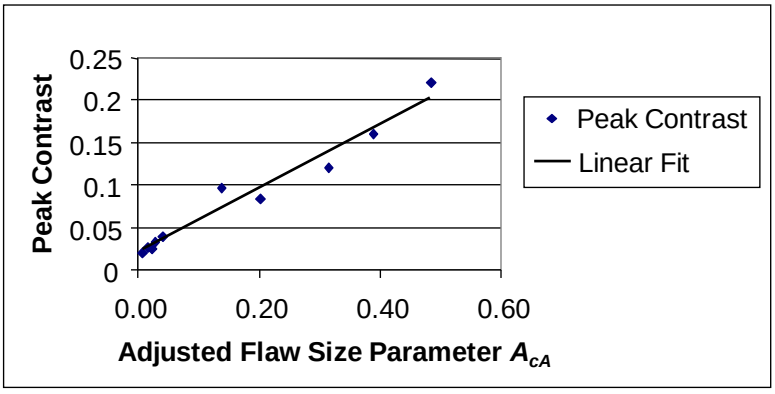

Figure 22: Use of Adjusted Flaw Size Parameter in Prediction of Peak Contrast

Persistence energy time, withholding heat time and peak contrast are measures of signal strength. FSP and adjusted FSP are measures of anomaly size. Therefore, these measurements are candidates for conventional probability of detection (POD) analysis where signal response to flaw size data is analyzed. Although, FSP and adjusted FSP are internal to the IR Contrast model, their values are displayed as they play an important role in demonstrating correlation between the anomaly size and the IR Contrast thermal measurements and FBH predictions and form the basis for POD analysis.

The product of peak time and persistence time provides a correlation to the product of depth and diameter. The withholding heat time and persistence energy time capture the strength of the IR indication to draw your attention for further analysis including the half-max width and the equivalent flat bottom hole analysis. Shallow anomalies have shorter persistence but higher amplitude. Deeper indications have lower amplitude. Wider indications have longer persistence. The persistence energy time captures the portion of evolution containing the peak of the contrast.

20. Contrast Evolution and Heat Flows

The contrast is zero until time t_{appear}. The rise time (= $t_{peak} - t_{appear}$) is much shorter than the decay time (= $t_{10R} - t_{peak}$). There is an inflection point in between the t_{peak} and t_{appear}. Also, there is an inflection point between t_{peak} and $t_{50R.}$ Different temperature gradients and heat flows exist in different time zones of the contrast evolutions of the FBH. Consider a FBH with a high γ value. For a post-flash time less than t_{50L}, the normal heat flow dominates and is therefore related more to the depth of the anomaly. The normal heat flow is highest immediately after the flash and reduces rapidly until time t_{50L}. The lateral heat flow is negligible immediately after the flash till the early detection time (t_{appear}). Therefore, the early detection time strongly relates to the depth but not to the diameter. Unfortunately, it is a bit cumbersome to locate the early detection time due the low contrast amplitude.

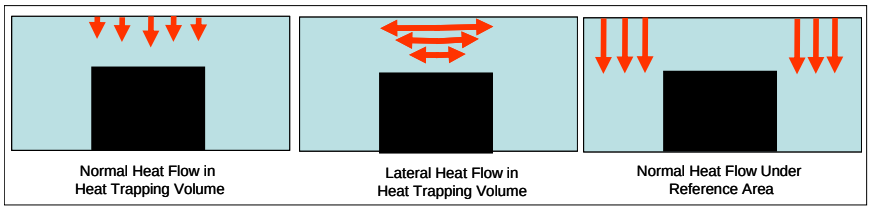

Figure 23: Directions of Heat Flow

As the normal heat flow reduces, the lateral heat flow increases in the trapped volume with time. Thus, the heat flow direction changes from vertical to a near lateral in the heat trapping volume. The lateral heat flow causes "spilling" of the heat from the boundary of the heat trapping volume into the surrounding volume. The normal conduction is dominant in the surrounding area for the period of the significant contrast (i.e. till t_{tail}). Here we assume a small value for ω so that the heat transit time to back surface is much longer than the heat transit time to the anomaly or the lateral transit times. Between time t_{50L} and the t_{peak}, the normal heat flow reduces significantly and the lateral heat flow

builds up in the trapped volume. The time t_{50L} is very close to the inflection point in the contrast evolution, a time at which the normal temperature gradient in the heat trapping volume becomes very low and the contrast continues to rise due to outpacing of the cooling in the surrounding area compared to the lateral heat flow (spilling). The inflection point near the t_{50L} signifies transition from dominant normal heat flow in the trapped volume to the dominant lateral heat flow and the resulting heat flow across the boundary of the heat trapping volume. This observation can be demonstrated by examining the contrast evolutions of FBH (or voids) with same characteristics but different widths (or diameters). Thus, t_{50L} is related to both depth and diameter of the anomaly. During the time period from t_{50L} to t_{peak}, the surrounding area cools faster than the anomaly area. A larger diameter anomaly has a longer peak time. The peak time signifies the maximum in the lateral heat flow across the boundary of the trapped volume. The peak time is related to both the depth and diameter.

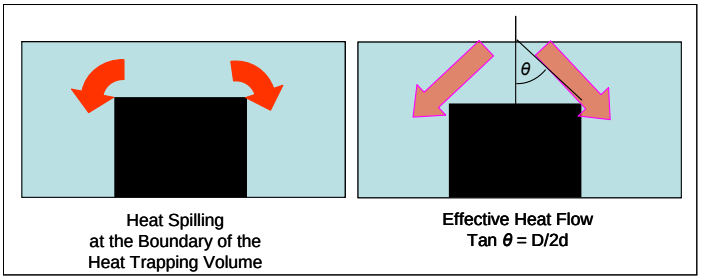

Figure 24: Heat Flow Around the Edge of a FBH

Beyond the peak time, the trapped volume continues to cool faster than the surrounding area. The lateral heat flow continues to reduce gradually from the peak time until the contrast reaches a zero value. The lateral heat flow in the trapped volume dominates in the post peak time zone. The lateral heat flow is not only affected by the depth of the anomaly but also by the lateral transit time or the diameter of the anomaly. The t_{50R} is also related to the anomaly width. The second inflection point may appear before or after the time t_{50R} depending upon anomaly parameters. The second inflection point in the contrast evolution indicates transition from rapid cooling to slower cooling across the boundary of the trapped volume.

To understand the overall direction of heat flow from the measurement point, a term called the "effective heat flow" is introduced. The effective heat flow direction can be approximated as from the anomaly center point on the surface to the closest inner corner of the FBH. The tangent of this angle is given by $\gamma/2$. The diffusivity in this direction can be called as an estimate of "the effective diffusivity" for the FBH. It is assumed that the effective diffusivity and the transit time from the center of the anomaly to the closest inner corner of the FBH have a controlling effect in influencing the contrast evolution. The contrast prediction model uses γ, which defines the direction of effective heat flow, to set-up the calibration. At any moment, the heat flow direction is different in different areas around the anomaly. For an anisotropic material, the diffusivity is different in different directions. For anisotropic materials the diffusivity may also be different at different locations. Thus, in reality, the heat flows that influence the contrast evolution

may be subject to varying diffusivity and direction with time. The IR Contrast model assumes that the normal and lateral diffusivities do not differ significantly and can be approximated in a single value of effective diffusivity. Although, some variation in effective diffusivity with anomaly depth has been accommodated in the model.

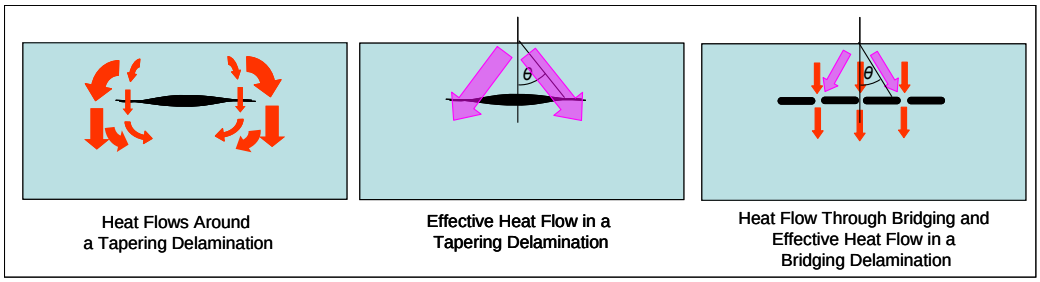

Figure 25: Heat Flows Through a Tapering Delamination and a Bridging Delamination

True delaminations are different from the flat bottom holes. Unlike in the FBH, the heat flows behind the delamination. Moreover, the gap between the two faces of the delamination may vary from the center towards the edge. The gap may be largest in the center. From the center of delamination to the edge, the gap may taper off to intermittent contact/gap and finally to zero gap or continuous material. The intermittent contact close to edge provides a path for heat conduction. Both, the heat conduction through the edge and the heat conduction behind the delamination cause change in the direction of the effective heat flow, changing the contrast evolution and the IR Contrast prediction. In some cases, the delamination may have varying degree of intermittent contact resulting in positive heat transmissivity (defined later). The degree of bridging affects the contrast evolution and the contrast prediction.

21. IR Contrast Application

Figure 26 shows the main interface window of the IR Contrast application with the three contrast evolutions. Differences between the measured data and the simulation are calculated and are indicated in the lower right of the application window. Numbers in black are based on the calculations on the raw contrast evolution curve. Numbers in red are based on the calculations on the filtered contrast evolution curve. Numbers in purple relate to the predicted contrast evolution curve.

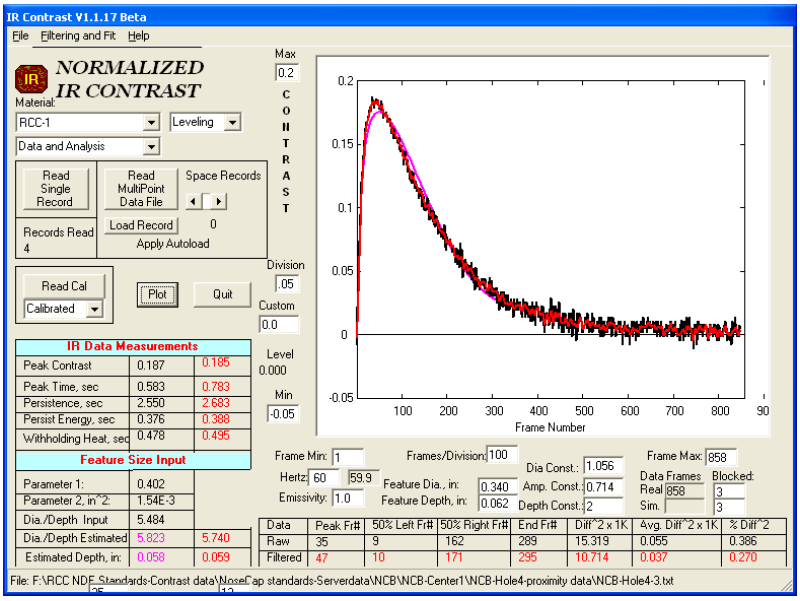

Figure 26: Main Interface for IR Contrast Application with the Three Evolutions

Figure 27 shows the filtering panel used in the IR Contrast application. It provides various filtering options and provides the values of the filtering indices. Also see section 17.

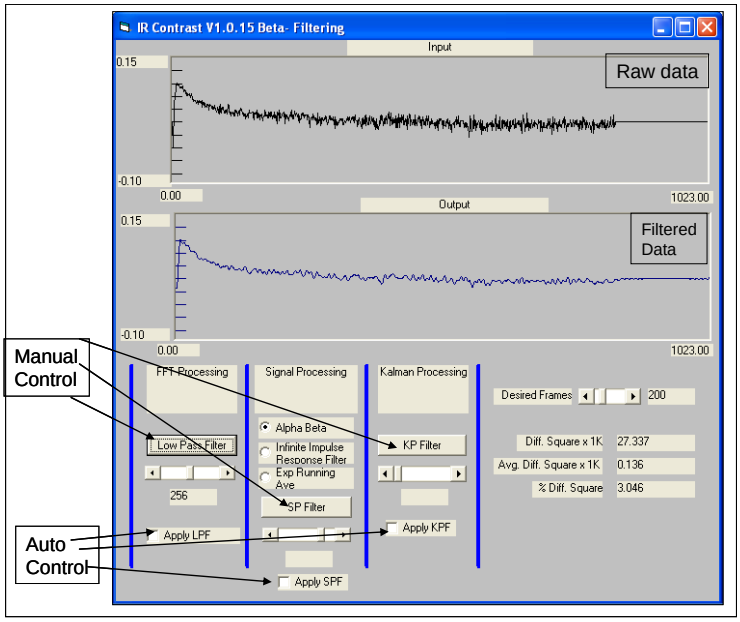

Figure 27: Signal Processing Panel

Figure 28 shows the simulation fit panel. It provides many simulation fit options including the automatic fit. Also see section 16.

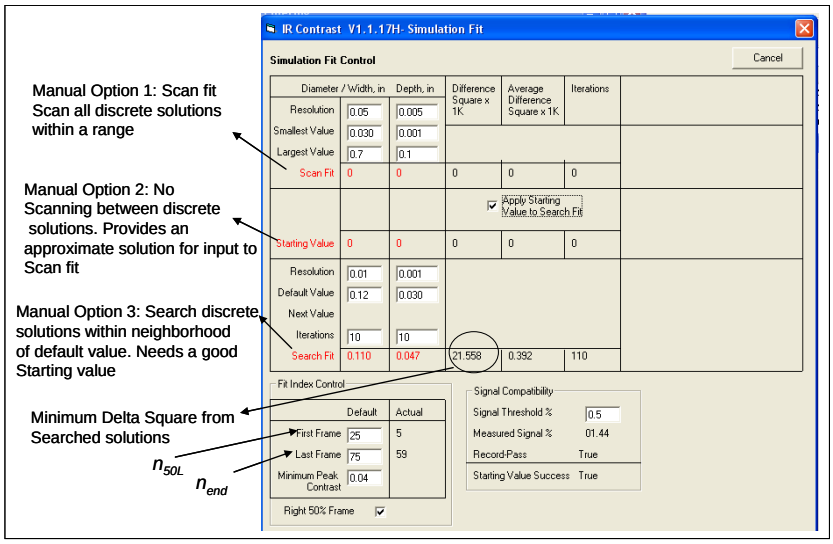

Figure 28: Simulation Fit Panel

Figure 29 shows the calibration panel for calibrating and setting up amplitude factor and depth constant as a function of anomaly depth (see section 38).

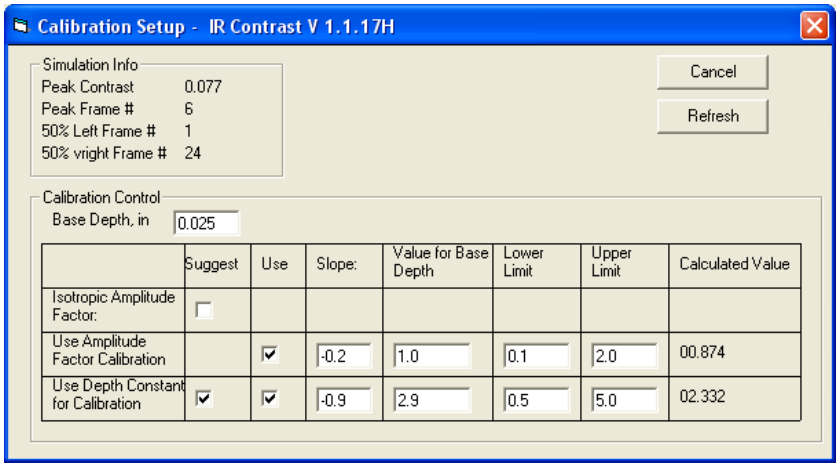

Figure 29: Calibration Panel

22. Half-max Width Measurement and Edge Detection

Width of indications, denoted by w_{hm}, can be directly measured from the IR data by choosing an appropriate frame. The technique assumes that the delamination gap thickness is uniform. Pixel intensities along a scan line drawn across the linear indication or through the center of a circular indication are plotted against the pixel position. For a randomly oriented indication boundary, a scan line is established normal the boundary and the technique is used for the edge detection. Maximum intensity pixel coordinate and its intensity are noted. Similarly, pixel coordinate and intensity of baseline level at left of the maximum intensity pixel and to the right of the maximum intensity pixel are noted.

The average of intensity of the maximum value and the base level value is used as the 50 percent intensity level. Then two pixel coordinates, one at left 50 percent of intensity and the other at right 50 percent of intensity, are located. Pixels between the left 50 percent peak to right 50 percent peak are counted and converted to length by multiplying by width of the image pixel to compute an approximate measure of anomaly width. This technique is called the "width measurement using the half-max technique". The technique is applied to frames between t_{50L} and t_{peak} assuming that the surface texture effects occur before t_{50L}. Simulation results show best match of half-max width measurement with the actual anomaly width for measurements done within this time range. For a randomly oriented indication boundary, scan lines are established along the entire boundary such that the lines are normal the boundary. The scan lines are used to plot the pixel intensity along the scan line and locate the 50 percent of intensity pixel as the location of edge of the indication. The half-max algorithm can be applied to normalized data cube. The normalized data cube is obtained by subtracting the pre-flash frame from all post-flash frames. A threshold based on ratio of half-max pixel intensity to average pixel intensity in the reference region is used to separate the indication data from noise. Thus, the half-max intensity to spatial noise ratio shall be more than 2-3 times for meaningful boundary estimation. Resolution of the half-max pixel can be improved by interpolation. The half-max estimation is in error if the delamination thickness is not uniform. Therefore, the half-max width estimation may be complemented by the EFBH or EUG width estimations.

23. Width Ratio

In order to compare EFBH estimation with the measured width, a quantity called the "width ratio" is introduced. The width ratio (ψ, psi) is defined as the ratio of the simulation estimated EFBH (or EUG) diameter to the half-max estimated width.

(47a)
$$\psi = \frac{D_{EFBH}}{w_{hm}}$$

(47b)
$$\psi = \frac{D_{EUG\%\mu}}{w_{hm}}$$

A correlation of width ratio measurements is established on the calibration standard FBH's with gamma. The ψ ratio is observed to be close to 1 for round FBH's. If the anomaly is not like a gapping delamination such that heat is partially conducted or transmitted through the anomaly, then the equivalent FBH estimation is expected to be smaller. Therefore, ψ is hypothesized to correlate to the degree of heat transmission through the anomaly. The heat transmission through anomaly occurs due to heat conduction through the air present in the delamination gap, contact between the delamination faces or the bridging of material in the delamination gap. It is hypothesized that a ratio close to 1 implies that the indication is similar to a flat-bottom hole or a gapping delamination. The lower values of width ratio will have more inaccuracies in depth assessment. Therefore, another ratio called the amplitude ratio is introduced. The ratio can be calculated for linear indications of flat bottom slots or linear delaminations.

The D_{EFBH} is expected to measure slightly more than the actual width due to effect of length but very little effect is expected in the accuracy of w_{hm}. Accordingly, if we compare ψ between a round FBH and a long slot with same depth and width equal to the diameter of the FBH, a higher ψ is expected for the slot. The effect of length contribution in the contrast evolution is minimal beyond a length of 1.5 times the width. This can be demonstrated by independent simulation.

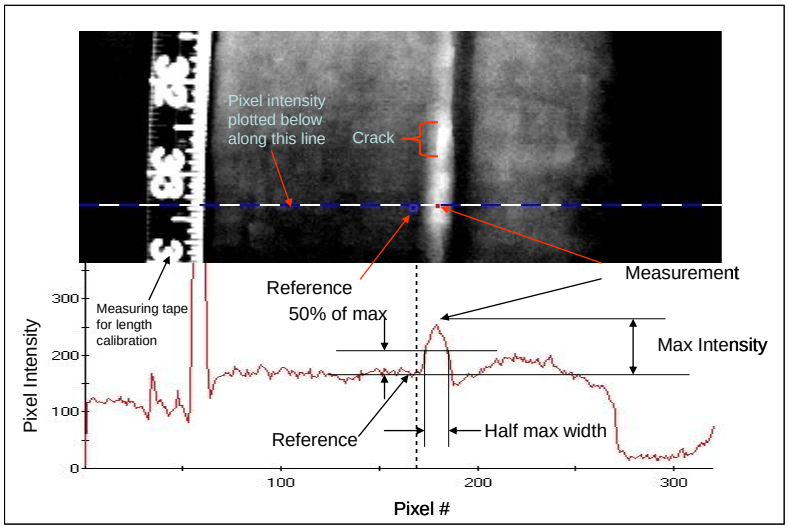

Figure 30: Half-max Width Measurement Technique

24. Amplitude Ratio, Transmissivity and Attenuation

In order to compare EFBH estimation with the measured half-max width, a quantity called the "amplitude ratio" is introduced. Similar to the width ratio, this ratio is intended to evaluate transmissivity of the anomaly. If a delamination has contact ($0 > \Gamma >$-1) between the faces, the heat will transmit through the delamination. A term related to the thermal mismatch factor ($-\Gamma$) is multiplied to the exponential term inside the summation sign in Eq. (1). In the contrast evolution Eq. (23), it is assumed to have a value of -1. A value of $0 < \Gamma <$ -1 results in lower peak contrast compared to the flat bottom hole of same size (Γ = -1), but the overall shape and the peak time is advanced due to change in direction effective heat flow (e.g. decrease in angle θ). Here, the half-max width (w_{hm}) is used as input to the simulation. Depth and the amplitude constant inputs to simulation are adjusted to match the simulation. The value of diameter constant is per calibration. The amplitude constant is changed to provide a best match with the measured data. This amplitude constant is denoted by C_{Ae} and is called the "anomaly evaluation amplitude constant". Ratio of the evaluation amplitude constant and calibrated amplitude constant is called the amplitude ratio. It denoted by ζ (zeta) and is given by,

$$\zeta = \frac{C_{Ae}}{C_A}. \tag{48}$$

The amplitude ratio compares the peak contrast (amplitude) of the anomaly with the peak contrast of an equivalent flat bottom hole with same depth and diameter. Thus, a ratio

close to 1 would imply that the anomaly is similar to the FBH. A lower value would imply that there is material bridging, thin gap or contact within the anomaly. The lower values also are likely accompanied by mismatch in shapes of the measured contrast and predicted FBH contrast evolutions. The material bridging provides adherence of the material above anomaly but a mere contact may not. The transmissivity measure or contrast attenuation μ is defined as.

(49) $$\mu = 1 - \zeta$$

Transmissivity measure ranges from 0 to 1. Higher transmissivity value indicates more heat transmission through anomaly. A value of 1 indicates full transmission and a value of 0 indicates no heat transmission similar to the no heat transmission in a FBH. The heat transmission through the anomaly is also due to partial contact or gap within the anomaly region. The heat may also transmit through the anomaly if the gap is too small as thinner air gaps are more conductive than the larger gaps. It is hypothesized that the effect of anomaly transmission results in reducing angle (θ) of effective heat flow. The effective angle of heat flow is related to γ and A_c. Therefore, the calibration curves which are functions of A_c can be developed for anomalies with controlled transmission (e.g. known air gap thickness or effective gap conductivity and thickness). Thus, the EFBH analysis can be extended to assumed equivalent uniform gap (EUG) diameter and depth.

25. Region of Interest Resolution

A selected image area with contiguous mosaic of fixed number of pixels is called region of interest (ROI). The smallest ROI contains a single pixel. The next larger ROI would contain 9 pixels in 3 rows and 3 columns. Usually, there are equal but odd number of pixel columns and rows to provide symmetry about the center pixel. Usually, the intensity of ROI is the average of all pixel intensities contained in the ROI and pixel coordinate of the center pixel is assigned to the ROI. Measurement accuracy of half-max width is affected by the size of the ROI. Therefore, a term called the "pixel resolution ratio", λ is defined as,

(50 A) $$\lambda = \frac{w_{hm}}{R}.$$

In order to compare the ROI size with the width of the anomaly, another ratio, λ' is defined as,

(50 B) $$\lambda' = \frac{w}{R}.$$

Where R = size of region of interest for the measurement pixel and w = width or diameter of the anomaly.

The size of single pixel is also known as the instantaneous field of view (IFOV). A quantity called slit response function (SRF) is determined experimentally for the IR

camera to determine resolution of the camera/lens combination. The slit response function provides relationship between the slit width (e.g. width of a warm object) at constant temperature with the measured relative intensity. Usually, the slit width should be minimum 3 to 5 pixels to register over 90 percent of maximum relative intensity. Thus, the width of an IR indication needs to be at least 4 times (λ = 4) the ROI size. An ROI with pixel size of 0.025 inch would be satisfactory to measure contrast on anomalies with width (or half-max width) larger than 0.1 inch. In other words, an indication with half-max width of 0.1 inch can be satisfactorily measured with an ROI with maximum dimension of 0.025 inch. Lower values of λ cause averaging of the pixel intensity of the measurement point resulting in lower contrast. If two ROI's with same size but different number of pixels are compared, an ROI with more pixels has less noise in the intensity value.

For curved surfaces, certain amount of defocusing is inevitable due to varying distance of the object surface from the lens. Defocusing reduces resolution by smearing edges of the indication. In the above case, the ROI needs to be smaller than 0.025 inch to account for smearing due to defocusing.

Although λ value of larger than 4 may be satisfactory to measure contrast, it is not sufficient to measure the half-max width. The half-max width measurement resolution (ROI size) shall be an order of magnitude smaller than the measurement (i.e. $\lambda > 10$). λ values lower than 10 are likely to introduce higher uncertainty in half-max width measurement and the width ratio. Smaller pixel size however provides better imaging of surface texture but provides more variation in contrast data for detection of subsurface delaminations. Thus, a very small pixel size may not provide most repeatable results. A pixel size that is one fourth of the feature size to be detected my provide a better compromise between contrast repeatability and resolution needed for half-max width measurement.

26. ThermoCalc Contrast Simulation on Flat Bottom Holes

The peak contrast amplitude and peak contrast time are the two most important features that define the approximate shape of the contrast evolution curve. ThermoCalc[6] simulation program was used to study correlation between normalized contrast peak time and peak amplitude for selected values of the diameter and depth of flat bottom holes. ThermoCalc is based on finite difference modeling of the test object temperature subjected to flash thermography. Figure 31 shows results of such a simulation. Figure 32 shows a similar contrast map from a calibrated IR contrast application on RCC. The two maps show similar trends, but are different in magnitude due to differences in material properties, assumptions and accuracy of models. These simulation results indicate that each combination of FBH diameter and depth provides a unique combination of the peak time and peak amplitude for higher values of contrast. Lines are drawn through constant diameter and constant depth data points to form a grid. The constant diameter grid lines do not intersect for peak contrast value above a certain threshold. The constant depth grid lines do not intersect each other. The plot indicates that it is possible to assess the depth

and diameter from the measured contrast evolution curve if the peak contrast amplitude is above a certain threshold within the calibration space for the depth and diameter. The plot also suggests that the peak contrast is higher for higher D/d γ (e.g. gamma = 20) values. The IR Contrast software is intended to capture the dependence of peak contrast and peak contrast time on the diameter and depth using the calibration. The shape of the contrast evolution is usually taken from a thermally isotropic material with high γ values. The IR Contrast prediction would be applicable to materials and anomaly with similar γ values.

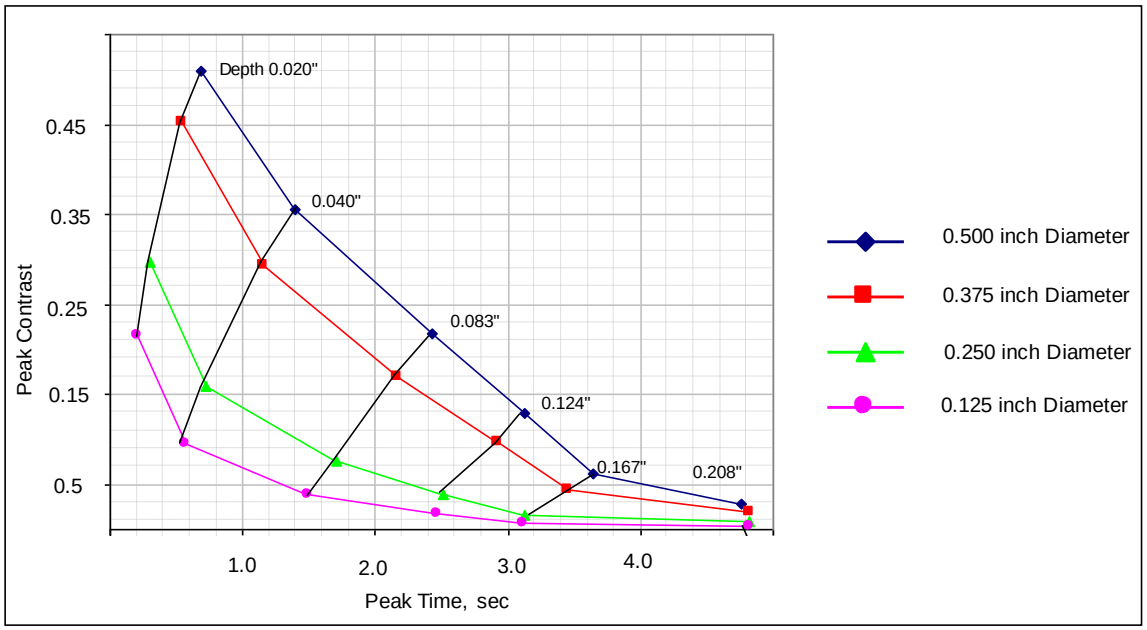

Figure 31: Example of Peak Contrast and Peak Contrast Time Simulation (Contrast Map) Using ThermoCalc

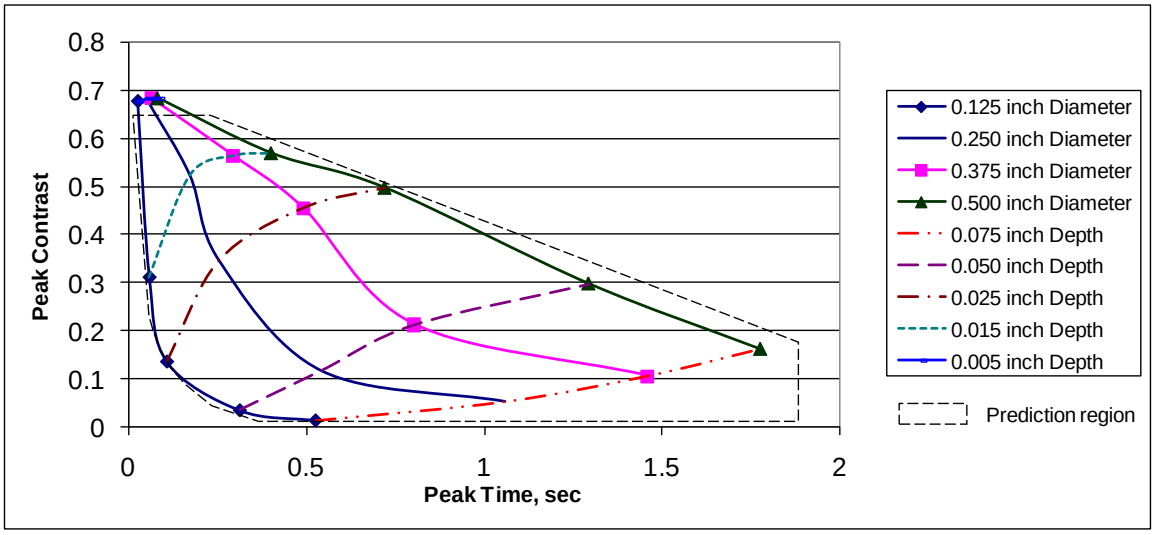

Figure 32: Example of Peak Contrast and Peak Time Simulation (Contrast Map) Using IR Contrast Calibration on RCC

The IR Contrast software seeks to estimate the EFBH diameter and depth of the anomaly. As the peak contrast value decreases below a certain threshold, accuracy of establishing unique values of depth and diameter decreases. Accuracy in locating the peak contrast time and other times (e.g. t_{50L} and t_{50R}) decreases significantly for lower peak contrast signal due to low signal to noise ratio. Deeper flaws provide long persistence time and lower peak amplitude causing flattening of the contrast evolution curve at the peak point reducing accuracy of locating the peak time. Consequently, accuracy of depth measurement is reduced. Similarly, sensitivity of peak contrast to the change in diameter decreases for deeper flaws. Thus, the accuracy of estimating γ and diameter also decreases for deeper flaws. Therefore, EFBH depth and diameter estimation is limited within certain range of depth and γ values. Thus, for deeper flaws, if approximate value of one of the two parameters e.g. depth or diameter is known, the other may be assessed with better accuracy instead of estimating both EFBH depth and diameter simultaneously.

27. Considerations for an Anisotropic Material

Consider a layered material with different thermal properties for each layer. The thermal response is affected by the variation in the layer thicknesses within a test object. The calibration standards should use the layer thickness covering the range of actual layer thicknesses. For a material with a coating layer, the thermal response is affected by the variation in thickness of the coating. An appropriate calibration file corresponding to the coating thickness should be used. The model uses three calibration constants e.g. the amplitude constant, diameter constant and depth constant as the primary means to match the prediction to the measured data. The validation process should assess the degree of fit using any of the indices discussed here. In some situations, it might be prudent to establish the reference evolution from a reference anomaly (e.g. a FBH or flat bottom slot) in the desired material with nominal properties and establish limits on prediction (γ and ω) in the neighborhood of the reference anomaly (e.g. γ_{ref} and ω_{ref}). It is not recommended to change the values of the evolution shape constants, although it is an option. The model uses a single value for diffusivity for prediction of a single contrast evolution.

Layered materials may be anisotropic in diffusivity. If the in-plane (lateral) and through thickness (normal) diffusivities are significantly different then the diffusivity experienced by the thermal conduction in the heat trapping volume and the surrounding area may be different at different post-flash times and may cause shape of the contrast evolution to be different compared to the contrast evolution from an isotropic material with same γ.

Thus, the lateral heat flow in the trapped volume is affected by the lateral diffusivity while the heat flow in the surrounding area is dominated by the normal diffusivity. The contrast evolution shape is affected by interaction of these two heat flows. If lateral heat diffusivity is significantly different than normal diffusivity then the contrast evolution

curve beyond t_{peak} is not likely to be useful for depth estimation as it relates more to difference between lateral diffusivity and normal diffusivity. The contrast evolution is dictated by heat diffusion in the reference and measurement ROI's. The primary factor affecting contrast evolution near the peak time is heat diffusion in the direction dictated by γ for the FBH. The diffusivity experienced by the heat flow not only depends upon the γ but also the layer thickness in the heat trapping volume and the in-plane and normal diffusivities in each layer. Thus, diffusivity is dependent on the direction of the dominant heat flow. At different times in contrast evolution the direction of the dominant heat flow changes and therefore the effective diffusivity experienced by the heat flow can be different at different points of time during the contrast evolution for an anisotropic material. For an anisotropic material correlation between the depth and effective diffusivity shall be established to improve the contrast prediction.

The depth estimation is likely to be more reliable based on the contrast evolution up to the peak time and particularly the portion of curve between t_{50L} and t_{peak}. If effective diffusivity does not differ significantly from the normal diffusivity, then the calibration profiles may compensate for the anisotropy. For a layered material with a given γ, the effective diffusivity of the FBH may be dependent on the depth. The IR Contrast model needs a single diffusivity value and may be limited to range of γ values for an anisotropic material to limit variation in the effective diffusivity.

28. Effect of Anomaly Shape

Comparison of the simulated evolution to the real evolution provides an estimation of the EFBH depth and diameter. The real anomalies may or may not be circular in shape. Anomalies may be elongated in shape and have a portion of perimeter concave outward. In such situations, we measure contrast at a point of maximum localized intensity on a line drawn across the localized width of the indication. The intensity at this point is affected mostly by the closest boundary of the anomaly (e.g. width) and to a lesser extent by the continuation of anomaly in length direction. IR measurement on the elongated flat-bottom holes indicate that as aspect ratio (φ) increases beyond one, the length contributes to contrast amplitude but the derivative of slope $\frac{d\overline{C}_w}{dl}$ is negative, implying diminishing contribution of length to the contrast amplitude with increasing length. In practice, the contrast evolution is not affected for aspect ratio of 1.5 and above for high gamma values. Consider a case with two anomalies at the same depth, one with round shape and the other with square shape such that the diameter equals the length of side of the square anomaly. The square anomaly has 27 percent larger area compared to the round anomaly and consequently has 13 percent larger equivalent FBH diameter. Thus, for elongated anomalies equivalent FBH diameter estimations are expected to be slightly larger than the physical width by 13 to 25 percent to account for effect of the shape and length. The EFBH depth and diameter are expected to bear correlation to actual width and depth of a delamination-like anomaly.

29. Effect of Surface Cracks Reaching the Anomaly

If cracks are present in the heat trapping volume, the thermal response or the contrast evolution is affected. The cracks may have partial contact between the faying surfaces. Depending on the degree of contact, gap thickness, size, location and number of cracks in the heat trapping volume and the surrounding material, the thermal response is affected. If the crack distribution (cracks per unit surface area) is uniform and the same as in the calibration standard then, the effect of cracks can be accounted for by calibration. Let us consider a special case of a linear anomaly with a single crack running lengthwise through the center. Such a crack bisects the heat trapping volume. Let us consider the effect on the contrast evolution from the single anomaly with a single crack in comparison to an identical anomaly without any cracks. The crack length is at least as long as the width. The measurement pixel is located in the center of the anomaly width and right next to the location of the crack. Therefore, as the heat conducts through the trapping volume, it reaches the crack boundary before it reaches the anomaly. The measurement pixel is located very close to the crack and the transit time from the measurement pixel to the crack is shorter than the transit time to the next closest boundary which is at a depth of the delamination. The effect of crack boundary is felt earlier by the measurement pixel. This results in the advancement of the peak contrast time or appearance of a separate peak. If the peak is advanced, it also may result in increase in the peak contrast value. However, the heat continues to diffuse to the anomaly and then around the edges of the anomaly. The persistence energy time is governed by the heat trapping volume and not by presence of a single crack. Therefore, as the contrast peak is advanced, the trailing side of the contrast evolution has lower amplitude so that the area under contrast evolution curve is unchanged. The shape of the contrast evolution curve is also changed accordingly. The simulation is based on the FBH without cracks and matching EFBH simulation to the contrast evolutions from the crack containing anomalies result in lower estimation of anomaly depth. It is hypothesized that the mismatch between the simulation and measured contrast evolutions at the peak contrast region indicates the severity of effect of the linear crack.

30.0 Optimization of Measurement and Reference Point

It is important to extract optimal contrast evolution from the IR data cube to achieve full potential of the IR Contrast analysis. Typically, three shapes of delamination-like anomalies are observed. These shapes are round, elliptical and elongated in the form of a strip. Let us take a case of a round anomaly. The measurement point is located close to the geometrical center as determined by the highest intensity pixel which is a unique pixel and can be easily located through user interface or by a computer algorithm. The contrast evolution is influenced by the measurement and the reference points. Locating the optimum reference point is not straight forward. The reference point can be located at a chosen radial distance and at any clocking orientation from the measurement point.

30.1 Radial Distance of Reference Point

The chosen radial distance is such that it locates the reference point just outside the anomaly footprint where the pixel intensity has no influence from the anomaly. As we continue to move the reference point closer to the measurement point, the contrast amplitude starts reducing. If the reference point is located within the boundary of the anomaly footprint, it is likely that the contrast evolution has less amplitude than maximum possible from the anomaly. If we move the reference point away from the anomaly, at a certain radial distance the maximum in the contrast amplitude is reached. If we move further away, the reference point is less related to the measurement point and bias due to local (including lateral) heat flow effects at the reference point influence the contrast evolution. Thus, there is an optimal radial distance range for the reference point where the contrast evolution is very close to the ideal maximum possible from the anomaly and is mostly invariant with further increase in distance of the reference point. Typically, the location of the optimal reference point is determined by analyzing a frame with time greater than t_{50R} to t_{tail}. The optimal reference point provides shallowest possible depth estimation and the largest possible EFBH diameter estimation.

30.2 Reference Point Clocking on Round Anomalies

If there were no lateral heat currents (or temperature gradients), then the clocking of the reference point should not matter. However, in practice there are always some lateral heat currents due to the test object curvature, uneven flash heating and change in material properties or thickness along the surface and proximity of the test object edge. The lateral heat current from the reference to the anomaly indicates that the reference area is relatively warmer and the contrast evolution will be lower than true contrast potential of the flaw. The reverse is true for the heat flow in the other direction. Let us assume that the lateral heat flow (0 deg) has the same direction in the vicinity of the flaw where we are interested in measuring both the measurement point and the reference point data. Consider two reference points, one in the upstream (180 deg) of lateral heat flow and the other in the downstream (0 deg) of the lateral heat flow with respect to the measurement point and located at the same radial distance from the measurement point. The two reference points have opposing effect on the contrast evolution, i.e. the upstream reference point causes the contrast evolution to lower and the downstream reference point causes it to be raised. Thus, if we average the two reference temperature profiles, it provides some compensation for the lateral heat flow. If the reference points are clocked at right angle (+/- 90 deg) to the heat flow, then the lateral heat flow has the least effect on the contrast evolution. The variation in contrast evolution due to clocking can be minimized by choosing the reference point such that the contrast at the tail end of the contrast evolution (at t_{tail}) is nearly zero. Thus, a search of the optimum reference point providing zero tail end contrast is needed if a single reference point is used. Another method involves choosing many reference points clocked uniformly over the 360 degrees and located at the same radial distance. We can average the temperature profiles of these reference points to create an artificial reference point for contrast computation. Here, we do not need to locate the optimal clocking. We still need to use optimal radial distance. The optimal clocking provides lowest EFBH depth prediction and the EFBH diameter

prediction somewhere in between the extremities of prediction from the un-optimized contrast evolutions.

30.3 Variation in Measurement Point Location

The measurement point is chosen as the point of peak amplitude (t_{peak}) of the pixel intensity. The ROI of the measurement point is chosen to be small, i.e. the size of a single pixel to minimize effect of signal averaging. Consider a case of round FBH where the reference point is located optimally and the location of the measurement point is changed from its optimal location. As the measurement point moves away from the optimal location, the contrast peak amplitude reduces and the peak time increases resulting in the increase in the EFBH depth estimation. It is observed that the EFBH diameter estimation diminishes slightly. The optimal measurement point provides the shallowest depth estimation. This, observation can be applied to a rectangular FBH. Consider a rectangular FBH and locate the measurement point at the center. The center location of the measurement point will be the optimum location. Imagine a centerline that runs parallel to the length of anomaly. If we move the measurement point along the centerline away from the optimum location, the contrast estimations are affected depending upon proximity of the reference to the closest end of the anomaly. If the distance of the measurement point from the end is less than the width of the FBH, then a slight decrease in EFBH diameter is expected similar to the case of round FBH. Similarly, as the measurement point is moved closer to the end, an increase in EFBH depth is expected. The slight decrease in width estimation can be accounted as error in measurements. The increase in depth signifies limit on the location of the measurement point.

30.4 Reference Point Locations for Elongated Anomalies

For elongated and elliptical flaws the uniform clocking over 360 degrees may not be applicable. Two reference points that are located on either side of the indication may be possible and averaging of the reference points may provide some compensation to the adverse effect of lateral heat flow. The reference point optimization schemes work only under assumption that nearly uniform lateral heat flow (surface temperature gradient) exists in the zone between the measurement point and the reference points. Thus, in practice although reference point optimization is possible, it may not provide full compensation especially if radial distance is too large. It is therefore, recommended to locate the anomaly area in the center of the hood where the flash intensity is most uniform and the test object surface can be most normal to the camera line of sight resulting in least lateral heat currents at the center of hood. Measurements performed at the center of symmetry of lateral temperature gradients are better as the temperature gradient is lower in the center compared to any other area.

31. Pixel Size and Pixel Averaging

Better image resolution is obtained using a small image pixel size. The measurement ROI is chosen as the point of maximum intensity in the frame of maximum contrast (t_{peak}). It

is located from the intensity versus distance profile along a line drawn across the longer axis of the IR indication. Larger ROI size may reduce the peak amplitude (peak clipping or averaging) due to averaging of intensity over many pixels. A λ of 4 (see also section 25) results in acceptable peak averaging. Reference ROI size is usually larger than the measurement ROI. The larger reference provides better confidence in the temperature evolution of the reference area due to noise reduction and suppression of the texture effect. As the size of reference ROI is increased, its distance from the measurement point needs to be increased to prevent the reference ROI from running into the anomaly indication area. Typically, the reference ROI shall be outside the anomaly foot print (as defined by the half-max measurement) at time larger than t_{50R}.

Increased distance between the measurement and the reference ROI may also cause issues with averaging over larger variation in the lateral heat flow or surface temperature gradients. Thus, reference ROI size cannot be increased beyond a certain limit. Use of a zoom lens reduces the pixel size and can provide better λ values. For example, a 13 mm lens used with a particular camera provided a pixel size of 0.040 inch at the hood opening. A 25 mm (zoom) lens provided a pixel size of 0.023 inch at the hood opening. Stability of camera with respect to the test object becomes more critical with zoom lens due to the smaller pixel size.

The anomaly indication is formed due to the heat diffusion. Immediately after the flash or at the beginning of the heat diffusion ($t < t_{50L}$), the absorbed heat is concentrated at the surface. If the object surface has surface texture in terms of surface roughness, then the incident heat flux has variation from the peak to the valley of roughness topography. The peaks in the surface texture absorb higher flux compared to the valley areas and the high points in the surface texture appear as hot spots with the size comparable to their physical size. The surface texture affects the lateral and normal heat conduction and is the other major factor causing hot spots in IR images immediately after flash time. A similar effect is observed when shallow surface cracks are present casing IR indication due to uneven cooling rates at either side of the crack. If a pixel size is larger than quarter of width ($\lambda <$ 4) of these features, then the pixel intensity can capture only a portion of the actual spot intensity. For a 0.023 inch pixel, the smallest IR indication half-max width can be 0.092 inch to have an acceptable (above 90 percent of maximum possible) intensity measurement. Thus, smaller (area and amplitude) indications appearing in the earlier frames are not measured adequately. For example, if we use a zoom lens to change $\lambda_{texture}$ from 1 to 5, a dramatic increase in the pixel intensity of texture indications is expected where pixels are located at the hot spots and decrease in intensity where pixels are located at the cooler spots. Thus, if surface texture is present in the part, the earlier portion of the contrast evolution curve ($t < t_{50L}$) may be more affected by the pixel size. With time, the heat diffuses and the texture indications fade away due to heat conduction. The smaller indications fade away before the larger ones. In most situations, we are interested in indications due to subsurface delaminations and not due to surface texture. We are interested in delaminations larger than a certain threshold size. Therefore, the $\lambda_{anomaly}$ for the threshold size shall be greater than 4. The apparent $\lambda_{anomaly}$ measured at time t_{50L} shall be greater than 4. The decay of the surface texture indications is dependent on the many factors such as spatial frequency of surface texture features and the depth of

the surface features (including the surface crack depth if any). Thus, the texture indications are superimposed on the subsurface anomaly indication.

32. Near Surface Resolution

Near surface resolution (depth) refers to ability to resolve the shallow delaminations. Shallow anomalies have shorter peak time and persistence. Figure 33 below illustrates that a higher frame rate provides a better time resolution and provides better definition of the contrast evolution. In the example, the 60 Hz and lower frame rates do not capture the peak in the contrast evolution. In order to run the automatic fit routines it is necessary to capture the peak of contrast. The near surface indications may be affected by the surface texture.

Also, depending on the extent of texture effect, the near surface delaminations may not be discernible in the contrast evolution. Higher frame rate helps in improving definition of the early portion of the contrast evolution. The near surface resolution is affected by the anomaly size (or gamma) and the pixel resolution among other factors.

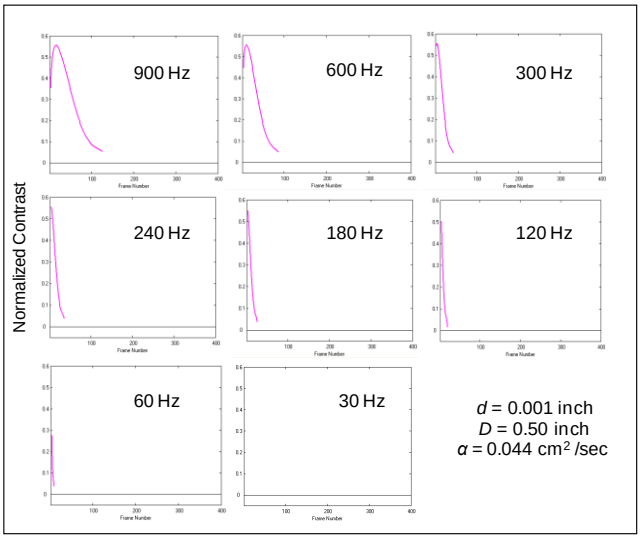

Figure 33: Effect of Frame Rate on Contrast Evolution of Shallow Anomalies

33. Limitations of IR Contrast Prediction

The predicted contrast evolution curve is based on "calibration" of the numerical model to the real contrast evolution curves within certain limits on γ and ω. Ideally, for contrast prediction, the material needs to be thermally isotropic; and the diffusivity and other thermal properties should be same as the calibration reference standard. The calibration is usually done on a reference piece of the same material and round flat-bottom holes are used to simulate the anomalies. The reference evolution can be based on the reference material itself. If the IR Contrast is calibrated on the flat-bottom round holes then, the IR Contrast approach predicts the diameter and depth of an equivalent flat-bottom hole

(EFBH) that provides a close match to the contrast measured on the test hardware with delamination-like anomaly. Comparison of the predicated contrast evolution curve to the measured contrast evolution curve is done under the following assumptions. The material properties between the calibration standard and the test object inspected are the same or correlated (e.g. thermal properties including coating thickness for a two-layer material). The test object thickness is similar to the calibration standard. The anomaly depth is much less than the test object thickness (e.g. $\omega << 1$). Omega values close to 1 are not desirable as the bottom of the test object influences the contrast signature. A precise limit on ω can be validated through calibration.

We assume that the contrast evolution curve and measurements on the contrast evolution (peak contrast, persistence energy time etc.) are only influenced by the anomaly characteristics (e.g. anomaly or FBH depth, width, gap thickness and length) and not by any factors that are not related to the anomaly characteristics such as proximity of the anomaly to the test object edge, proximity of the anomaly to edge of the flash zone, the less than optimal choice of reference point location, lateral heat flow not related to the anomaly, and uneven flash heating. It is assumed that the contrast evolution curve is positive and has similar shape to the contrast evolution curve on the flat-bottom holes (or other programmed anomalies) in the calibration reference standard. Factors not related to the anomaly characteristics are assumed to be small and assumed not to distort the contrast evolution from its expected shape similar to an ideal shape (i.e. positive skewed distribution with sharper rise and gradual decay).

Natural anomalies are like delaminations and differ from the FBH's. The contrast evolutions of the FBH and delaminations of same size are likely to differ to some extent due to additional mass below the delamination compared to the FBH. If the delamination-like controlled anomalies are available for calibration, then it is advisable to establish the reference evolution and the calibration curves on these anomalies to improve contrast prediction. In general, the additional mass under the delamination should cool the surface above anomaly faster, possibly implying need to use slightly higher depth constant (e.g. higher diffusivity) in the simulation.

34. Effect of Emissivity, Flash Duration, and Orientation of Object Surface

The IR Contrast technique assumes a high emissivity (> 0.8). Thus, the pixel intensity is assumed to a positive power (3 to 10 approximately) of the surface temperature. The polished inner sides of the hood help to reflect the flash energy on to the test object maximizing the incident energy on the test object. The lamps are hot after the flash and the test object reflects the heat radiation from the lamps in proportion to the test object reflectivity. The shiny inner sides of the hood act as four front side mirrors and provide multiple mirror images of the flash lamps which provide portion of the pixel intensity that is not related to the test object surface temperature. If a test object has lower emissivity, high emissivity paint can be applied to the test object to improve the emissivity to some

extent. However, applying paint introduces more variables such as the thermal properties of the paint which introduce other sources of errors.

The emissivity is dependent on the wavelength of the incident radiation. The test object may have different emissivity in visible and infrared wavelengths. The flash radiation constitutes visible white light but after the visible radiation stops the lamps radiate infrared radiation (called afterglow) at much lower intensity. The slow decay after the peak intensity time in the flash is undesirable as it has effect of reducing contrast. A square flash pulse of a given duration provides the most contrast but is impractical. It is recommended to keep the flash duration constant (e.g. 3 ms) during calibration and inspection.

The test object should have high emissivity for visible light and thermal radiation. The object surface angle with the camera line of sight affects thermal absorption, radiation and resulting contrast measurements.

The hood uses two long flash lamps with length along the inner roof and on either side of the camera lens. The lamps provide fairly uniform incident light radiation (< 5 percent variation) at the hood opening. Thus, the heat illumination can be thought to have a direction parallel to “the center axis of the hood”. The camera lens is located at the center of the hood. Consider a flat test object that is located at the hood opening with the camera “optics axis” (optic centerline) pointing to the center of hood opening. The line of sight from camera lens center to the area at the center of hood is collinear with the optic axis and normal to the test object surface. In areas of object away from the center of the hood, the line of sight makes an angle called the line of sight angle with the normal to the object surface. The heat emission in the direction of the line of sight is received by the camera. The line of sight angle increases as the distance of the area increases from the optic axis.

The emissivity changes as cosine of the radiation angle with normal to the surface for a diffuse radiator. It is assumed to follow the Lambert’s law. Thus, the measured intensity is maximum if the ROI is located on the optic axis. If both, the measurement point and the reference point, have about the same line of sight angle, then the effect of angle on the contrast is minimized. Centering the area where contrast measurements are extracted provides the best possible measurements.

Consider a curved test object with a sloping step. Direction of the surface normal is not collinear with the hood axis at many locations on the surface of the test object including at the sloping surface. Angle between the surface normal and the hood axis can be considered to be the incident angle of the flash radiation. The intensity of the incident radiation is proportional to the cosine of the incident angle. The absorption of incident energy is also proportional to the cosine of the angle for a diffuse radiator. Thus, surfaces with surface normals that are not collinear with the hood axis receive less flash radiation and they absorb less from the received radiation. If the surface also makes a line of site angle with the camera then the emitted radiation is proportional to the cosine of the line of site angle and is less than the optimal. Thus, angle of the object surface affects the

pixel intensity and measured temperature from the pixel intensity. The curvature and the object surface angle also result in undesirable surface or lateral temperature gradients.

35. IR Contrast Technique to Measure Test Object Diffusivity

The calibration profiles of the diameter and amplitude constants are about the same for thermally isotropic materials. This implies that once we calibrate the predicated evolution on a set of different FBH's with high γ values, it is applicable to other materials under certain conditions such as the requirement of high emissivity and similar range of γ values. The procedure involves calibrating the predicated contrast evolutions using the measured contrast on FBH's of a reference material with known diffusivity (α_{ref}). The calibration involves plotting the diameter and amplitude constants (e.g. C_d and C_A) versus size parameter (A_C) using value of the depth constant equal to 1 ($C_{d\text{-}ref} = 1$). To measure diffusivity on an isotropic material of interest, FBH's with identical γ values are machined in the sample. We obtain measured contrast evolutions on the sample. Next, using the measured evolutions we find the best simulation fit with actual diameter and depth as input. We use the diameter and amplitude constant from the calibration profiles of the reference material. The only variable in seeking the best simulation fit is the depth constant which is chosen by trial and error. Using following equation we can determine diffusivity of the material.

(51) $$\alpha = \alpha_{ref} \frac{C_d}{C_{d-ref}}$$

36. Effect of Material Parameters on the Contrast Evolution

The peak contrast and peak contrast time are two very important parameters in the IR Contrast analysis. The peak contrast value is controlled by the size parameter A_c and it is independent of diffusivity. Consider an identical FBH in two materials with different diffusivities. If we compare the contrast evolutions, the two peak contrast values are same but the peak contrast time for the material with higher diffusivity is shorter compared to the other material. The effect of increase in the diffusivity is similar to decreasing depth of the FBH provided the γ value is kept the same. Effect of doubling depth is equivalent to changing diffusivity to one fourth. The effect of change in the diffusivity and depth is illustrated in Figure 34.

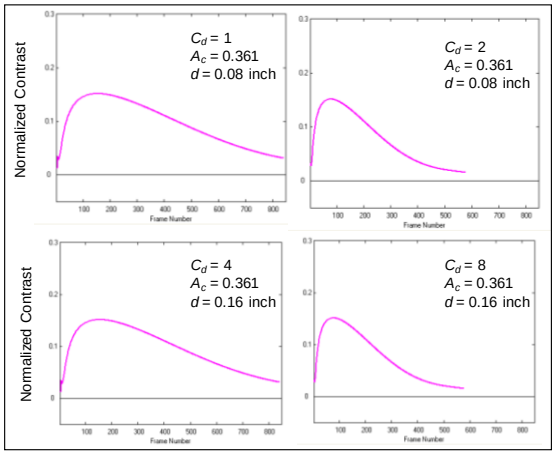

Figure 34: Effect of Diffusivity and Depth Constant on the Contrast Evolution

Change in the diffusivity of the test object due to mechanisms such as mass loss, off-gassing or chemical reaction, can be assessed by monitoring the peak time (or t_{50L}). The change in peak time provides a measure to assess the change in diffusivity provided we assume that anomaly dimensions and transmissivity do not change. If we monitor an anomaly contrast evolution, then lack of change in the peak contrast (including peak time) suggests that there is no change in the anomaly size and transmissivity. Effect of change in the diameter on the contrast is illustrated in Figure 35. Increase in the diameter increases both the peak contrast and peak contrast time.

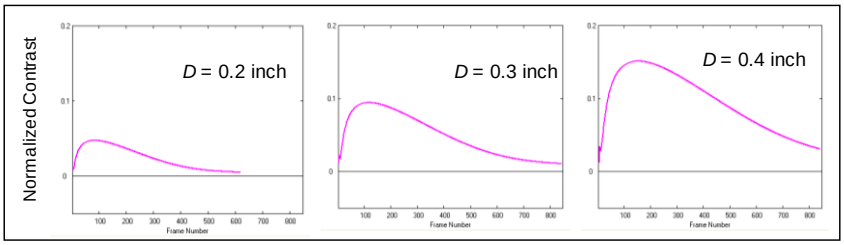

Figure 35: Effect of Change in Diameter on the Contrast Evolution

The effect of anomaly transmissivity on the contrast is illustrated in Figure 36. Depending upon the anomaly mismatch factor or the transmissivity, the peak amplitude is affected.

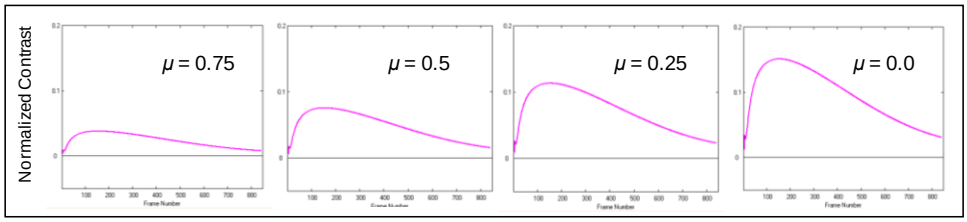

Figure 36: Effect of Attenuation μ on the Contrast Evolution

37. IR Contrast Calibration Steps for an Anisotropic Material

Calibration standards with FBH's are needed for the calibration. Choose two depth values (low and high) to establish a depth range of interest. At each depth, choose low and high values for diameter to establish a diameter range of interest. Choose several hole sizes that span the range of diameters. Fabricate the standards and measure the depth and diameter accurately. Assign a unique number to each hole. It is important to know the thermal diffusivity of the material accurately. If the diffusivity is not known, measure the diffusivity using a flash thermography technique given in ASTM E 1461. If the part emissivity is lower than 0.75, then apply a high emissivity coating. Parts with the same material will have to be inspected with the same emissivity coating.

Next, perform the flash thermography inspection and capture the contrast evolutions on the holes of the chosen standards. Open the IR Contrast application if not open. Choose the material that has the closest diffusivity to the calibration standard. Choose the frame rate for the simulation that matches the frame rate in the actual contrast evolutions. Choose the depth constant so that the diffusivity times the depth constant matches the estimated diffusivity of the material. If the chosen diffusivity value is in error, it will cause changes in the calibration curves. As long as the same diffusivity value is chosen during the data analysis it will not cause any additional errors. Thus, the calibration curves are referenced to ratio of part diffusivity and assumed or estimated effective diffusivity. The value of effective diffusivity can be changed by changing the value of the depth constant.

Open the IR Contrast application if not open. Choose a contrast evolution from one of the lower depth holes. Always examine for levelness of the contrast evolution. Contrast for the beginning frame (first frame) and the end frame shall be at same level and close to zero. If the evolution is not level, re-extract the contrast evolution by choosing a different reference ROI. Input the correct diameter and depth of the FBH. Refresh the plot. Ensure that the "un-calibrated" mode is on. Ensure that other inputs (e.g. frame rate, depth constant etc.) are correct. The simulation may not match the actual contrast evolution. Note the peak-time (or frame) of the actual contrast evolution. Change the diameter constant such that the peak-time of the simulation matches with the actual peak-time. Change the amplitude constant to match the amplitude of the signal. Note value of the flaw size parameter (A_c), diameter constant and the depth constant. Load another contrast evolution from a hole with same depth but with different diameter. Repeat the process. Analyze all holes at the low depth. Repeat analysis of contrast evolutions of all holes at higher depth. Plot the diameter constant and amplitude constant against the flaw size parameter. Establish a single best fit diameter calibration curve for both depths.

The amplitude constant data for each depth is likely to indicate a separate trend line. Choose only the low depth flaw amplitude constant versus the flaw size parameter data to establish the amplitude constant calibration curve. Create the calibration file. Calibration file is a text file with a table containing three columns. The first column is the flaw size parameter. The second column is the diameter constant and the third column is the

amplitude constant. The lowest flaw size parameter value is 0.01 and the highest is 1.0. Choose at least 10 values of the flaw size parameter in the table.

Open the IR Contrast application if not open. Choose "calibrated" mode and load the calibration file. Load a contrast evolution from a low depth hole. Verify other input values. Use "Auto-fit" window to find automatic match of simulation with the signal. Observe if values of the diameter and depth used in the simulation match with the actual diameter and depth of the hole. If the match is good for all holes at low depth, load a contrast evolution of a hole with high depth with highest gamma. Unclick the "Auto-fit" option.

Open the amplitude factor calibration window. Choose "apply amplitude factor" calibration. Type the low depth value as the base depth value. Type the actual depth and diameter values in the simulation input. Observe the simulation contrast evolution. Use the amplitude slope of 1 for the base depth. Change the amplitude factor slope and refresh the plot to match simulation with the actual signal. Note the amplitude factor slope value. Repeat the process by loading another high depth contrast evolution. Note the amplitude factor slope that provides the best match. The slope factor may be positive or negative. Average all the slope factors and use the average value. Re-analyze all high depth contrast evolutions using the same amplitude factor value.

38. Calibration Curves for RCC by Calibrating for Depth Dependence of Diffusivity

RCC is a three layer material with outer layers made from silicon carbide (SiC) and the middle layer made from carbon-carbon material. Consider a round FBH or a round void-like anomaly. The diffusivity value that controls the contrast evolution is dictated by the location and direction of the dominant heat flow that starts from the measurement ROI and passes towards the edge of the anomaly as well as by the (normal) heat flow from the reference ROI. The heat flow (direction and flux) changes with the time and effective diffusivity experienced by such heat flow changes with direction and time. The effective diffusivity as a function of depth of the flaw should be known before the calibration curves can be established. Here we choose two sets of flat bottom holes. One set has a depth at a shallow (low) depth of interest and the other is at the deeper (high) depth of interest. It is not necessary to know the exact effective diffusivity in order to establish the calibration curve. However, it is important to assign a reasonable estimate of the diffusivity to the low depth holes. Using the chosen diffusivity, the simulated contrast evolutions of the low depth holes are obtained and used to establish the diameter constant and amplitude constant. The low (or high) depth can be chosen to be the base depth. Let us chose the low depth as the base depth for the following plots.

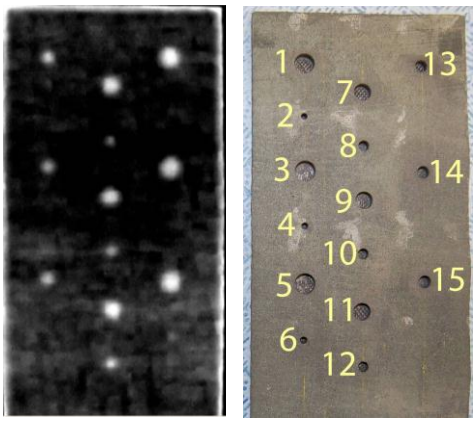

IR Image of D2 Photo of D2

Figure 37: Images of Calibration Standard D2

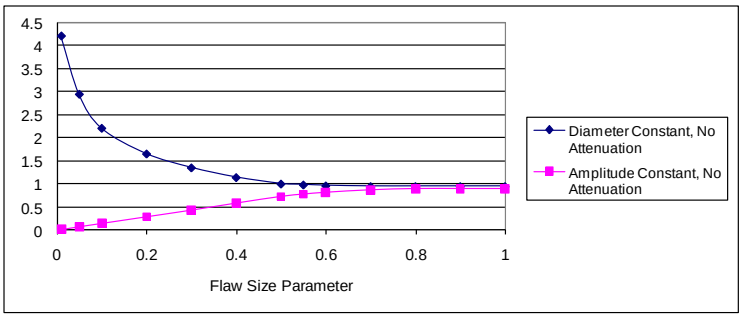

Figure 38: Calibration Curve from Base Depth Holes

Use the high depth hole contrast evolutions and choose a diffusivity value that provides about same diameter constant to flaw size parameter relationship as the low depth contrast evolutions. The depth constant calibration is controlled by the following empirical equation.

(52) $$C_{d,d} = C_{d,b} + S_d Log\left(\frac{d}{d_b}\right)$$

$C_{d,d}$ = depth constant at depth d
$C_{d,b}$ = depth constant for base depth (e.g. 2.9)
S_d = slope for the depth constant (e.g. -0.9)
d = delamination, FBH or uniform gap depth
d_b = base depth for a calibration FBH
$\chi = \frac{d}{d_b}$, depth to base depth ratio or simply depth ratio

Figure 39 provides an example of a plot of the depth constant calibration equation.

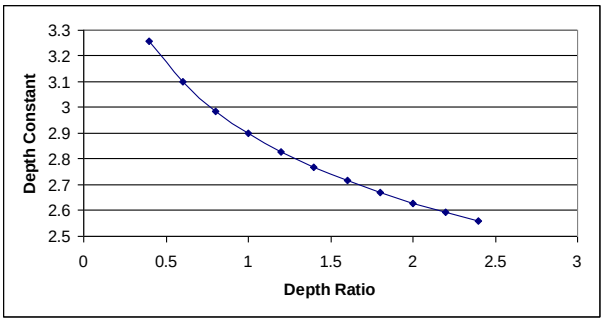

Figure 39: Depth Constant versus Depth Ratio

The amplitude constant may be depth dependent too. Figure 40 shows an example of a plot of the amplitude factor calibration equation.

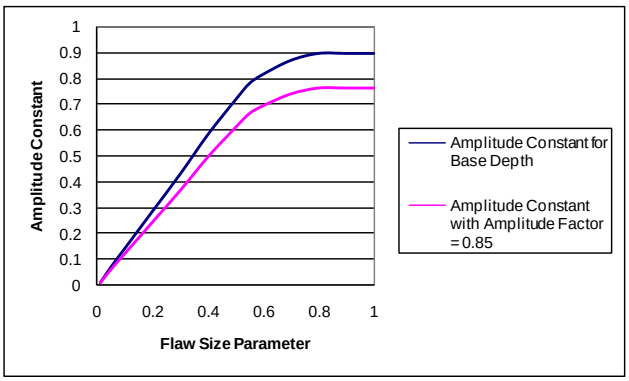

Figure 40: Amplitude Constant versus the Flaw Size Parameter

The following equation captures the relationship between the amplitude constant for base depth and variable depth.

(53) $$C_{A,d} = C_{AF,d} C_{A,b,\mu}$$

(54) $$C_{AF,d} = C_{AF,b} + S_{AF,d} Log\left(\frac{d}{d_b}\right)$$

$C_{A,d}$ = amplitude constant for a give depth d
$C_{AF,d}$ = amplitude factor for a given depth d
$C_{A,b,\mu}$ = amplitude constant from the calibration curve for a base depth and given attenuation μ
$C_{AF,b}$ = amplitude factor at base depth, usually 1
$S_{AF,d}$ = slope for the amplitude factor (e.g. -0.1)

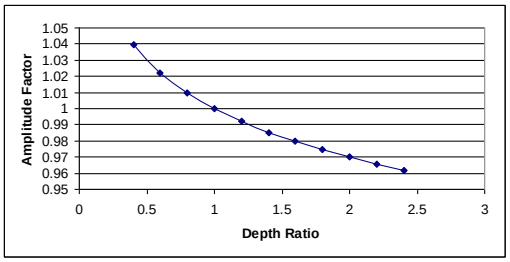

Figure 41: Amplitude Factor versus the Depth Ratio

As an example, two RCC standards were used for the calibration. RCC Standard D1 had 0.025 inch deep holes and RCC standard D2 had 0.050 inch deep holes. Results of the calibration as depth prediction on the standard D1 and D2 are shown in Figure 42.

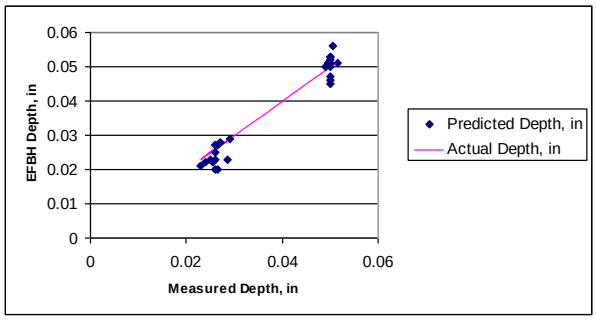

Figure 42: Comparison of Actual and Predicted Depth

Results of the calibration as the diameter prediction on standard D1 and D2 are shown in Figure 43.

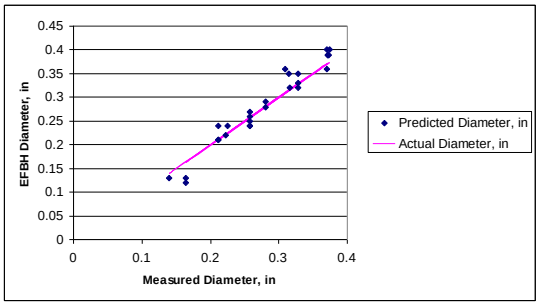

Figure 43: Comparison of Actual and Predicted Diameter

39. Calibration for Specified Attenuation ($\mu_{\%}$) for a Thin Delamination

For the flash IR thermography, it is assumed that air gap exists in the delamination. The heat transmits through the air gap. Thin gaps transmit heat by air conduction. Thick gaps transmit heat by convection which is negligible. The radiative heat transfer is mostly

independent of the gap thickness and is not a major contributor to the heat transmission across the gap of the delamination. Higher contact pressure at the gap interface provides larger contact area. Therefore, the contact pressure probably affects the amount of heat conduction.

As the energy is transmitted through the gap, the registered peak amplitude is reduced compared to the amplitude from a corresponding FBH. The calibration curves for a uniform thin gap are different from that of a corresponding FBH. Ideally, physical reference standards with known and uniform gaps shall be fabricated to establish the calibration curves for known gaps. However, using ThermoCalc simulation, it can be shown that a gap of less than 0.010 inch is needed to reduce the contrast amplitude significantly. It may be impractical to create controlled gaps less than 0.001 inch.

An alternate approximate approach is to use a ThermoCalc (or other) simulation. In using the ThermoCalc simulation, we choose many uniform gap voids with differing widths but same depth. The chosen depth is equal to the base (low) depth. We choose a different gap thickness for each run. We choose a large gap thickness (0.150 inch) to represent the case of a FBH. We choose several other values with lowest gap thickness at about 0.0005 inch. We calculate peak-time ratio and peak amplitude ratio with respect to the peak-time and amplitude of the FBH. The peak-time ratio is plotted against peak amplitude ratio for each gap thickness with different diameters. See Figure 44. Here we choose a desired amplitude attenuation level (e.g. 30 percent). From the plot, we read value of the peak-time ratio for the chosen amplitude ratio. We create a table of the peak-time ratio for the given size of the gap. See Table 2. We use the IR Contrast simulated contrast evolution (use calibration mode) to note the peak amplitude and peak-time for each gap width. We compute the 30 percent attenuation amplitude by multiplying by 0.7 (1.0 -peak amplitude ratio). We calculate the corresponding peak frame by multiplying the FBH peak frame (IR Contrast simulation) by the peak-time ratio. Now we choose the "un-calibrated" mode to input trial values for the calibration constants that provide the best match with the calculated peak frame and peak amplitude.

The real delaminations may have thin gaps and the contrast evolution is attenuated. The relationship between the peak-time and peak contrast can be studied by using ThermoCalc simulation for many void thicknesses that range from very thin (g = 0.0005 inch) to very thick (e.g. 0.150 inch). The thick voids can be considered to be like a flat bottom hole. The contrast evolutions for the FBH's of various widths can be used as the base to compute the peak contrast (amplitude) ratio and the peak-time ratio for the corresponding hole sizes for each gap thickness. Here, we make an assumption that the ThermoCalc simulation can provide acceptable correlation between the peak contrast ratio and the peak-time ratio for a material with known properties. See Figure 44. The lowest values of peak-time ratio correspond to a gap of 0.0005 inch in this plot.

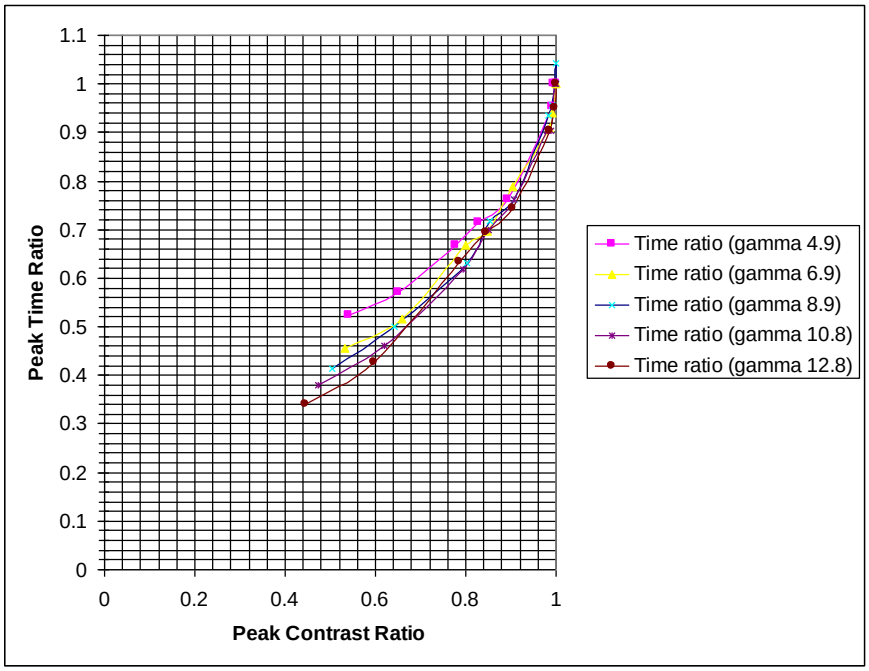

Figure 44: An Example of Relationship between Peak-time Ratio and Peak Contrast Ratio Based on ThermoCalc Simulation for a Void Depth of 0.040 inch

Using the above results, we can establish a correlation between gamma (void width) and the peak-time ratio for a chosen attenuation in the simulated peak contrast. 50 percent attenuation corresponds to an air gap thickness of approximately 0.001 inch. The attenuation is similar to one minus the amplitude ratio ζ (i.e. 1- ζ). See also Section 24. While the attenuation is used to compare the peak contrasts of simulated evolutions, the amplitude ratio is used to compare the peak contrast of actual evolution with the peak contrast of the simulated evolution.

Void Width, in	Gamma	Peak Time Ratio for 50% Attenuation
0.512	12.8	0.34
0.433	10.8	0.39
0.354	8.9	0.41
0.276	6.9	0.44
0.197	4.9	0.51

Table 2: An Example of Correlation Between Gamma and the Peak-time Ratio at Chosen Depth of 0.040 inch

The above data can be used to generate the calibration curves for the chosen attenuation. First load the calibration curve (mode: calibrated) for the FBH (0 percent attenuation or $\mu_{\%} = 0$). For each void width and depth, determine and note down the peak-time and the peak amplitude. Then change the mode of the software to "un-calibrated". Now compute the attenuated amplitude and the peak frame from the corresponding ratios. The diameter

and amplitude constants are determined by trial-and-error. The diameter constant is altered to match the peak-time followed by the change in the amplitude constant to match the amplitude. Figure 27 shows the calibration panel in the IR Contrast application.

(55) $$C_{D,\mu} = C_{D,0} - S_{D,\mu}(A_c)^{\eta}$$

(56) $$C_{A,\mu} = C_{A,0} S_{A,\mu}$$

Where, μ = attenuation or transmissivity measure,
$C_{D,\mu}$ = diameter constant for attenuation μ,
$C_{D,0} = C_D$ =diameter constant for no attenuation,
$S_{D,\mu}$ = slope for the diameter constant,
A_C = flaw size parameter,
$C_{A,\mu}$ = amplitude constant for attenuation μ,
$C_{A,0}$ = amplitude constant at for no attenuation,
$S_{A,\mu}$ = slope for the amplitude constant and
η = chosen by best fit(for example $\eta = 0.25$), depends upon μ.

40. Calibration Curves for Contrast Attenuation

Figure 45 provides an example of calibration curves for no attenuation (FBH) and with 30 percent and 50 percent attenuation.

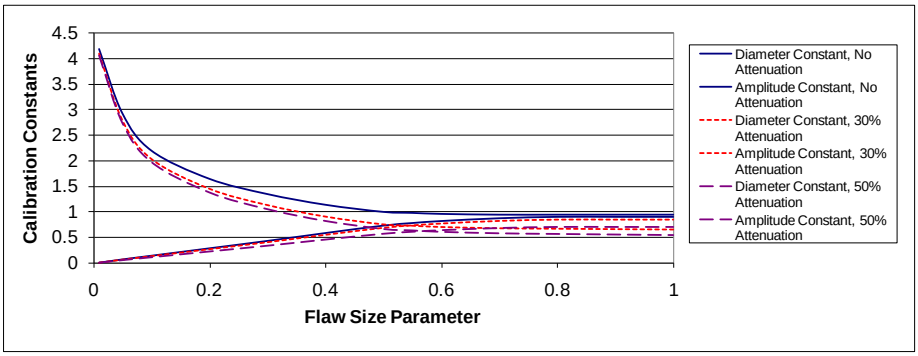

Figure 45: An Example of Calibration Curves for No Attenuation, 30 percent Attenuation and 50 percent Attenuation

Figure 46 shows a plot of the slope constants versus the contrast attenuation. A curve fit equation may be used to describe the slope constants as a function of the contrast attenuation.

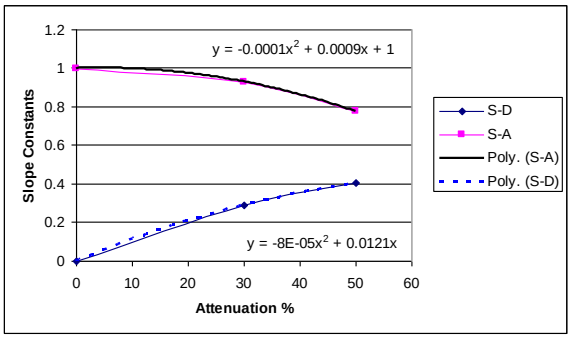

Figure 46: Slopes of Calibration Curves. ThermoCalc Simulation Used to Determine 30 percent and 50 percent Attenuation Slopes

70 percent attenuation calibration curves can be calculated by extrapolating curves from Figure 46. Similarly interpolation may be used. The corresponding calibration curves are shown in Figure 47.

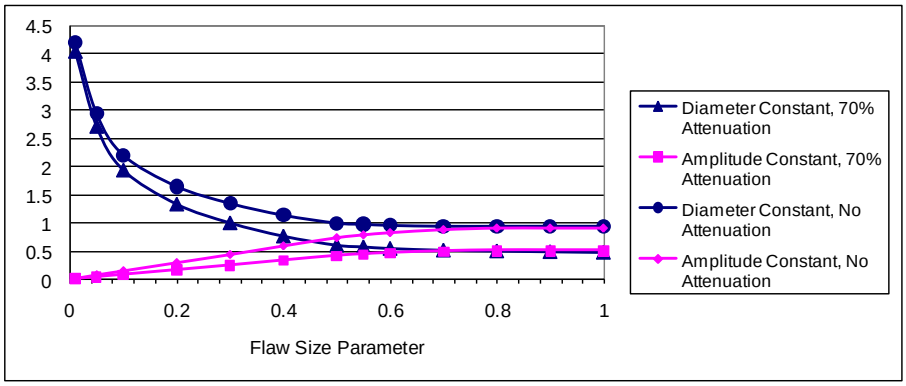

Figure 47: Slopes of Calibration Curves. Extrapolation of Slope Curves Used to Determine 70 percent Attenuation Slopes

41. Contrast Maps for Attenuated Calibrations

Figure 48 shows, an example of a map of the peak contrast and peak time for flat bottom holes in RCC. The map is also known as the "contrast map". The map indicates the IR Contrast prediction region. At the upper left corner and lower right corner the prediction is not accurate in terms of the diameter. Also, the low amplitude evolutions have higher error in the prediction.

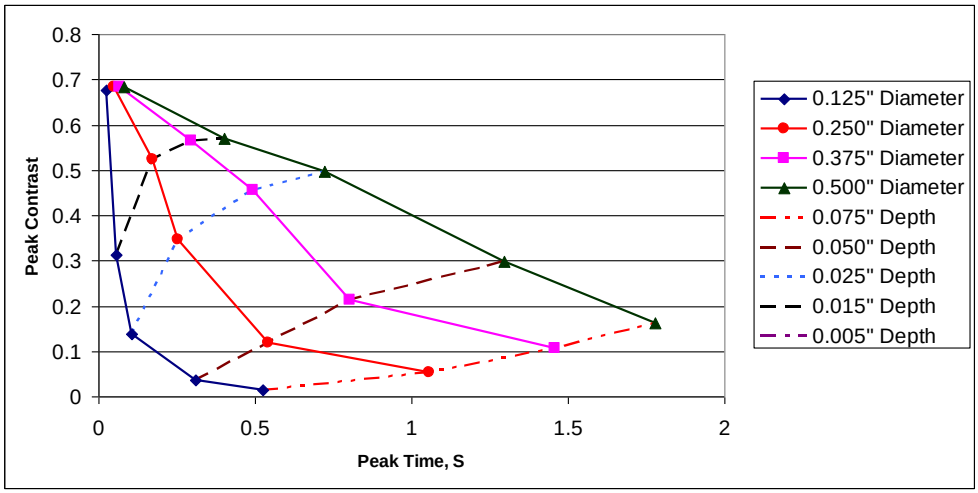

Figure 48: Peak Contrast versus Peak Time Contrast Map for 0 percent Attenuation (EFBH)

Figure 49 shows, an example of a map of the peak contrast and peak time for uniform round thin gaps with 50 percent attenuation in RCC. For thin gaps with 50 percent attenuation, the contrast map indicates much lower peak contrast and peak times. The contrast application can choose a FBH calibration or the corresponding percent attenuation calibration. When finding a simulation match on contrast evolutions from FBH, the percent attenuation calibration may not be able to find a match. Similarly, when finding a simulation match on the contrast evolutions from thin delaminations, the FBH calibration may not be able to find a match. The degree of match can be viewed as the contrast plots and quantified as delta square values. It is postulated that the 50 percent attenuation is good approximation for gaps of the order of 0.001 inch. The map indicates severe contrast attenuation at 0.5 sec for 50 percent attenuation.

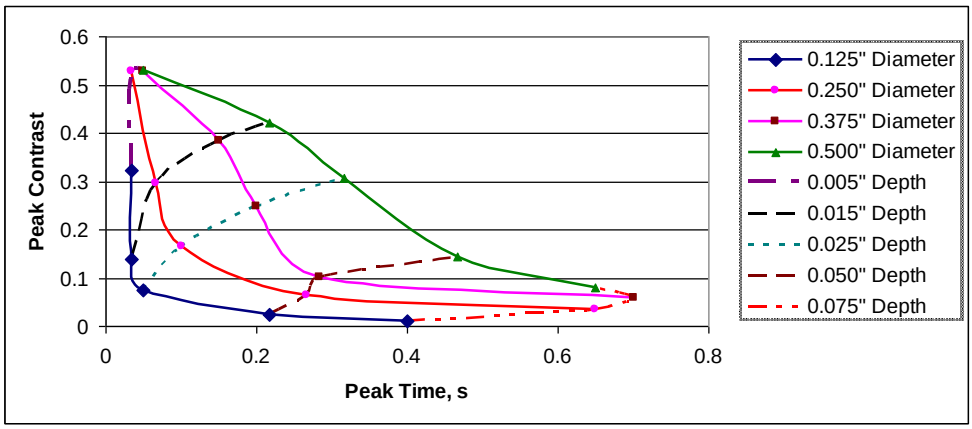

Figure 49: Peak Contrast versus Peak Time Map for 50 Percent Attenuation in EUG

42. Accounting for Long Indications in the Analysis

For long indications, the EFBH or EUG width estimations are higher than the actual width due to the length to width aspect ratio of greater than 1. The effect can be studied on a slot standard. Figure 50 shows a slot standard and IR image of holes 3, 4 and 5. The figure also illustrates the half-max boundary (in yellow) detection. The half-max boundary closely matches the actual vertical edges of the three anomalies.

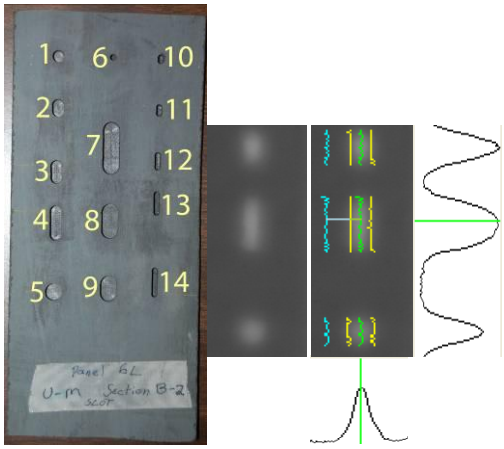

Figure 50: Slot Specimen, IR Image at 0.67 sec of Hole 3 (Top), Hole 4 (Middle) and Hole 5 (Bottom) and Their Half-Max Vertical Boundary

Figure 51 shows that on a long 0.25 inch wide slot (#4) EFBH estimations are 60 percent wider than the actual but on the round hole (#5), the prediction is close.

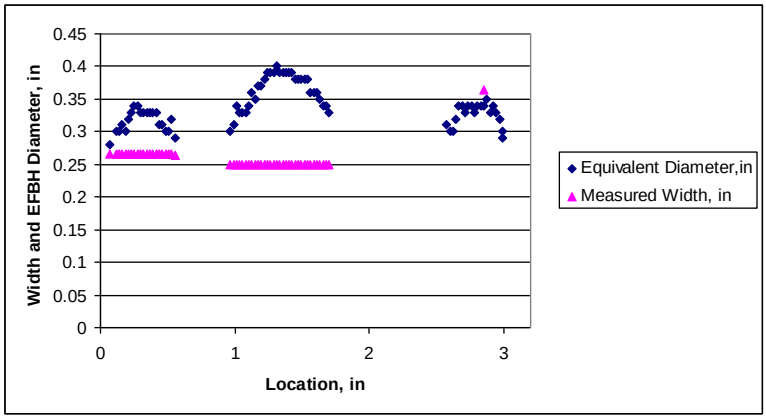

Figure 51: Comparison of Actual Width with Predicted EFBH Diameters for Holes 3, 4 and 5

If the data contains only long indications, it may be advantageous to set-up calibration on long slot (aspect ratio >3) standards using width in place of the diameter. In this situation,

correction for the length effect will not be needed for most of the length of the indication except near ends.

43. Contrast Evolutions of Surface Texture

Figure 49 indicates that compared to the contrast map for the FBH's, the near surface delaminations attenuate relatively less than the deeper delaminations. The air-gap at the delamination is similar to a contact resistance or a thermal mismatch factor between layers. Thermal mismatch factor between two layers is based on the ratio of effusivities of the two materials. The thermal mismatch between the top layer and the next layer may vary periodically along the interface in a laminated structure which uses fabric and matrix. Similarly, the emissivity and diffusivity of top layer may vary periodically along the surface. Variation in the diffusivity, emissivity and mismatch factor between the top two layers as well as the surface texture or roughness pattern is referred to as the surface/near surface thermal texture. Figure 52 illustrates the positive and negative early peaks due to texture. The blue square outlines the reference area and the red spot indicates the measurement spot. Figure 52 implies that a hot spot in IR image of the surface (thermal) texture would provide an early peak. Here, we assume that measurement ROI size is smaller than or equal to the width of the hot spot. Similarly, a cold spot should provide a negative peak in the contrast evolution. Thus, in detection of delaminations, it is important to properly interpret the early time peaks as possibly due to surface texture. These indications may superimpose on the signal from shallow delaminations reducing depth resolution in evaluating shallow delaminations.

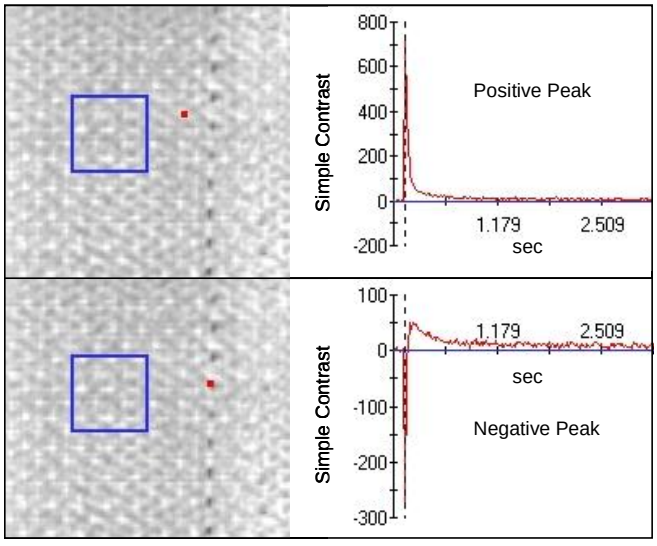

Figure 52:Example of Texture Peak and Dip (Negative Peak) in Graphite Epoxy Laminate

44. Similarities and Differences between Flash Thermography IR Contrast and Ultrasonic Pulse Echo Analysis

Due to familiarity of an NDE engineer with the ultrasonic testing, it is important to point out similarities and differences between the pulse echo ultrasonic A-scan analysis and the IR Contrast analysis. IR Contrast algorithm is used to analyze delamination-like anomalies. The IR Contrast concept is similar to flaw sizing in ultrasonic inspection of wrought metal. In the ultrasonic technique, usually a plate of wrought metal is inspected for internal separations. The part may be immersed in water along with the ultrasonic transducer.

A longitudinal ultrasonic pulse is triggered at the transducer and is transmitted through water to the part where a portion of the ultrasonic pulse is reflected and a portion is transmitted into the part. The pulse reflects off the anomaly and some of the reflected pulse energy, after passing through the water-to-metal interface, is received back by the transducer. The ultrasonic instrument provides an A-scan display. The A-scan shows waveform of the received pulse. The horizontal or X-axis is the time of the waveform. The X-axis can be calibrated in distance or length of the one-way sound-path of the pulse reflections from the top surface of the part. The beginning portion of the A-scan has the waveform of the initial pulse applied to the transducer. The remaining portion of the A-scan indicates reflected pulse energy. The reflected pulse amplitude is affected by the depth and size of the reflector.

Flat bottom hole reference standards are used to calibrate the inspection technique for depth and depth-amplitude correlation. In addition, area-amplitude correlations can also be established externally.

The ultrasonic pulse has a beam width. The aperture and curvature of the transducer influences the beam width. The beam width usually changes with the distance from the transducer. For an unfocussed transducer, the aperture primarily controls the amount of energy received. For a focused transducer, both beam width at the reflector and the aperture influence the amount of energy received.

The IR Contrast evolution shows some similarities with the ultrasonic pulse-echo A-scan, especially when the ultrasonic signal is rectified on positive side and the envelope (or video) mode is used. The horizontal axis is time in both cases. The peak-time in both cases relates to the depth of the anomaly from the part surface. In the ultrasonic technique, the ultrasound material velocity is used to convert the peak-time to the reflector depth by multiplying one-way transit time observed in the A-scan by the velocity of ultrasound. In IR Contrast analysis, material heat diffusivity is primarily used to convert the peak-time to depth although width of the contrast envelope (persistence time) also affects this correlation. The persistence time is affected by the width of the anomaly. The ultrasonic pulse width is normally not related to the flaw size. Both techniques use flat bottom hole standards for amplitude/depth calibration. In the ultrasonic technique, the depth versus amplitude calibration can be incorporated in real-time such that the chosen area of the flaw provides same amplitude at a range of flaw

depths. In the IR Contrast analysis, the calibration is applied to a separate simulated contrast evolution. The actual contrast evolution is not altered by the calibration. Similar to the ultrasonics, the area/amplitude correlation is also established for the IR Contrast. Typically, FBH at two depths of interest are chosen.

As the flaw size increases, the amplitude of reflected ultrasonic pulse increases but as the size of the flaw grows comparable to the aperture or the beam width at the flaw, the growth in the amplitude slows and reaches a saturation value. A similar relationship is observed for very high gamma (diameter/depth) flaws in the IR Contrast evolution. The contrast signature is not affected by further increase in the gamma. For elongated flaws, typically the growth in length beyond two times of the width does not increase the peak contrast significantly for shallow flaws.

Tighter delaminations transmit ultrasound depending upon the amount of contact area and contact pressure or bonding. Also, very thin gaps transmit small percentage ultrasound but thick gaps do not. Tighter delaminations conduct heat depending upon the amount of contact pressure. While thin delaminations (0.0005 inch gap) can conduct and convect heat, they cannot conduct detectable ultrasound at megahertz frequencies. Unless there is a contact pressure or bond between dry and hard surfaces, very little ultrasound energy is transmitted.

In the ultrasonic pulse echo technique, a single delamination may register multiple echoes in the A-scan. In the IR Contrast analysis, only one envelope is registered by a single delamination. In case of multiple delaminations of about same size that are stacked, only the nearest delamination is detected by both ultrasonics and the Flash IR technique. In a special case, where a vertical surface crack or cracks connect to a subsurface delamination, two peaks may be observed in the contrast evolution as described in the following case study. The first peak is usually very sharp (short persistence time) and is due to the surface cracks or surface (or near-surface) thermal texture. In graphite-Epoxy laminates, weave pattern of the top layer may provide the surface thermal texture. Depending upon the pixel location a sharp peak or a sharp dip may be observed in earlier times.

In ultrasonics, the near surface resolution is limited by the surface roughness, ultrasound wavelength, pulse width and the beam diameter. In flash thermography, the surface texture reduces the near-surface resolution. In order to image the texture satisfactorily, the IR image pixel size should be less than a third of the texture wavelength (or the width of the texture hot spot or feature in the IR image). In order to detect a thin gap sub-surface delamination under the texture, the width of the sub-surface delamination should be more than the texture wavelength and it should not be aligned with the texture.

The second peak has lower amplitude and longer persistence time; and is due to the delamination. In some situations, the two peaks may merge into one envelope with only one distinct peak location which is heavily influenced by presence of the crack. Ultrasonic echoes from vertical cracks are very small in the longitudinal wave pulse echo ultrasonic inspection compared to the echo from a delamination.

45. Case Study: RCC Joggle Area Test Piece with Subsurface Delamination

We analyze an RCC test piece with delamination. Figure 53 shows an IR image of a test piece (6L-2A_25-30y_ss_200P06L004). The two white dots in the center indicate near surface delaminations known as flakes.

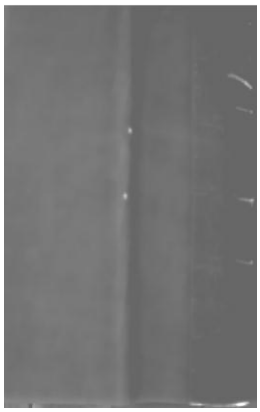

Figure 53: IR Image of RCC Joggle Area Anomaly

Figure 54 shows the half-max boundary (w_{hf}) in yellow. The green line indicates the high intensity locations chosen as the measurement points and the blue line shows the reference locations. A contrast data file is extracted based on the measurement and reference points and is analyzed by the IR Contrast application for diameter and depth.

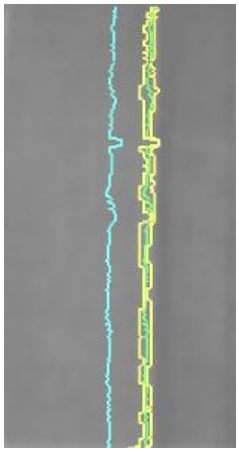

Figure 54: Contrast Extraction Locations and Half-max Boundary

Figure 55 shows a typical contrast evolution at a chosen measurement pair (measurement ROI and corresponding reference ROI) when craze cracks are not present close to the measurement ROI.

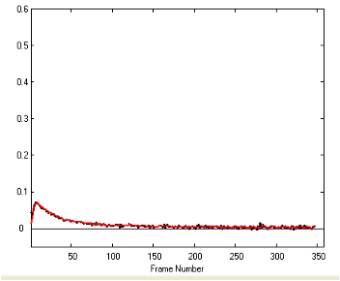

Figure 55: Typical Contrast Evolution without Craze Crack Influence

Figure 56 shows a typical contrast evolution for a chosen measurement pair when craze cracks are present near the measurement ROI. The initial peak in the evolution is due to the crack, the later peak is due to the delamination. The IR Contrast application allows choice of signal matching either to the initial peak or to a later peak by allowing omission of contrast in the initial frames after flash. The IR Contrast technique can assess severity of the cracks as mapped into the EFBH's.

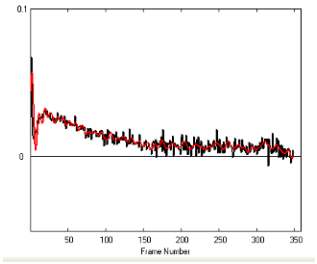

Figure 56: Typical Contrast Evolution with Craze Crack Influence

The craze cracks may be connected to the delamination and the initial and later peaks may get merged as shown in Figure 57 and 58.

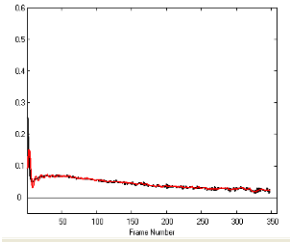

Figure 57: Typical Contrast Evolution with Craze Crack Influence, Second Peak Less Distinct

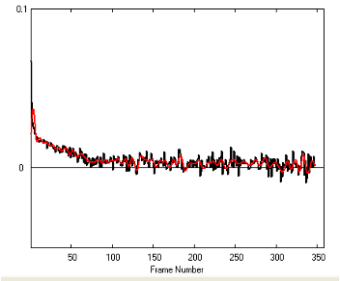

Figure 58: Contrast Evolution with Craze Crack Influence, No Second Peak

Figure 59 shows the peak contrast plot. Two peaks at 1.8 inch and 2.8 inch are due to flake spots.

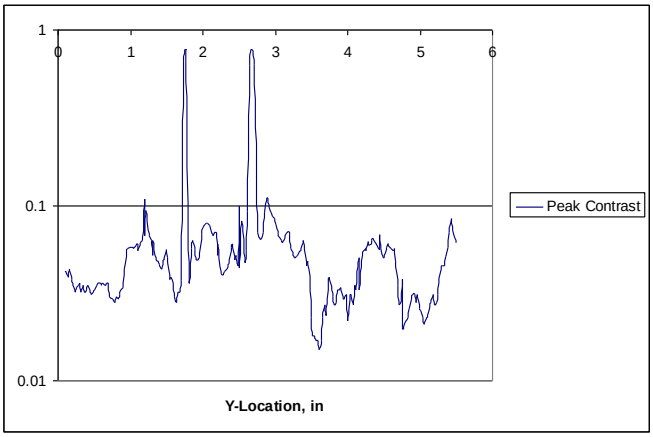

Figure 59: Peak Contrast along the Indication

Figure 60 shows the peak time plot. In most of the region, the peak time is less than 0.5 sec. In some locations it is larger than 0.5 sec.

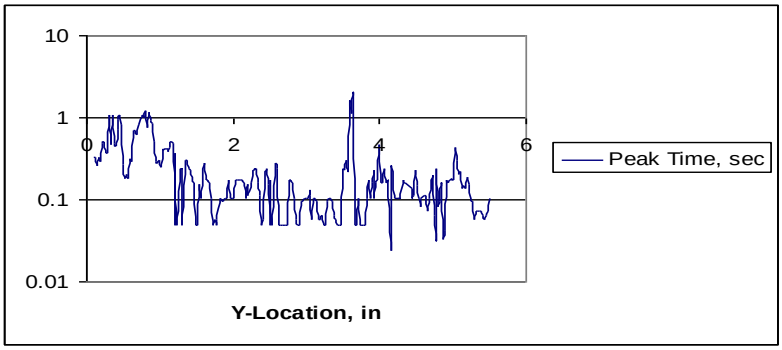

Figure 60: Peak Time along the Indication

Figure 61 shows the persistence time plot. It shows the two dips at 1.8 inch and 2.8 inch corresponding to flake locations. The plot indicates relatively high persistence time within region from 0 inch to 1 inch and at 3.5 inch.

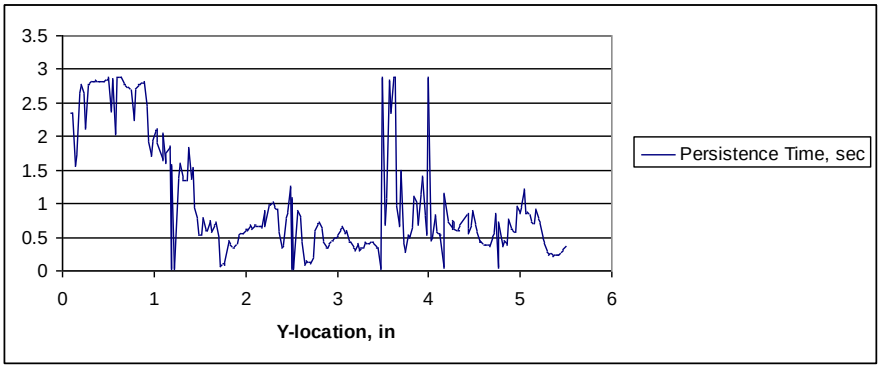

Figure 61: Persistence Time along the Indication

Figure 62 shows the persistence energy time. It shows the two peaks at flake locations. The plot indicates relatively high persistence within a range from 0 inch to 1 inch. Persistence time and persistence energy time plots have similar shape in many locations and relate more to width of the delamination.

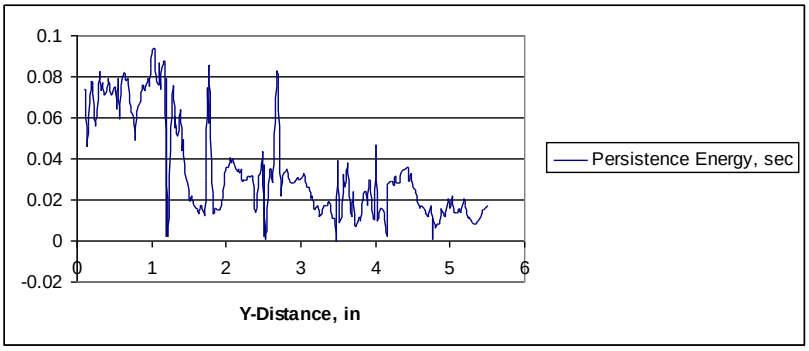

Figure 62: Persistence Energy Time along the Indication

Figure 63 provides IR Contrast (D_{EFBH} and d_{EFBH}) and half-max predictions. The IR Contrast (D_{EFBH}) and half-max (w_{hm}) widths seem to provide same order of magnitude measurements. The flake indications show lower half-max and higher EFBH width, indicating a relatively higher gap thickness**.** Indications that show higher half-max width and lower EFBH width imply that the gaps are thinner. See Figure 63 (Y-distance of 2.4 inch).

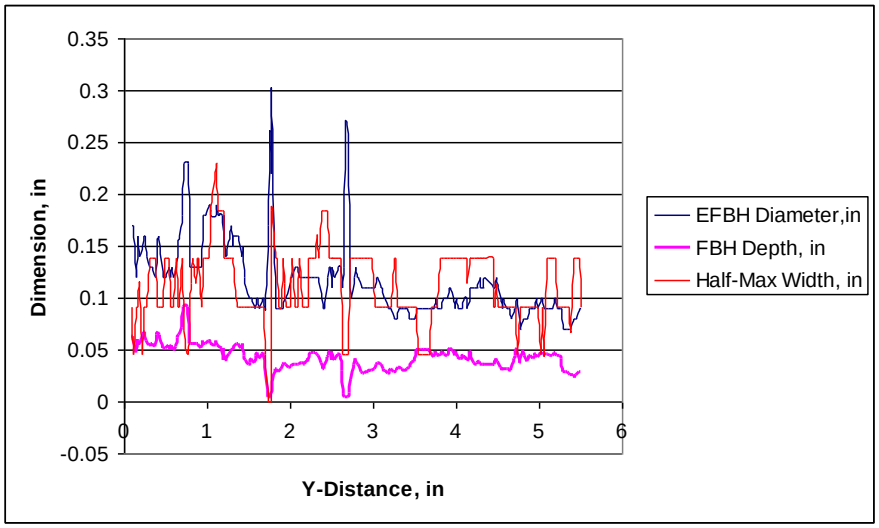

Figure 63: EFBH Diameter, Depth and Half-max Width Estimations

The results (D_{EUG} and d_{EUG}) of attenuation contrast analysis with percent attenuation ($\mu_{\%}$) of 0, 30 and 50 percent are shown in Figure 64. The depth prediction (d_{EFBH}, $d_{EUG,\%\mu 50}$ and $d_{EUG,\%\mu 30}$) in the three attenuation analysis is about same. The 50 percent attenuation diameter ($D_{EUG,\%\mu 50}$) is about 1.6 times the 0 percent attenuation diameter.

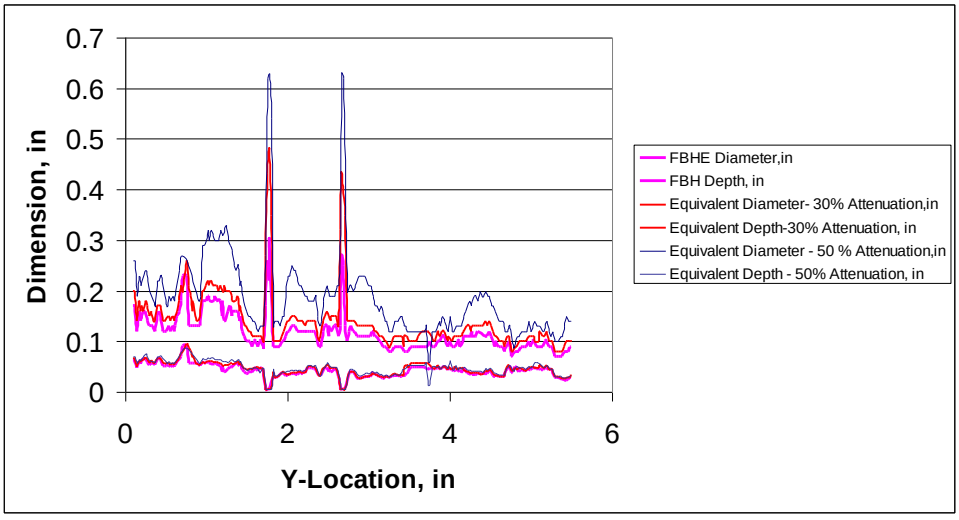

Figure 64: IR Contrast Diameter and Depth Prediction

As expected, analysis with thinner gaps shows higher diameter estimation. Since the indication is long, the EFBH and attenuation diameters are expected to be approximately two times of actual width. The delamination is not like a flat bottom hole but more like a thin gap delamination. We would assume that the delamination is close to 50 percent attenuation (or a gap of 0.001 inch approximate). Therefore, to obtain an approximate estimate of width we divide the EUG diameter by about 1.6 (0.25 inch wide delamination at 0.040 inch depth). The comparison is shown in Figure 65. The EFBH and the adjusted

50 percent attenuation EUG estimations are in good agreement implying EFBH estimations on the long RCC indications may provide comparable estimations to 50 percent attenuation measurements with adjustment for the aspect ratio.

Indications that have about the same value for both EFBH width and half-max width (or the adjusted 50 percent attenuation width) indicate that the gap thickness assumed in the 50 percent attenuation analysis are applicable. The attenuation analysis is based on use of thermal simulation, assumed delamination depth and expected width of a longitudinal delamination. Whereas the EFBH analysis does not use the thermal (ThermoCalc) simulation but assumes a range of delamination depth and width. If results from the EFBH and the attenuation analysis look comparable, one may choose to use EFBH analysis only due less effort required to perform the analysis.

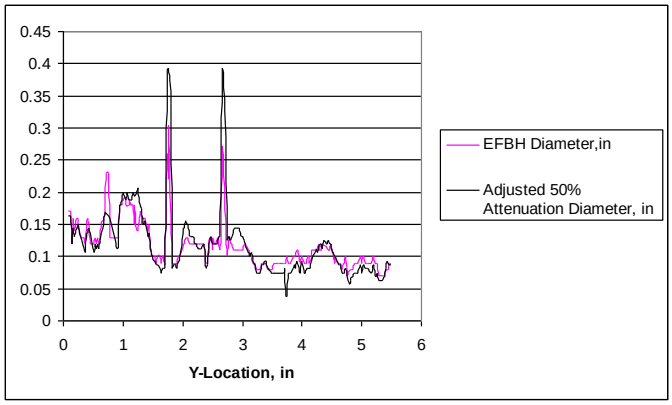

Figure 65: Comparison of EFBH Diameter and 50 Percent Attenuation EUG Diameter

Silicon carbide coating spallation is postulated to relate to the buckling strength across the width of the linear indication. The buckling strength is proportional to the inverse of gamma square. A plot of inverse of gamma square is shown in Figure 66. Low values indicate lower buckling strength. Correlation of this quantity with the pull strength needs to be investigated.

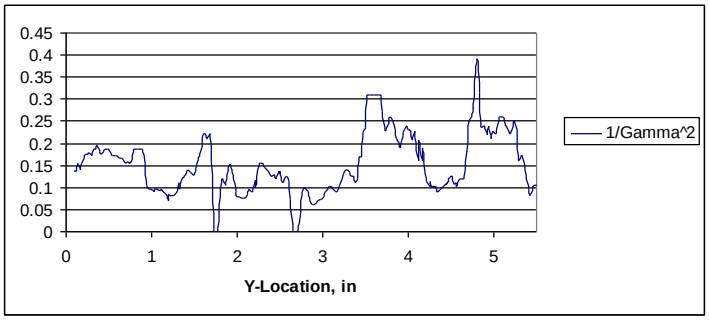

Figure 66: Inverse of Gamma Square

Figure 67 provides one of the three microscopy cross sections of this specimen. The IR Contrast width estimations seem to match the width measurements in the aero-surface (horizontal surface) regions. IR Contrast depth estimations are of the same order as indicated by the microscopy section.

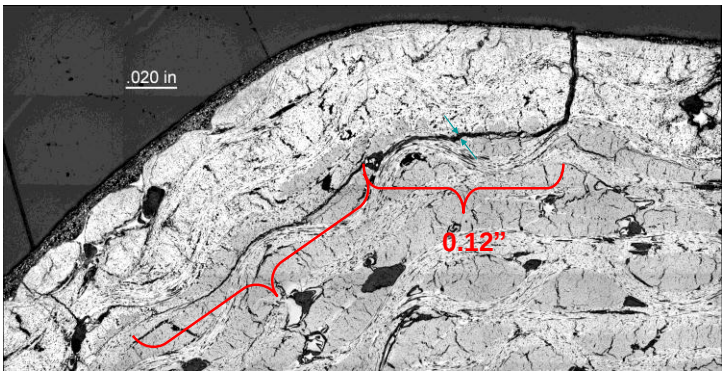

Figure 67: Typical Cross Section of the Specimen

The flash thermography response is limited to the horizontal (or aero) surface. The sloping surface receives less flash heat and the IR response is weak in this area. Thus, the half-max and IR Contrast EFBH or EUG diameter measurements should be compared to the microscopy measurement of delamination width of 0.12 inch, which is under the aero-surface. The half-max, EFBH and adjusted 50 percent attenuation EUG widths do compare with the microscopy measurements. It is better to measure both half-max and the EFBH width or half-max width and the adjusted 50 percent attenuation EUG width to corroborate the measurements to increase confidence in these measurements. Both the half-max and EFBH/EUG diameter measurements can provide error in the estimation by themselves due to the fact that the real delaminations are not like flat bottom holes or uniform gaps. The real delamination may have a tapering gap towards its boundary and craze cracks. Estimating a delamination width by analyzing the signal in time (IR Contrast) and in space (half-max) provides higher confidence in estimations.

46. Conclusions Regarding IR Contrast/Half-Max Technique

The IR Contrast approach provides two methodologies to analyze the flash thermography video data for characterization of delamination-like anomalies. The first methodology involves measurements such as the peak contrast, persistence energy time and peak time which can be plotted against the location of the measurement. These measurements show some correlation to the anomaly depth and width. The second methodology involves matching the calibration-based predicted contrast evolution to the measured contrast evolution. The matching of the simulated evolution to the measured contrast provides size and depth of the equivalent flat bottom hole or equivalent uniform gap with known attenuation. The EFBH/EUG depth and diameter are hypothesized to bear correlation to the width and depth of the measured anomaly. Comparison of the EFBH/EUG evolutions with measured contrast evolutions, to provide evaluation of delaminations in terms of

depth, width and presence of surface cracks, confirms this hypothesis. The half-max edge detection complements the IR Contrast EFBH/EUG width predictions and the reverse is also true. The difference in the two width measurements is thought to be due to non-uniformity of the gap thickness, value of gap thickness as well as the limitations of the two estimations. The paper provides information on the IR Contrast/half-max analysis of flash thermography data.

47. Recommendation for Analyzing Linear Delaminations

Analysis of more validation data is ideally needed to support some of these recommendations. The analysis does not specifically address the tapering nature of the delamination gap or the bridging between delaminations. The boundary of delamination can be located using destructive microscopy but we need to locate the boundary non-destructively. In the IR technique, for a nonmetal like RCC, the heat flows through the air gap if the gap thickness is less than about 0.010 inch. The contrast evolution is attenuated to 50 percent at about 0.0005 inch to 0.001 inch of air gap thickness. In reality, a gap of approximately 0.001 inch has been observed on many specimens with delaminations. Also, the peak time profile indicates that the contrast map is likely to be close to the contrast map for 50 percent attenuation. Therefore, it is recommended to choose an attenuation level of 50 percent for the EUG analysis as the lower bound. Similarly, the 0 percent attenuation is also recommended for the EFBH analysis as the upper bound. For conservatism, a larger of the two width estimates is recommended. The length-to-width aspect ratio correction is recommended for the EUG estimations. Also, depending upon the delamination depth and width, the EFBH estimations are recommended. Analysis of the validation data should help in choosing the right attenuation level. It is postulated that, although delamination gaps less than 0.0005 inch do exist, they are likely to have smaller continuous areas (short in length and width). These gaps are likely to be separated by material continuity or contact. In order to apply higher attenuation such as 70 percent attenuation, the assumption that the IR evolution is extracted from a continuous gap is necessary. Also smaller gap delaminations may not be detectable by the IR technique due to low signal to noise ratio.

Comparison of the adjusted 50 percent attenuation width (or EFBH width) with the half-max width allows assessment of gap thickness. If we call the 50 percent attenuation gap as the standard gap, then we can describe the gap thickness as thicker than, thinner than, or equal to the standard gap. If the half-max width is larger than the adjusted 50 percent attenuation width ($\psi_{\mu 50\%} < 1$), then the delamination gap is thinner than the standard gap. If the half-max width is smaller than the adjusted 50 percent attenuation width ($\psi_{\mu 50\%} > 1$), then the gap is thicker than the standard gap. If the half-max width is equal to the adjusted 50 percent attenuation width ($\psi_{\mu 50\%} = 1$), then the gap thickness is equal to the standard gap thickness. Here the real gaps may not be uniform, and the gap thickness assessment is meant to relate only to the average gap thickness.

The half-max width estimation is also affected by the non-uniformity of the gap thickness**.** The half-max width estimation is also affected by the pixel size in comparison

to width of the feature being measured. The half-max width estimation has some error due to above factors. A larger of the half-max and EFBH/EUG width estimate is recommended. Based on the validation data, a lower percent threshold (e.g. 40 percent) may be better suited in the half-max width estimation. The half-max boundary location is estimated locally while the EFBH/EUG boundaries are estimated symmetrical about the measurement ROI's. For tracking purposes, the half-max boundary may be more reproducible. The half-max and the EFBH/EUG width estimations have limitations in evaluating the real delamination data, therefore, it is recommended to use both estimations as both estimations allow conservative compensation for the effect of gap non-uniformity and gap thickness variation. The higher of the two estimations, e.g. adjusted 50 percent attenuation width and half-max width, is recommended as the estimate of width of the linear indication to reduce risk of under estimation of the width. Also, the results are expected to be more accurate in the calibration range of delamination depth.

48. REFERENCES

1. Maldague, X. P.V., Nondestructive Evaluation of Materials by Infrared Thermography, Springer-Verlag London, (1993).
2. Carslaw H.S. and Jaeger J.C., Conduction of Heat in Solids, Clarendon Press, Oxford, (1959).
3. Spicer J. W.M., Active Thermography for manufacturing and Process Control, Short Course Notes SC05, Thermosense, SPIE – The International Society for Optical Engineering (April 1995).
4. EchoTherm and Mosaic, Thermal Wave Imaging, Inc.
5. Software: Thermofit Pro V 2.0, V. Vavilov, Innovation Inc., Introscopy Institute, Tomsk, Russia 634029
6. Software: ThermoCalc V1.0 and ThermoCalc Pro 1.1, V. Vavilov, Innovation Inc., Introscopy Institute, Tomsk, Russia 634029

7. Koshti A. M., Estimating Temperature Rise in Pulsed Thermography using Irreversible Temperature Indicators, Proc. SPIE vol. 4702, p. 191-201, Smart Nondestructive Evaluation for Health Monitoring of Structural and Biological Systems, March 2002